Development of light-addressable potentiometric sensor systems and their applications in biotechnological environments

Dissertation
zur
Erlangung des Doktorgrades
der Naturwissenschaften
(Dr. rer. nat.)

dem

Fachbereich Pharmazie
der Philipps-Universität Marburg
vorgelegt von
Carl Frederik Werner
aus Göttingen

Marburg/Lahn 2014

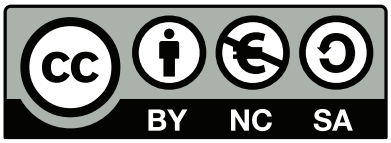

Vom Fachbereich Pharmazie
der Philipps-Universität Marburg als Dissertation am 16. Mai 2014 angenommen.
Erstgutachter: Prof. Dr. M.J. Schöning
Zweitgutachter: Prof. Dr. M. Keusgen
Tag der mündlichen Prüfung am 19. Mai 2014

Erklärung

Ich versichere, daß ich meine Dissertation

> Development of light-addressable potentiometric sensor systems and their applications in biotechnological environments

selbständig ohne unerlaubte Hilfe angefertigt und mich dabei keiner anderen als der von mir ausdrücklich bezeichneten Quellen bedient habe.

Die Dissertation wurde in der jetzigen oder einer ähnlichen Form noch bei keiner anderen Hochschule eingereicht und hat noch keinen sonstigen Prüfungszwecken gedient.

Jülich, den 16. März 2014

Abstract

The simultaneous analysis of multiple analytes and spatially resolved measurements of concentration distributions with a single sensor chip are an important task in the field of (bio-)chemical sensing. Together with the miniaturisation, this is a promising step forward for applications and processes that profit from (bio-)chemical sensors. In combination with biological recognition elements, like enzymes or cells, these biosensors are becoming an interesting tool for e.g., biotechnological, medical and pharmaceutical applications. One promising sensor principle is the light-addressable potentiometric sensor (LAPS). A LAPS is a semiconductor-based potentiometric sensor that allows determining analyte concentrations of aqueous solutions in a spatially resolved manner. Therefore, it is using a focused light source to address the area of interest. The light that illuminates the local area of the LAPS chip generates a photocurrent that correlates with the local analyte concentration on the sensor surface. Based on the "state of the art", further developments of LAPS set-ups were carried out within this PhD thesis. Furthermore, by utilising enzymes and whole cells, the benefits of these LAPS set-ups for biotechnological, medical and pharmaceutical applications are demonstrated.

During the present thesis, three different LAPS set-ups were developed: The first LAPS set-up makes use of a field-programmable gate array (FPGA) to drive a 4×4 light-emitting diode (LED) array that defines 16 measurement spots on the sensor-chip surface. With the help of the FPGA, the driving parameters, like light brightness, modulation amplitude and frequency can be selected individually and all LEDs can be driven concurrently. Thus, a simultaneous readout of all measurement spots is possible and chemical images of the whole sensor surface can be achieved within 200 ms. The FPGA-based LAPS set-up is used to observe the frequency behaviour of LAPS chips. Electrical equivalent circuitries are employed to compare the frequency response of the photocurrent with the electrical sensor impedance that can also be determined with the FPGA-based LAPS set-up. In this way, the optimal modulation-frequency range for driving the light sources is figured out as well as the physical parameters that have influence on the frequency behaviour. Furthermore, the photocurrent generation mechanisms are discussed. In a second LAPS set-up, a commercially available organic-LED (OLED) display is used as light source. The OLED panel consists of 96×64 pixels with a pixel size of 200 µm $\times$ 200 µm and thus, an over 16 times higher lateral resolution compared to the IR-LED array. To achieve modulation frequencies in the kHz range

that are fitting to the LAPS-frequency behaviour, a new method to drive the OLED display has been developed, since the typical refresh rates of the displays are at about 100 Hz. It was demonstrated that chemical images of the whole sensor surface can be obtained in 2.5 min, which is about 40 times faster than traditional addressing methods. Since the lateral resolution of LAPS is not only specified by the light source, but also by the LAPS chip itself, the lateral resolution of the LAPS structures is characterised. Therefore, the third LAPS set-up has been developed, which utilises a single laser diode that can be moved by an XY-stage. By scanning a specially patterned LAPS chip, a lateral resolution of the LAPS structures in the range of the pixel size of the OLED display is demonstrated.

Label-free imaging of biological phenomena is investigated with the FPGA-based LAPS. With the help of an enzymatic layer with the enzyme acetylcholine esterase (AChE) the detection of the neuronal transmitter acetylcholine (ACh) is demonstrated. The dynamic and static response as well as the long-term stability is characterised and compared with another semiconductor-based chemical imaging sensor based on charge-coupled devices (CCD) using the same enzymatic layer. The response of both sensors towards different ACh concentrations is discussed and shows a similar behaviour of both sensors, which is in agreement with theoretical models.

The usage of the FPGA-based LAPS as whole-cell-based biosensor is studied with the model organism *Escherichia coli*. Here, the metabolic activity of the *E. coli* cells is investigated by determining the extracellular acidification. The primary aim of these measurements is the development of a new monitoring system for biogas digesters, in order to monitor the metabolic activity of the organisms involved in the fermentation process. Therefore, an immobilisation technique for embedding the microorganisms in polyacrylamide gel on the sensor surface has been developed. The immobilisation is realised in an on-chip differential arrangement by making use of the addressability of LAPS. This way, external influences such as sensor drift, temperature changes and external pH changes can be compensated. In a comparative study of the extracellular acidification rate between immobilised *E. coli* and *E. coli* that are in suspension, acidification rates in the same order were determined, demonstrating that the immobilisation does not have any influence on the metabolic activity. Further measurements with this cell-based LAPS system underline the sensitivity towards different nutrient concentrations, namely glucose. The ability to observe the extracellular acidification of microorganisms and the sensitively towards nutrient concentrations enables to detect high-order effects, like toxicity or pharmacological activity in complex analytes.

Contents

Acronyms

ACh acetylcholine.
AChE acetylcholine esterase.
APS ammonium persulfate.
ATP adenosine triphosphate.

CCD charge-coupled device.
CMOS complementary metal-oxide-semiconductor.
CMP chemical-mechanical polishing.

DLP digital light processing.

ECIS electric cell-substrate impedance sensing.
EIS electrolyte/insulator/semiconductor.

FFT fast Fourier transform.
FPGA field-programmable gate array.

GPIO general purpose input/output.

IR-LED infrared light-emitting diode.
ISFET ion-sensitive field-effect transistor.
IUPAC International Union of Pure and Applied Chemistry.

LAPS light-addressable potentiometric sensor.
LB lysogeny broth.
LED light-emitting diode.
LSI large-scale integration.

MIS metal/insulator/semiconductor.

OLED organic light-emitting diode.

PBS phosphate buffered saline.
PDM pulse-density modulator.
PLL phase-locked loop.
PSoC Programmable System-on-Chip.

RMS root mean square.

SLPT scanned light pulse technique.
SPI serial peripheral interface.
SPIM scanning photo-induced impedance microscopy.

TEMED tetramethylethylenediamine.
TIA transimpedance amplifier.

VHDL very high-speed integrated circuit hardware description language.

1 Introduction

Light-addressable potentiometric sensors (LAPS) are part of field-effect-based (bio-) chemical sensors. LAPS are able to determine the analyte concentration of an aqueous solution in a spatially resolved manner. Therefore, a focused light pointer is used to illuminate the sensor chip to define a local measurement spot, where a photocurrent will be generated that depends on the local analyte concentration. This present thesis aims to be the successor of a thesis by Dr. Torsten Wagner from the year 2008 [1]. The aim of the thesis of Dr. Wagner was the development of miniaturised and self-contained measuring instruments for pharmaceutical applications based on a LAPS. Selected measurements showed that LAPS has a wide field of applications in the areas of chemistry, biotechnology and pharmacy, that is due to the possibility to autoclave the LAPS chips, which is ideal for cell-culture applications. Furthermore, it was demonstrated that self-contained LAPS-based measuring instruments could be build up with commercially available parts without the need of external measurement devices, which makes an industrial implementation possible. Based on these results, a further development of different LAPS set-ups, their enhancements and characterisation is done in the present thesis. In addition, their capability in the field of whole cell-based biosensors is demonstrated and discussed.

This introduction will give a short overview of the current "state of the art" of field-effect-based potentiometric (bio-)chemical sensors, especially LAPS. Hereafter, an overview of whole cell-based biosensors is given as possible application. The section 1.4 will guide through the publications that are collected in the present cumulative thesis.

1.1 Field-effect-based potentiometric sensors

Field-effect-based potentiometric sensors belong to the field of semiconductor-based sensors. Thus, they adopt most of the advantages compared to conventional sensors (like ion-sensitive electrodes), e.g., small size and solid-state nature, mass fabrication, short response time and integration of compensation and data processing circuits [2]. Field-effect-based potentiometric sensors are utilising the field effect to determine and "amplify" the potential on their sensor surface. The first developed sensor in this group was the ion-sensitive field-effect transistor (ISFET), published by Bergveld in 1970 [3].

Field-effect-based potentiometric sensors in general consist of an electrolyte/transducer/insulator/semiconductor structure (see Fig. 1.1a, left). With the help of a reference electrode in the electrolyte and a rear-side contact on the semiconductor layer, a bias voltage V_{bias} is applied across the structure. The sensing principle involves mainly two effects: The effect of the concentration-depending surface potential and the field effect used to read out the surface potential. The field effect is usually described by metal/insulator/semiconductor (MIS) structures, where the electrolyte/transducer layer is replaced by a metal layer. The theory of MIS structures is specified with energy-band diagrams and can be found in detail elsewhere [4]. Qualitatively, the mechanisms of the field effect can be described as followed: Due to the applied bias voltage, a space-charge region at the insulator/semiconductor interface is formed. The width of the space-charge region varies with the applied bias voltage and shows three distinct conditions. In the case of an ideal MIS structure with *p*-doped[1] silicon, the conditions are:

- Accumulation ($V_{\text{bias}} < 0$): Positive mobile charge carriers (holes) accumulate on the interface and no space-charge region will be formed.
- Depletion ($V_{\text{bias}} > 0$): The holes are pushed away from the interface due to the electrical field. Thus, a region depleted of mobile carriers is formed at the interface, which, due to the uncovered acceptor atoms is charged negatively. It is called the space-charge region.
- Inversion ($V_{\text{bias}} \gg 0$): If the voltage increased more, the electron (minority charge carrier) concentration on the interface exceeds the hole concentration and a thin layer of *n*-type silicon, a so-called inversion layer, is formed. The width of the space-charge region has reached its maximum.

In the case of real MIS structures, the transition between accumulation and depletion condition occurs not at $V_{\text{bias}} = 0\,\text{V}$, instead it occurs at the so-called flat-band voltage V_{FB}, which depends, amongst others, on charges in the insulator and on surface states. If the metal layer of the MIS structure is replaced by an electrolyte/transducer layer, an additional potential φ forms at the interface electrolyte/transducer that in turn depends on the analyte concentration. This potential will modulate the flat-band voltage and thus, the space-charge region [5]. In the case of a H^+-ion concentration-sensitive transducer material (e.g., SiO_2, Ta_2O_5 or Si_3N_4), the surface-potential building mechanism is based on the site-binding theory [6]. The surface of a metal oxide always contains neutral amphoteric hydroxyl groups (MOH). At a material-specific pH value, the so-called point of zero charge pH_{pzc}, the surface potential equals zero. At higher H^+-ion activities ($pH < pH_{pzc}$) the surface hydroxyl groups bind protons (MOH_2^+)

[1] A *n*-type MIS structure shows an identical behaviour but the polarity of the voltage and the charge of the charge carriers are reversed.

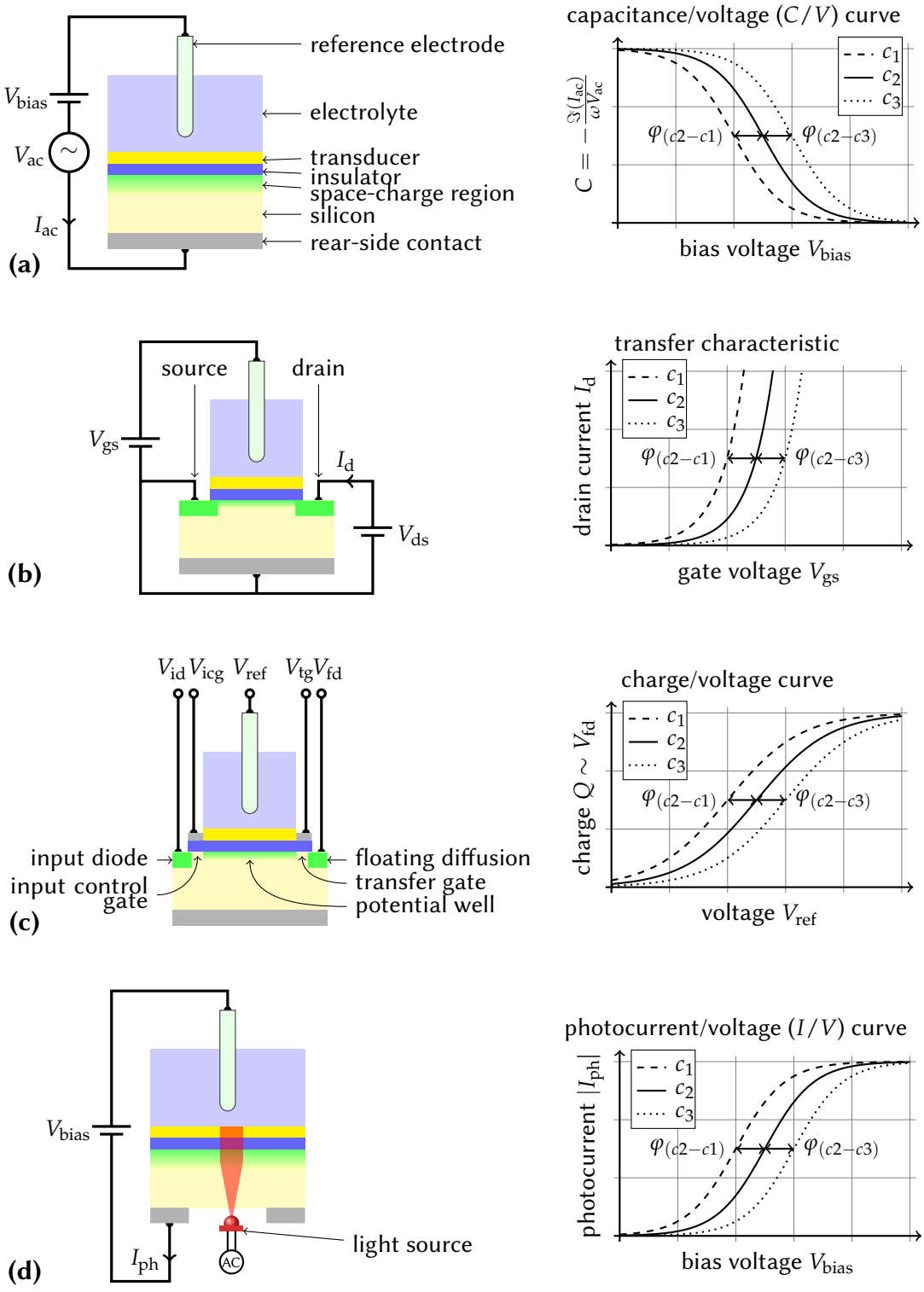

Figure 1.1: Schematic drawings of field-effect potentiometric sensors (left) and their response curves for different analyte concentrations ($c_1 > c_2 > c_3$) (right): EIS sensor (a), ISFET (b), CCD-based sensor (c) and LAPS (d).

and the oxide surface is charged positively. At lower H^+-ion activities ($pH > pH_{pzc}$) the surface hydroxyl groups release protons (MO^-) and the oxide surface is charged negatively. The amount of potential variation depends on the density of surface-active sites and the ion concentration of the bulk solution, which can reach at maximum a Nernstian sensitivity (59.2 mV pH^{-1} at 25 °C) [5]. In the case of Si_3N_4 in addition to the hydroxyl groups, amine groups (SiNH) are present as second type of active sites [7, 8].

Since the analyte-concentration-depending surface potential varies the flat-band voltages and in consequence the space-charge region, one important part of field-effect potentiometric sensors is the principle to read out the space-charge region variations. There are different sensor types that are using different techniques (see also Fig. 1.1):

- The ion-sensitive field-effect transistor (ISFET) determines the conductivity of the inversion layer [3, 5, 9].
- Sensors based on capacitive EIS structures determine the capacitance of the space-charge region [5, 10, 11].
- Sensors based on CCD determine the amount of charge that can be filled in the potential well, built by the space-charge region [12, 13].
- Light-addressable potentiometric sensors (LAPS) generate a photocurrent inside the space-charge region [5, 14–16].

Since the direct output signals of these sensors are different (e.g., current, capacitance, charge) and various due to additional amplification circuitries it is wise to use the change of the surface potential as a common sensor-output signal. In the case of the ISFET, this is an IUPAC[2] recommendation to achieve a better comparison with ion-selective electrodes [17]. The surface potential can be determined in several ways. One way is to calculate the voltage shift of the response curves (e.g., transfer characteristic (ISFET), capacitance/voltage curve (EIS), photocurrent/voltage curve (LAPS) or charge/voltage curve (CCD)) of the sensors at different analyte concentrations. Another way is to use a feedback-control circuit that keeps the sensor signal (e.g., current, capacitance, charge) at a constant value by varying the bias voltage (see Fig. 1.2). By using the controlled bias voltage as sensor-output signal, the potential change, which results from the ion activity, can be directly recorded and visualised over time. These controlled modes (e.g., constant-charge mode for ISFET [17], constant capacitance mode for EIS sensors [10] or constant current mode for LAPS [18]) also help to achieve a wide linear range of the sensors. To determine the quantitative ion concentration, usually, field-effect potentiometric sensors are calibrated with different analyte concentrations prior to the measurements.

[2] International Union of Pure and Applied Chemistry

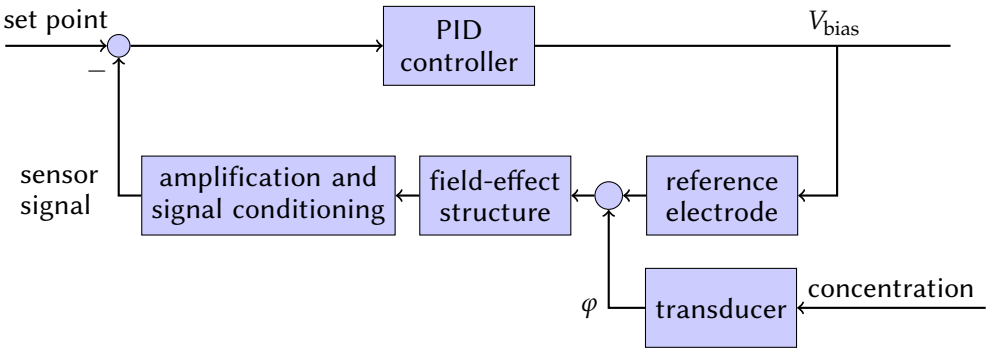

Figure 1.2: A feedback-control loop that keeps the sensor signal (e.g., current, capacitance, charge) of a field-effect potentiometric sensor at a constant value (set point) by varying the bias voltage. The controlled bias voltage V_{bias} is used as sensor-output signal. Thus, changes in the potential φ, which result from different ion concentrations, can be directly recorded and visualised over time.

1.2 Light-addressable potentiometric sensors

Light-addressable potentiometric sensors (LAPS) enable the monitoring of analyte concentrations in a spatially resolved manner on the sensor surface [14–16]. Therefore, they can be used to record chemical images that visualise the analyte-concentration distribution. Chemical images are useful, e.g., to observe the diffusion of analytes [19, 20], chemical reactions [21] or the growth of cell colonies [22, 23]. Another possibility of spatially resolved measurements is the observation of multiple parameters with a single sensor by means of different sensitive membranes or recognition elements on the sensor surface [14, 21, 24–26]. There are other 2-dimensional potentiometric chemical imaging sensors, which are utilising arrays of ISFETs or CCD-based sensors [27–30]. However, the LAPS offers the advantage, that it consists of a lateral, unstructured electrolyte/insulator/semiconductor (EIS) structure and the area of interest (measurement spot) is addressed by a focused light beam. This results in a smoother and unstructured sensor surface and a free addressing of the sensor spot compared to array-based imaging sensors, which is helpful for e.g., the immobilisation of biological recognition elements. Furthermore, there is no need of sophisticated encapsulating of conducting paths or electrical circuitries on the sensor surface.

The LAPS principle was introduced 1988 by Hafemann *et al.* [14]. It was based on the scanned light pulse technique (SLPT) [31] with the intention to measure in aqueous solutions. As field-effect-based potentiometric sensor, the LAPS consists of an EIS structure and a bias voltage V_{bias} is applied across the structure (see Fig. 1.1d, left). A focused and modulated light source illuminates the semiconductor at the position of the measurement spot. The light results in electron-hole pairs inside the semiconductor that will be separated in the space-charge region and induce an externally measurable

alternating photocurrent. Plotting the photocurrent amplitude against the applied bias voltage results in photocurrent/voltage (I/V) curves, where the three conditions of the space-charge region are visible (see Fig. 1.1d, right). The variation of the flat-band voltage due to different analyte concentrations results in a shift of the I/V curve along the bias-voltage axis. Thus, driving the sensor in depletion condition, a concentration-depending signal could be achieved. However, by driving the sensor in inversion condition, the local impedance could be analysed, as it is used in the scanning photo-induced impedance microscopy (SPIM) [32].

Since one important component of a LAPS device is the light source, which defines the ability of spatially resolved measurements, different types of LAPS set-ups were introduced. Furthermore, there are different methods to read-out and process the resulting photocurrent, which leads to several LAPS read-out modes. The next two subsections gives a short overview and discussion about existing and possible LAPS set-ups and read-out modes.

1.2.1 LAPS light-driving methods

Illuminating the semiconductor is possible from two directions: Front-side and rear-side illumination. Front-side illumination results in a higher photocurrent and better lateral resolution compared to rear-side illumination, because the electron-hole pairs are generated directly inside the space charge region [33]. In case of rear-side illumination most of the light is absorbed by the semiconductor substrate and the electron-hole pairs have to diffuse towards the space-charge region, resulting in a lower lateral resolution. The wavelength of the light source is usually chosen in the infrared region, since silicon has a high transparency in this range. This way the photocurrent amplitude and lateral resolution can be improved [34]. However, regarding the front-side illumination, it has to be taken into account that the light has to go through the analyte, possible immobilised recognition elements (e.g., additional membranes, enzymes or whole cells) or even parts of the measurement cell (e.g., microfluidic channels) that can adsorb some light and thus, will influence the sensor signal, or the light will have some impact to these components.

The light source itself defines the measurement resolution, the scanning range, the measurement speed and the signal amplitude. In the past, different light sources for LAPS have been proposed in literature. Conventional set-ups use a single focused laser on a mechanical XY-stage [21, 34, 35]. Since the sensor plane is scanned in a raster-like manner, these set-ups have a rather high spatial resolution; however, they are rather slow due to the required mechanical movement. Another approach is the use of multiple light sources in an array arrangement, e.g., by light-emitting diodes (LEDs) [25, 36–38]. These set-ups are faster, but are limited in their spatial resolution because of the

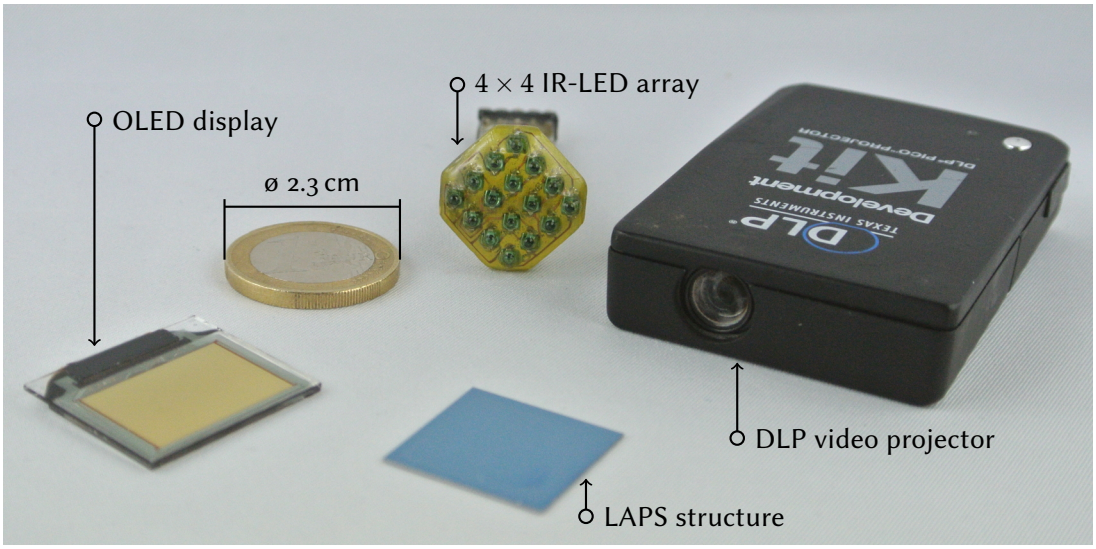

Figure 1.3: Possible light sources that were used for LAPS set-ups, in addition a LAPS structure is presented. The 4×4 IR-LED array is mostly used in this thesis and driven by an FPGA (see chapter 2). The OLED display is used in chapter 4. In [42] the application of the DLP video projector is described.

geometrical size of the LEDs. The combination of both methods, a linear arrangement of light-sources that scan along the sensor chip, like a flat-bad scanner, is presented in [39, 40]. Multiple light sources can be driven simultaneously at different modulation frequencies to measure several measurement spots at the same time [25, 36, 38, 39]. The resulting photocurrent has to be separated into the different frequency components and mapped to the corresponding position. This can lead to fast measurements of chemical images, enabling the monitoring of chemical reactions and diffusion processes [41]. Recently, the use of commercial imaging techniques, like a digital light processing (DLP) video projector [42] or an organic light-emitting diode (OLED) display [43], were presented as possible light sources for LAPS. These techniques allow to design LAPS systems that are free from any mechanical movement and to define free measurement areas by customising the size of the illuminated area. In Fig.1.3, some possible light sources that were applied for LAPS are depicted.

1.2.2 LAPS read-out methods

Since the excitation signal of LAPS (the light) is intensity-modulated, the resulting photocurrent is an alternating current at the same modulation frequency. Thus, the photocurrent at a certain frequency has a complex value and can be expressed in either real and imaginary part or amplitude and phase shift. The photocurrent amplitude is typically in the range of a few µA. If a LAPS is driven with multiple light sources

simultaneously, each with a different modulation frequency, the photocurrent in turn consists of multiple frequency components, each with a complex value belonging to a single measurement spot. Usually, for an I/V curve the photocurrent amplitude of a measurement spot is plotted against the applied bias voltage (see also Fig. 1.1d, right). Therefore, most LAPS set-ups only determine the photocurrent amplitude, since this results in a less complex device. However, Miyamoto *et al.* [44, 45] showed that the phase shift can also be used for ion sensing. Using the phase shift has the advantage to be less sensitive to fluctuations of the light intensity and distribution of defects in the silicon substrate compared to photocurrent-amplitude measurements. In order to determine the surface potential from the photocurrent, either the photocurrent amplitude or phase shift could be used. To obtain the surface potential, different methods are available: I/V curves, constant-current mode and constant-voltage mode.

The recording of an I/V curve results in more information then only the surface potential at the measurement spot at a specific time. However, the bias-voltage sweep takes some time, thus the temporal resolution is low. Recording the whole I/V curve helps to identify other influences to the measurement, e.g., intensity variations of the light source, distributions and defects in the semiconductor substrate, interface stages, charges in the oxide and analyte-conductivity variations [46].

The constant-current mode [18], or constant-phase mode [45], which utilises the phase shift of the photocurrent instead of the amplitude, uses a controlled feedback loop to keep the photocurrent at a constant value by varying the bias voltage (see Fig. 1.2). This mode is similar to the constant-charge mode of an ISFET or the constant-capacitance mode of an EIS sensor and uses the controlled bias voltage as output signal. Thus, the output signal represents the time-depending surface potential. However, since there is only one bias voltage that is applied over the whole LAPS structure, it has to be changed and controlled for each measurement spot independently in sequence. This results in slow measurement times. Furthermore, since the bias voltage has to be controlled for each measurement spot separately according to the local surface potential, thus, depending on the measurement-spot sequence and the surface-potential distribution, this results in a "randomly" change of the applied bias voltage during switching through the different measurement spots.

The constant-voltage mode is the fasted mode. Here, the bias-voltage is kept constant at a linear range at depletion condition and the photocurrent is measured for each measuring spot. This mode is used to record high-resolution chemical images with an enormous number of measurement spots or to achieve a high temporal resolution. The corresponding surface potential can be calculated by using a previously recorded I/V curve as a reference. Since the bias voltage is kept constant, the measurement range of this mode is low and depending on the linear region of the depletion condition. Due

to some defects and inhomogeneities in the substrate and the additional layers of the sensor chip, it might be necessary to apply some additional image corrections to those chemical images [46].

1.3 Whole cell-based biosensors

The usage of whole cells as complex biological recognition element for biosensors offers at least three advantages [47]:

1. Effects such as toxicity, mutagenicity, or pharmacological activity become accessible to measurements.
2. Internal amplification cascades can be used to increase the sensitivity of the device.
3. Whole cells are the smallest biological entity which is self-sustaining.

Furthermore, whole cell-based biosensors will add value to modern technological fields, like biomedical research, pharmaceutical applications and environmental monitoring, e.g., clinical diagnostics, toxicology, pharmacology and drug screening and environmental monitoring for toxins [48, 49]. These kinds of biosensors give indications of the true "bioactivity" of agents, whereas a conventional immunoassay provides only binding information [48]. Therefore, these sensors are widely discussed in the literature [22–25, 34, 47–73]. Cell-based biosensors are composed of mainly two transducers [48]:

1. Primary transducer: Cells that convert the bioactive substance in cellular signals.
2. Secondary transducer: Detects the cellular signal and outputs electrical signals that can be analysed and processed.

Cell reactions are very different to various bioactive substances. Therefore, several methods to read out the cellular signals have arisen:

- Electrical signals of electrogenic cells (e.g., neural cells or heart muscle cells) can be read out with micro-electrodes [47, 48, 50] or field-effect devices [49, 51, 52].
- Morphology changes, adhesion and cellular movements of adherent growing cells can be observed by impedimetric methods [47, 49, 50, 53–55]. This is also called electric cell-substrate impedance sensing (ECIS) [53].
- Analysing the energy metabolism by determining the uptake of nutrients and/or release of metabolic end products by means of (bio-)chemical sensors [22–25, 34, 47, 49, 50, 52, 54, 56–73].

Several commercially available devices to analyse cellular activities have been launched on the market, some of them analysing multiple parameters, like the Bionas AS 2500 device or the Cellasys IMOLA device that can measure the O_2 uptake, extracellular acidification and the electric cell-substrate impedance [54, 59].

1.3.1 Observing the energy metabolism of cells

Cells take up nutrients and oxidants and metabolise them in the catabolic pathway. The metabolic end products (e.g., organic acids and carbon dioxide) that are not used for synthesis are excreted to the cellular environment. Cellular metabolism is necessary for cells to keep them alive, to grow, to reproduce, to maintain their structure and to adapt to their environment. The metabolic pathways can be dived into aerobic and anaerobic metabolism, depending on the presence of oxygen. One typical metabolite is glucose. Under aerobic conditions, glycolysis and respiration occurs, which leads to the following sum equation:

$$\mathrm{C_6H_{12}O_6} + 6\,\mathrm{O_2} \longrightarrow 6\,\mathrm{CO_2} + 6\,\mathrm{H_2O} \tag{1.1}$$

The glucose ($\mathrm{C_6H_{12}O_6}$) will be converted into water and carbon dioxide. The standard Gibbs free energy of this reaction is $\Delta G'^{\circ} = -2870\,\mathrm{kJ\,mol^{-1}}$, which results in a maximum of about 32 mol adenosine triphosphate (ATP) per mole glucose, for most mammalian cells [74]. Under anaerobic conditions, the glucose will run through glycolysis and lactic acid fermentation for the most mammalian cells:

$$\mathrm{C_6H_{12}O_6} \longrightarrow 2\,\mathrm{H_3C{-}CHOH{-}COO^-} + 2\,\mathrm{H^+} \tag{1.2}$$

One mole glucose results in two mole lactate ($\mathrm{H_3C{-}CHOH{-}COO^-}$) and a standard Gibbs free energy of $\Delta G'^{\circ} = -198\,\mathrm{kJ\,mol^{-1}}$ [74]. Some bacteria such as *E. coli* produce various organic acids under anaerobic conditions. This process is called the mixed acid fermentation. A typical fermentation balance of organic acids from *E. coli* by utilising on mole glucose is [74]:

$$\begin{aligned}\mathrm{C_6H_{12}O_6} \longrightarrow\ & 0.84\,\mathrm{H_3C{-}CHOH{-}COO^-} + 0.44\,\mathrm{H_3C{-}COO^-} \\ & + 0.42\,\mathrm{H_3C{-}CH_2OH} + 0.29\,\mathrm{(OOC{-}CH_2{-}CH_2{-}COO)^{2-}} \\ & + 0.02\,\mathrm{HCOO^-} + 1.88\,\mathrm{H^+} + 0.44\,\mathrm{CO_2} + 0.43\,\mathrm{H_2}\end{aligned} \tag{1.3}$$

By the mixed acid fermentation, glucose is converted to lactate ($\mathrm{H_3C{-}CHOH{-}COO^-}$), acetate ($\mathrm{H_3C{-}COO^-}$), ethanol ($\mathrm{H_3C{-}CH_2OH}$), succinate ($\mathrm{(OOC{-}CH_2{-}CH_2{-}COO)^{2-}}$), formate ($\mathrm{HCOO^-}$) and carbon dioxide. The standard Gibbs free energy is about $\Delta G'^{\circ} = -208\,\mathrm{kJ\,mol^{-1}}$ [74], thus the mixed acid fermentation yields about $10\,\mathrm{kJ\,mol^{-1}}$ more energy than the lactic acid fermentation.

The nutrient- or product-concentration changes in the micro-environment of the microorganisms could be analysed by (bio-)chemical sensors. There are two parameters that are frequently used in cell-based biosensors: The change of the $\mathrm{O_2}$ concentration

[54, 59] to monitor the respiration[3] or the extracellular pH-value changes [22–25, 34, 52, 54, 60–73]. The pH-value changes resulting from the extracellular acidification[4] can be determined in a reliable way by means of pH-sensitive field-effect sensors, e.g., the ISFET or LAPS. Usually, the end products of the metabolic pathway of microorganisms are organic acids that lead to the extracellular acidification and thus, to a measurable pH-value change. The amount of pH-value change depends on the amount of acids excreted by the cells, the dissociation of these acids in the surrounding media and the strength of the pH buffer. Thus, under same conditions of number of cells, nutrient concentration and pH-buffer strength, the pH-value change correlates with the metabolic activity.

The extracellular acidification is determined in small volumes by measuring the time-varying pH value between periodical changes of the measurement medium. The duration for the measurement of the time-varying pH value should be short, in order to avoid high pH-value changes that will reduce the metabolic activity of the cells. Typically, low pH-buffered measurement media with a buffer capacity of about $1\,\mathrm{mmol\,l^{-1}}$ are used to achieve measurable pH changes. Since mammalian cells usually produce about $10^8\,H^+\,s^{-1}$ per cell, Owicki *et al.* [63] suggest a cell concentration on the sensor of about $10^6\,\mathrm{cells\,ml^{-1}}$, depending on the uncertainty of time-varying pH measurements of the used sensor.

1.3.2 Immobilisation of living cells

In order to determine cellular signals with electrochemical sensors it is necessary to locate the living cells near the sensor surface. By means of immobilisation the cells should be attached to the sensor surface in a way they stay alive. This way, changing of the measurement medium would be possible without (or only little) loss of cells. Ideally, the immobilisation should have no effect to the cellular activity of the organisms and should provide a high degree of covering. The number of cells on the sensor surface should be kept at an optimal value in order to obtain measurable signals. To achieve an optimal supply by substrates to the cells, the thickness of the immobilisation layer should be as thin as possible. There are different immobilisation methods for living cells, like adherent growing, covalent binding, entrapment and encapsulation (see Fig. 1.4) [75, 76].

Adherent growing is the simplest method, as long as the cells will grow adherent on the sensor surface and will ideally building a continuous cell layer. The forces involved are mostly electrostatic such as van der Waals forces, ionic or hydrogen bonding interactions [76]. However, by this method, the cells are not protected and cell losses due to shear forces induced by e.g., high flow rates should be considered.

[3] or the O_2 production of plant cells to monitor their photosynthesis.
[4] or alkalisation, if cells consume more acids (e.g., volatile fatty acids) then they produce.

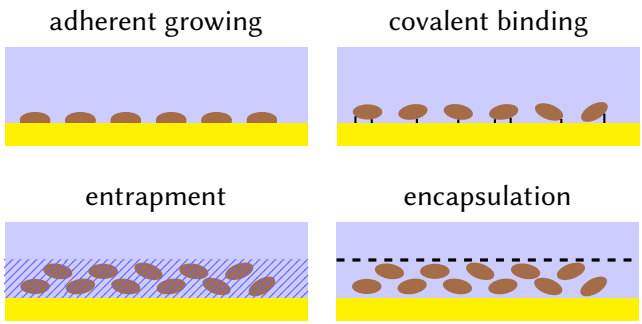

Figure 1.4: Different immobilisation methods to attach living cells to the sensor surface. With adherent growing, the cells grow immediately on the sensor surface. With covalent binding, cross-linker molecules between the cells and the sensor surface are used. With the entrapment method, the cells are embedded in a matrix (e.g., a gel layer) on the sensor surface. With the encapsulation method, the cells are captured under a semipermeable membrane.

By means of coatings with e.g., collagen A or fibronectin, adherent growing can be achieved for some mammalian cells [77]. Furthermore, it was shown that neuronal cells preferably grow on special micro-structures and porous surfaces [23, 78, 79].

Another method is the covalent binding, which involves the formation of covalent bonds between the cells and the sensor surface [76]. The bonds are formed between functional groups, present on the sensor surface and functional groups on the cell membrane. Reactive chemical groups can be formed by e.g., previous plasma treatments of the sensor surface [80].

Instead of binding cells directly to the sensor surface, they could also be immobilised by embedding them in a matrix on the sensor surface. The entrapment method is preferably used, if the cells are not growing adherent, like many bacteria [81]. The matrices are typically gels (e.g., agarose, alginate or polyacrylamide) or natural biofilms [81–84]. Cells are freely distributed in the gel layer, but restricted in movement by the lattice structure of the gel. The porosity of the gel lattice has to be controlled to ensure that the structure is tight enough to prevent leakage of cells, yet at the same time allowing free movement of the substrate and products [76]. By utilising gel entrapment, the cell density can be controlled and the cells embedded in the gel are protected against leakage and against contamination of other cells. Disadvantageously, it must be mentioned that some substances, necessary to form the gel, may have a toxic effect and thus, can reduce the cellular activity of the immobilised cells. Furthermore, with the gel-entrapment method, the cells are not directly linked to the sensor surface, which makes it impractical to analyse morphology changes of cells by impedance measurements or to determine extracellular potentials.

The encapsulation method is similar to entrapment. With the help of a semipermeable membrane, a separate compartment with cells is formed on top of the sensor [76]. The semipermeable membrane protects the cells against leakages, thus the pore sizes of the membrane must be smaller than the cell sizes but big enough to enable the transport of metabolites and products.

The immobilisation could act as a barrier to the mass transfer. This can have a significant influence on the reaction kinetics, especially by using the entrapment or encapsulation method. This phenomenon also occurs related to enzyme-based biosensors, where the enzymes are immobilised on the sensor surface. Usually, theses enzyme-based sensors are driven in diffusion limitation. The resulting measurement signal is in this case depending on the analyte concentration [85–88]. If the biosensor is designed in a way that the reaction kinetic is diffusion-limited, then an equilibrium between substrate delivery to the enzyme layer and product delivery to the bulk solution will occur and the product concentration on the sensor surface will become a function of the substrate concentration. In this case, the product to be determined is the H^+-ion concentration or in other words, the pH value, the measurement value also depends on the pH-buffer capacity of the test solution.

In reference [88] a mathematical model is described, which includes several phenomena that occur related to enzyme-potentiometric biosensors utilising a pH-sensitive membrane. In principle, these can also occur in case of cell-based sensors, where the change of the pH value is analysed and the cell layer acts as a barrier to the mass transfer. The model in reference [88] takes the following considerations into account:

- The enzymes are immobilised on the sensor surface and the sensor will analyse the pH value on the interface enzyme layer/sensor surface.
- The substance from the test solution (e.g., substrate and pH-buffering agents) diffuses into the enzyme layer. Inside the enzyme layer, the analyte will be irreversibly converted by the enzymatic reaction into acids and/or bases.
- The catalytic activity of the enzymes is sensitive to the pH value of their environment.
- The produced acids and/or bases dissociate, in most cases, only partially within the pH range of their environment. In addition, the dissociated H^+ and/or OH^- ions can be covered by the buffering agents.
- The products diffuse to the sensor surfaces and back to the test solution. Thus, together with the buffering agents, the H^+ ions have an alternate diffusion path.
- Inside the enzyme layer, all substances will form concentration profiles. Especially, the pH-value gradient leads to a spatial variation of the enzymatic activity in the enzyme layer and a spatial variation of the dissociation.
- When a steady state is reached, time-invariant concentration profiles of the analyte

and products are established in the enzyme layer, and the mass flux of the analyte into the film equals the total mass flux of all the reaction products out of the film.

Under such conditions, the pH value in the enzyme layer on the sensor surface is related to the analyte concentration in the test solution. The conclusions of the model, in case that the reaction kinetic is limited by diffusion, are:

- The response characteristics are strongly affected by the concentration and the dissociation of the buffers present in the test solution, as well as by the dissociation of the acids and bases produced during the enzymatic reaction.
- The sensitivity is not related to the enzymatic activity or amount of enzymes as long as the reaction kinetic is limited by diffusion.

However, this model describes only the behaviour in case of diffusion limitation. If the enzymatic activity of the enzyme layer is rather low, the biosensor begins to saturate at lower concentrations, which in turn implies lower upper detection limits. This model describes the behaviour of an enzyme-based biosensor with pH-sensitive transducer, but the principles can also be transferred to a cell-based biosensor. Thus, driving a cell-based biosensor by analysing the metabolic end products, in diffusion-controlled conditions, it would be possible to be sensitive to the nutrient concentration in the test solution.

1.4 Content of the work

The content of this present thesis can be divided into two parts:

1. Development and characterisation of new LAPS set-ups as well as investigations on the LAPS principle: Chapter 2 to 5.
2. Applications of LAPS as biosensor utilising enzymes and cells: Chapter 5 to 7.

The described LAPS set-ups in this thesis represent further stages of development of the set-ups presented in the thesis of Dr. Torsten Wagner [1]. The last set-up, developed in [1], was the so-called FFT-based LAPS, which utilised a 4×4 infrared light-emitting diode (IR-LED) array [25]. These 16 IR-LEDs could be driven simultaneously at different frequencies and were driven each one by a discrete electrical circuitry as frequency generator. By means of the fast Fourier transform (FFT) algorithm, the amplitude of each excitation frequency was calculated and assigned to the corresponding measurement spot, thus all 16 measurement spots could be read out simultaneously. The LAPS set-up that was built upon the FFT-based LAPS is described in **chapter 2** and utilised a field-programmable gate array (FPGA) to drive the IR-LEDs. The FPGA represents a replacement of the 16 discrete frequency generators, which offers the same features

and in addition, the possibility to drive even more LEDs. This results in a low circuit complexity and more compact measurement instruments. Furthermore, the FPGA-based LAPS offers in addition the possibility to adjust the brightness of each LED individually, which is used in an integrated signal correction mode to e.g., equalise the light brightness of each LED.

Since the LAPS structures are EIS structures, they also could be read out like a capacitive EIS sensor. To do so, a measurement mode for determining the electrical impedance of the LAPS structure was added to the FPGA-based LAPS (see **chapter 3**). Furthermore, the possibility to measure the phase shift of the photocurrent was implemented. Thus, it was possible to measure the frequency behaviour of the LAPS and its impact on amplitude and phase shift of the photocurrent for the first time. The impedance and frequency-behaviour measurements were compared to each other with the help of electrical equivalent circuitries. These measurements help to understand the LAPS principles and frequency-depending parameters of LAPS structures in more detail.

To record high-resolution chemical images, it is advantageous to use more than 16 measurement spots, and thus to improve the lateral resolution. This was demonstrated, in **chapter 4** by adapting a commercially available OLED display with 96×64 pixels and a pixel size of $200\,\mu m \times 200\,\mu m$ as light source. Thus, this OLED display allows an over 16 times higher resolution compared to the IR-LED array of the FPGA-based LAPS set-up. One main aspect of the development of the OLED-based LAPS was to ensure that the excitation frequency of the OLED-display pixels is in an optimal range for LAPS measurements. Therefore, a new developed driving method for the OLED display optimised for LAPS-based measurements is demonstrated. The new method enables to define modulation frequencies between 1 kHz and 16 kHz and hence, reduces the measurement time of a chemical image by a factor of 40 compared to the traditional addressing of an OLED display. Furthermore, section 4.5.1 describes an additionally implemented scanning-LAPS set-up that utilises a movable laser diode. This scanning-LAPS set-up was used to characterise the physical limitation of the lateral resolution of the LAPS chips.

To observe dynamic chemical processes, e.g., diffusion of analytes, chemical reactions or cellular signals it is necessary to have a high refreshing rate of those chemical images. A measurement at a speed of 5 frames per second was realised with the FPGA-based LAPS by using the constant-voltage mode. This is described in **chapter 5** and in addition, a comparison of the FPGA-based LAPS and a CCD-based imaging sensor was done. **Chapter 5** compares both mentioned imaging sensors as acetylcholine-sensitive sensors utilising an enzymatic layer of acetylcholinesterase as a possible application for biosensors.

In **chapter 6** and **chapter 7**, the FPGA-based LAPS is used as whole cell-based biosensor. The primary intention of these experiments was to demonstrate the usage of this type of biosensor for monitoring and controlling biogas digesters. Therefore, the metabolic activity of microorganisms was determined, in order to get an information about their "welfare" during the biogas process and hence, to be able to control the biogas digester. With the help of the pH-sensitive LAPS chip, the extracellular acidification was determined under anaerobic conditions. An immobilisation protocol based on polyacrylamide has been developed to immobilise the microorganisms on the sensor surface. With the help of addressability of the LAPS an on-chip differential set-up was developed. Thus, external influences such as sensor drift, temperature and external pH changes can be minimised. **Chapter 6** describes the immobilisation and discusses the acidification measurements of *E. coli* in suspension and after immobilisation using culture medium. In **chapter 7**, the nutrient-concentration sensitivity of this biosensor in terms of glucose sensing is demonstrated for the first time. Furthermore, the functional principle of this new set-up is discussed and can be compared with enzyme-based field-effect sensors using diffusion limitation.

References

[1] T. Wagner. "Lichtadressierbare potentiometrische Sensoren für den Einsatz in der Pharmazie". German. PhD thesis. Philipps-Universität Marburg, 2008.

[2] C. Jimenez-Jorquera, J. Orozco, and A. Baldi. "ISFET based microsensors for environmental monitoring". In: *Sensors* 10.1 (2009), pp. 61–83. DOI: 10.3390/s100100061.

[3] P. Bergveld. "Development of an ion-sensitive solid-state device for neurophysiological measurements". In: *IEEE Transactions on Biomedical Engineering* BME-17.1 (1970), pp. 70–71. DOI: 10.1109/TBME.1970.4502688.

[4] S. M. Sze. *Physics of Semiconductor Devices*. 2nd ed. New York: John Wiley & Sons, 1981.

[5] A. Poghossian and M. J. Schöning. "Silicon-based chemical and biological field-effect sensors". In: *Encyclopedia of Sensors*. Ed. by C. A. Grimes, E. C. Dickey, and M. V. Pishko. Vol. X. Santa Clarita, California, USA: American Scientific Publishers, 2006, pp. 1–71.

[6] D. E. Yates, S. Levine, and T. W. Healy. "Site-binding model of the electrical double layer at the oxide/water interface". In: *Journal of the Chemical Society, Faraday Transactions 1: Physical Chemistry in Condensed Phases* 70 (1974), pp. 1807–1818. DOI: 10.1039/F19747001807.

[7] M. Grattarola, G. Massobrio, and S. Martinoia. "Modeling H^+-sensitive FETs with SPICE". In: *IEEE Transactions on Electron Devices* 39.4 (1992), pp. 813–819. DOI: 10.1109/16.127470.

[8] M.-N. Niu, X.-F. Ding, and Q.-Y. Tong. "Effect of two types of surface sites on the characteristics of Si_3N_4-gate pH-ISFETs". In: *Sensors and Actuators, B: Chemical* 37 (1996), pp. 13–17. DOI: 10.1016/S0925-4005(97)80067-6.

[9] P. Bergveld. "Future applications of ISFETs". In: *Sensors and Actuators B: Chemical* 4.1–2 (1991), pp. 125–133. DOI: 10.1016/0925-4005(91)80187-0.

[10] M. Klein. "Characterization of ion-sensitive layer systems with a C(V) measurement method operating at constant capacitance". In: *Sensors and Actuators, B: Chemical* 1.1-6 (1990), pp. 354–356. DOI: 10.1016/0925-4005(90)80229-S.

[11] P. Fabry and L. Laurent-Yvonnou. "The C-V method for characterizing ISFET or EOS devices with ion-sensitive membranes". In: *Journal of Electroanalytical Chemistry and Interfacial Electrochemistry* 286.1-2 (1990), pp. 23–40. DOI: 10.1016/0022-0728(90)85062-A.

[12] K. Sawada, S. Mimura, K. Tomita, T. Nakanishi, H. Tanabe, M. Ishida, and T. Ando. "Novel CCD-based pH imaging sensor". In: *IEEE Transactions on Electron Devices* 46.9 (1999), pp. 1846–1849. DOI: 10.1109/16.784183.

[13] K. Sawada, T. Shimada, T. Ohshina, H. Takao, and M. Ishida. "Highly sensitive ion sensors using charge transfer technique". In: *Sensors and Actuators, B: Chemical* 98.1 (2004), pp. 69–72. DOI: 10.1016/j.snb.2003.09.027.

[14] D. G. Hafeman, J. W. Parce, and H. M. McConnell. "Light-addressable potentiometric sensor for biochemical systems". In: *Science* 240.4856 (1988), pp. 1182–1185. DOI: 10.1126/science.3375810.

[15] J. C. Owicki, L. J. Bousse, D. G. Hafeman, G. L. Kirk, J. D. Olson, H. G. Wada, and J. W. Parce. "The light-addressable potentiometric sensor: Principles and biological applications". In: *Annual Review of Biophysics and Biomolecular Structure* 23 (1994), pp. 87–113. DOI: 10.1146/annurev.bb.23.060194.000511.

[16] T. Wagner and M. J. Schöning. "Light-addressable potentiometric sensors (LAPS): recent trends and applications". In: *Electrochemical Sensor Analysis*. Ed. by S. Alegret and A. Merkoci. Vol. 49. Amsterdam: Elesevier, 2007, pp. 87–128.

[17] A. K. Covington. "Terminology and conventions for microelectronic ion-selective field effect transistor devices in electrochemistry (IUPAC Recommendations 1994)". In: *Pure and Applied Chemistry* 66.3 (1994), pp. 565–569. DOI: 10.1351/pac199466030565.

[18] T. Yoshinobu, H. Ecken, A. Poghossian, A. Simonis, H. Iwasaki, H. Lüth, and M. J. Schöning. "Constant-current-mode LAPS (CLAPS) for the detection of penicillin". In: *Electroanalysis* 13.8-9 (2001), pp. 733–736. DOI: 10.1002/1521-4109(200105)13:8/9<733::AID-ELAN733>3.0.CO;2-N.

[19] T. Yoshinobu, T. Harada, and H. Iwasaki. "Application of the pH-imaging sensor to determining the diffusion coefficients of ions in electrolytic solutions". In: *Japanese Journal of Applied Physics* 39.4A (2000), pp. L318–L320. DOI: 10.1143/JJAP.39.L318.

[20] K. Miyamoto, H. Ichimura, T. Wagner, M. J. Schöning, and T. Yoshinobu. "Chemical imaging of the concentration profile of ion diffusion in a microfluidic channel". In: *Sensors and Actuators B: Chemical* 189 (2013), pp. 240–245. DOI: 10.1016/j.snb.2013.04.057.

[21] T. Yoshinobu, H. Iwasaki, Y. Ui, K. Furuichi, Y. Ermolenko, Y. Mourzina, T. Wagner, N. Näther, and M. J. Schöning. "The light-addressable potentiometric sensor for multi-ion sensing and imaging". In: *Methods* 37.1 (2005), pp. 94–102. DOI: 10.1016/j.ymeth.2005.05.020.

[22] M. Nakao, S. Inoue, R. Oishi, T. Yoshinobu, and H. Iwasaki. "Observation of microorganism colonies using a scanning-laser-beam pH-sensing microscope". In: *Journal of Fermentation and Bioengineering* 79.2 (1995), pp. 163–166. DOI: 10.1016/0922-338X(95)94085-6.

[23] T. Yoshinobu, H. Ecken, A. B. M. Ismail, H. Iwasaki, H. Lüth, and M. J. Schöning. "Chemical imaging sensor and its application to biological systems". In: *Electrochimica Acta* 47.1-2 (2001), pp. 259–263. DOI: 10.1016/S0013-4686(01)00564-3.

[24] B. Stein, M. George, H. E. Gaub, J. C. Behrends, and W. J. Parak. "Spatially resolved monitoring of cellular metabolic activity with a semiconductor-based biosensor". In: *Biosensors & Bioelectronics* 18.1 (2003), pp. 31–41. DOI: 10.1016/S0956-5663(02)00109-4.

[25] T. Wagner, R. Molina, T. Yoshinobu, J. P. Kloock, M. Biselli, M. Canzoneri, T. Schnitzler, and M. J. Schöning. "Handheld multi-channel LAPS device as a transducer platform for possible biological and chemical multi-sensor applications". In: *Electrochimica Acta* 53.2 (2007), pp. 305–311. DOI: 10.1016/j.electacta.2007.04.006.

[26] J. R. Siqueira, R. M. Maki, F. V. Paulovich, C. F. Werner, A. Poghossian, M. C. F. de Oliveira, V. Zucolotto, O. N. Oliveira, and M. J. Schöning. "Use of information visualization methods eliminating cross talk in multiple sensing units investigated

for a light-addressable potentiometric sensor". In: *Analytical Chemistry* 82.1 (2010), pp. 61–65. DOI: 10.1021/ac9024076.

[27] T. Hizawa, K. Sawada, H. Takao, and M. Ishida. "Fabrication of a two-dimensional pH image sensor using a charge transfer technique". In: *Sensors and Actuators B: Chemical* 117.2 (2006), pp. 509–515. DOI: 10.1016/j.snb.2006.01.056.

[28] S. Takenaga, Y. Tamai, M. Ishida, and K. Sawada. "Charge accumulation type hydrogen ion image sensor with high pH resolution". In: *Japanese Journal of Applied Physics* 50.2 (2011), p. 027001. DOI: 10.1143/JJAP.50.027001.

[29] B. Nemeth, M. S. Piechocinski, and D. R. Cumming. "High-resolution real-time ion-camera system using a CMOS-based chemical sensor array for proton imaging". In: *Sensors and Actuators B: Chemical* 171–172 (2012), pp. 747–752. DOI: 10.1016/j.snb.2012.05.066.

[30] P. Shields, B. Nemeth, R. Green, M. Riehle, and D. Cumming. "High-speed imaging of 2-D ionic diffusion using a 16x16 pixel CMOS ISFET array on the microfluidic scale". In: *IEEE Sensors Journal* 12.9 (2012), pp. 2744–2749. DOI: 10.1109/JSEN.2012.2200249.

[31] O. Engstrom and A. Carlsson. "Scanned light pulse technique for the investigation of insulator–semiconductor interfaces". In: *Journal of Applied Physics* 54.9 (1983), pp. 5245–5251. DOI: 10.1063/1.332752.

[32] S. Krause, H. Talabani, M. Xu, W. Moritz, and J. Griffiths. "Scanning photo-induced impedance microscopy—an impedance based imaging technique". In: *Electrochimica Acta* 47.13–14 (2002), pp. 2143–2148. DOI: 10.1016/S0013-4686(02)00088-9.

[33] M. George, W. J. Parak, I. Gerhardt, W. Moritz, F. Kaesen, H. Geiger, I. Eisele, and H. E. Gaub. "Investigation of the spatial resolution of the light-addressable potentiometric sensor". In: *Sensors and Actuators, A: Physical* 86.3 (2000), pp. 187–196. DOI: 10.1016/S0924-4247(00)00455-6.

[34] M. Nakao, S. Inoue, T. Yoshinobu, and H. Iwasaki. "High-resolution pH imaging sensor for microscopic observation of microorganisms". In: *Sensors and Actuators B: Chemical* 34.1-3 (1996), pp. 234–239. DOI: 10.1016/S0925-4005(96)01903-X.

[35] W. Moritz, I. Gerhardt, D. Roden, M. Xu, and S. Krause. "Photocurrent measurements for laterally resolved interface characterization". In: *Fresenius' Journal of Analytical Chemistry* 367.4 (2000), pp. 329–333. DOI: 10.1007/s002160000409.

[36] Z. Qintao, W. Ping, W. J. Parak, M. George, and G. Zhang. "A novel design of multi-light LAPS based on digital compensation of frequency domain". In: *Sensors and Actuators, B: Chemical* 73.2-3 (2001), pp. 152–156. DOI: 10.1016/S0925-4005(00)00696-1.

[37] T. Yoshinobu, M. J. Schöning, R. Otto, K. Furuichi, Y. Mourzina, Y. Ermolenko, and H. Iwasaki. "Portable light-addressable potentiometric sensor (LAPS) for multisensor applications". In: *Sensors and Actuators, B: Chemical* 95.1-3 (2003), pp. 352–356. DOI: 10.1016/S0925-4005(03)00437-4.

[38] K. Miyamoto, Y. Kuwabara, S. Kanoh, T. Yoshinobu, T. Wagner, and M. J. Schöning. "Chemical image scanner based on FDM-LAPS". In: *Sensors and Actuators, B: Chemical* 137.2 (2009), pp. 533–538. DOI: 10.1016/j.snb.2008.12.008.

[39] T. Wagner, C. F. Werner, K. Miyamoto, H.-J. Ackermann, T. Yoshinobu, and M. J. Schöning. "FPGA-based LAPS device for the flexible design of sensing sites on functional interfaces". In: *Physica Status Solidi A: Applications and Materials Science* 207.4 (2010), pp. 844–849. DOI: 10.1002/pssa.200983320.

[40] T. Wagner, C. F. Werner, K. Miyamoto, M. J. Schöning, and T. Yoshinobu. "A high-density multi-point LAPS set-up using a VCSEL array and FPGA control". In: *Sensors and Actuators, B: Chemical* 154.2 (2011), pp. 124–128. DOI: 10.1016/j.snb.2010.03.009.

[41] A. Itabashi, N. Kosaka, K. Miyamoto, T. Wagner, M. J. Schöning, and T. Yoshinobu. "High-speed chemical imaging system based on front-side-illuminated LAPS". In: *Sensors and Actuators B: Chemical* 182 (2013), pp. 315–321. DOI: 10.1016/j.snb.2013.03.016.

[42] T. Wagner, C. F. Werner, K. Miyamoto, M. J. Schöning, and T. Yoshinobu. "Development and characterisation of a compact light-addressable potentiometric sensor (LAPS) based on the digital light processing (DLP) technology for flexible chemical imaging". In: *Sensors and Actuators, B: Chemical* 170 (2012), pp. 34–39. DOI: 10.1016/j.snb.2010.12.003.

[43] K. Miyamoto, K. Kaneko, A. Matsuo, T. Wagner, S. Kanoh, M. J. Schöning, and T. Yoshinobu. "Miniaturized chemical imaging sensor system using an OLED display panel". In: *Sensors and Actuators B: Chemical* 170 (2012), pp. 82–87. DOI: 10.1016/j.snb.2011.02.029.

[44] K. Miyamoto, T. Wagner, T. Yoshinobu, S. Kanoh, and M. J. Schöning. "Phase-mode LAPS and its application to chemical imaging". In: *Sensors and Actuators, B: Chemical* 154.1 (2011), pp. 28–32. DOI: 10.1016/j.snb.2009.12.022.

[45] K. Miyamoto, T. Wagner, S. Mimura, S. Kanoh, T. Yoshinobu, and M. J. Schöning. "Constant-phase-mode operation of the light-addressable potentiometric sensor". In: *Sensors and Actuators, B: Chemical* 154.2 (2011), pp. 119–123. DOI: 10.1016/j.snb.2010.01.004.

[46] K. Miyamoto, Y. Sugawara, S. Kanoh, T. Yoshinobu, T. Wagner, and M. J. Schöning. "Image correction method for the chemical imaging sensor". In: *Sensors and Actuators, B: Chemical* 144.2 (2010), pp. 344–348. DOI: 10.1016/j.snb.2008.10.069.

[47] C. Ziegler. "Cell-based biosensors". In: *Fresenius' Journal of Analytical Chemistry* 366.6-7 (2000), pp. 552–559. DOI: 10.1007/s002160051550.

[48] A. M. Aravanis, B. DeBusschere, A. J. Chruscinski, K. H. Gilchrist, B. K. Kobilka, and G. T. Kovacs. "A genetically engineered cell-based biosensor for functional classification of agents". In: *Biosensors and Bioelectronics* 16.7–8 (2001), pp. 571–577. DOI: 10.1016/S0956-5663(01)00171-3.

[49] A. Poghossian, S. Ingebrandt, A. Offenhäusser, and M. J. Schöning. "Field-effect devices for detecting cellular signals". In: *Seminars in Cell & Developmental Biology* 20.1 (2009), pp. 41–48. DOI: 10.1016/j.semcdb.2009.01.014.

[50] J. J. Pancrazio, J. P. Whelan, D. A. Borkholder, W. Ma, and D. A. Stenger. "Development and application of cell-based biosensors". In: *Annals of Biomedical Engineering* 27.6 (1999), pp. 697–711. DOI: 10.1114/1.225.

[51] W. Parak, M. George, J. Domke, M. Radmacher, J. Behrends, M. Denyer, and H. Gaub. "Can the light-addressable potentiometric sensor (LAPS) detect extracellular potentials of cardiac myocytes?" In: *IEEE Transactions on Biomedical Engineering* 47.8 (2000), pp. 1106–1113. DOI: 10.1109/10.855939.

[52] H. Yu, H. Cai, W. Zhang, L. Xiao, Q. Liu, and P. Wang. "A novel design of multifunctional integrated cell-based biosensors for simultaneously detecting cell acidification and extracellular potential". In: *Biosensors & Bioelectronics* 24.5 (2009), pp. 1462–1468. DOI: 10.1016/j.bios.2008.08.045.

[53] I. Giaever and C. R. Keese. "A morphological biosensor for mammalian cells". In: *Nature* 366.6455 (1993), pp. 591–592. DOI: 10.1038/366591a0.

[54] P. Mestres and A. Morguet. "The Bionas technology for anticancer drug screening". In: *Expert Opinion on Drug Discovery* 4.7 (2009), pp. 785–797. DOI: 10.1517/17460440903018840.

[55] H. Yu, J. Wang, Q. Liu, W. Zhang, H. Cai, and P. Wang. "High spatial resolution impedance measurement of EIS sensors for light addressable cell adhesion monitoring". In: *Biosensors and Bioelectronics* 26.6 (2011), pp. 2822–2827. DOI: 10.1016/j.bios.2010.08.032.

[56] I. Karube and K. Nakanishi. "Immobilized cells used for detection and analysis". In: *Current Opinion in Biotechnology* 5.1 (1994), pp. 54–59. DOI: 10.1016/S0958-1669(05)80070-9.

[57] L. Bousse. "Whole cell biosensors". In: *Sensors and Actuators B: Chemical* 34.1–3 (1996), pp. 270–275. DOI: 10.1016/S0925-4005(96)01906-5.

[58] S. Mohri, J. Shimizu, N. Goda, T. Miyasaka, A. Fujita, M. Nakamura, and F. Kajiya. "Measurements of CO_2, lactic acid and sodium bicarbonate secreted by cultured cells using a flow-through type pH/CO_2 sensor system based on ISFET". In: *Sensors and Actuators, B: Chemical* 115.1 (2006), pp. 519–525. DOI: 10.1016/j.snb.2005.10.029.

[59] Y. Eminaga, M. Brischwein, J. Wiest, J. Clauss, S. Becker, and B. Wolf. "Self calibration of a planar dissolved oxygen sensor". In: *Sensors and Actuators B: Chemical* 177 (2013), pp. 785–791. DOI: 10.1016/j.snb.2012.11.104.

[60] J. W. Parce, J. C. Owicki, K. M. Kercso, G. B. Sigal, H. G. Wada, V. C. Muir, L. J. Bousse, K. L. Ross, B. I. Sikic, and H. M. McConnell. "Detection of cell-affecting agents with a silicon biosensor". In: *Science* 246.4927 (1989), pp. 243–247. DOI: 10.1126/science.2799384.

[61] J. W. Parce, J. C. Owicki, and K. M. Kercso. "Biosensors for directly measuring cell affecting agents." In: *Annales de Biologie Clinique (Paris)* 48.9 (1990), pp. 639–641.

[62] H. M. McConnell, J. C. Owicki, J. W. Parce, D. L. Miller, G. T. Baxter, H. G. Wada, and S. Pitchford. "The cytosensor microphysiometer: biological applications of silicon technology". In: *Science* 257.5078 (1992), pp. 1906–1912. DOI: 10.1126/science.1329199.

[63] J. C. Owicki and J. W. Parce. "Biosensors based on the energy metabolism of living cells: The physical chemistry and cell biology of extracellular acidification". In: *Biosensors & Bioelectronics* 7.4 (1992), pp. 255–272. DOI: 10.1016/0956-5663(92)87004-9.

[64] F. Hafner. "Cytosensor Microphysiometer: technology and recent applications". In: *Biosensors & Bioelectronics* 15.3-4 (2000), pp. 149–158. DOI: 10.1016/S0956-5663(00)00069-5.

[65] M. Sole, N. Rius, and J. G. Loren. "Rapid extracellular acidification induced by glucose metabolism in non-proliferating cells of *Serratia marcescens*". In: *International microbiology* 3.1 (2000), pp. 39–43. URL: http://revistes.iec.cat/index.php/IM/article/view/4c457c0c4ac46.002.

[66] M. Lehmann, W. Baumann, M. Brischwein, R. Ehret, M. Kraus, A. Schwinde, M. Bitzenhofer, I. Freund, and B. Wolf. "Non-invasive measurement of cell membrane associated proton gradients by ion-sensitive field effect transistor arrays for microphysiological and bioelectronical applications". In: *Biosensors & Bioelectronics* 15.3-4 (2000), pp. 117–124. DOI: 10.1016/S0956-5663(00)00065-8.

[67] M. L. Pourciel-Gouzy, W. Sant, I. Humenyuk, L. Malaquin, X. Dollat, and P. Temple-Boyer. "Development of pH-ISFET sensors for the detection of bacterial activity". In: *Sensors and Actuators, B: Chemical* 103.1-2 (2004). The 17th Euopean Conference on Solid-State Transducers, University of Minho, Guimares, Portugal, September 21-24, 2003, pp. 247–251. DOI: 10.1016/j.snb.2004.04.056.

[68] M. Lehmann and W. Baumann. "New insights into the nanometer-scaled cell-surface interspace by cell-sensor measurements". In: *Experimental Cell Research* 305.2 (2005), pp. 374–382. DOI: 10.1016/j.yexer.2005.01.014.

[69] F. Bettaieb, L. Ponsonnet, P. Lejeune, H. B. Ouada, C. Martelet, A. Bakhrouf, N. Jaffrézic-Renault, and A. Othmane. "Immobilization of *E. coli* bacteria in three-dimensional matrices for ISFET biosensor design". In: *Bioelectrochemistry* 71.2 (2007), pp. 118–125. DOI: 10.1016/j.bioelechem.2007.02.004.

[70] M. Castellarnau, N. Zine, J. Bausells, C. Madrid, A. Juárez, J. Samitier, and A. Errachid. "Integrated cell positioning and cell-based ISFET biosensors". In: *Sensors and Actuators, B: Chemical* 120.2 (2007), pp. 615–620. DOI: 10.1016/j.snb.2006.01.057.

[71] M. Castellarnau, N. Zine, J. Bausells, C. Madrid, A. Juarez, J. Samitier, and A. Errachid. "ISFET-based biosensor to monitor sugar metabolism in bacteria". In: *Materials Science & Engineering, C: Biomimetic and Supramolecular Systems* 28.5-6 (2008), pp. 680–685. DOI: 10.1016/j.msec.2007.10.074.

[72] N. Hu, D. Ha, C. Wu, J. Zhou, D. Kirsanov, A. Legin, and P. Wang. "A LAPS array with low cross-talk for non-invasive measurement of cellular metabolism". In: *Sensors and Actuators A: Physical* 187 (2012), pp. 50–56. DOI: 10.1016/j.sna.2012.08.023.

[73] N. Hu, C. Wu, D. Ha, T. Wang, Q. Liu, and P. Wang. "A novel microphysiometer based on high sensitivity LAPS and microfluidic system for cellular metabolism study and rapid drug screening". In: *Biosensors and Bioelectronics* 40.1 (2013), pp. 167–173. DOI: 10.1016/j.bios.2012.07.010.

[74] G. Fuchs and H. Schlegel. *Allgemeine Mikrobiologie*. German. 8th ed. Stuttgart: Georg Thieme Verlag, 2006.

[75] K. Nilsson. "Methods for immobilizing animal cells". In: *Trends in Biotechnology* 5.3 (1987), pp. 73–78. DOI: DOI:10.1016/S0167-7799(87)80015-X.

[76] G. F. Bickerstaff. "Immobilization of enzymes and cells: Some practical considerations". In: *Immobilization of enzymes and cells*. Ed. by G. F. Bickerstaff. Vol. 1. Methods in Biotechnology. Totowa, New Jersey: Humana Press, 1997, pp. 1–11. DOI: 10.1385/0-89603-386-4:1.

[77] I. Hirata, H. Iwata, A. M. Ismail, H. Iwasaki, T. Yukimasa, and H. Sugihara. "Surface modification of Si_3N_4-coated silicon plate for investigation of living cells". In: *Japanese Journal of Applied Physics* 39.11 (2000), pp. 6441–6442. DOI: 10.1143/JJAP.39.6441.

[78] S. Bayliss, L. Buckberry, I. Fletcher, and M. Tobin. "The culture of neurons on silicon". In: *Sensors and Actuators A: Physical* 74.1–3 (1999), pp. 139–142. DOI: 10.1016/S0924-4247(98)00346-X.

[79] P. Heiduschka, I. Romann, H. Ecken, M. J. Schöning, W. Schuhmann, and S. Thanos. "Defined adhesion and growth of neurones on artificial structured substrates". In: *Electrochimica Acta* 47.1-2 (2001), pp. 299–307. DOI: 10.1016/S0013-4686(01)00573-4.

[80] K. S. Siow, L. Britcher, S. Kumar, and H. J. Griesser. "Plasma methods for the generation of chemically reactive surfaces for biomolecule immobilization and cell colonization – a review". In: *Plasma Processes and Polymers* 3.6-7 (2006), pp. 392–418. DOI: 10.1002/ppap.200600021.

[81] S. Fukui and A. Tanaka. "Immobilized microbial cells". In: *Annual Review of Microbiology* 36.1 (1982), pp. 145–172. DOI: 10.1146/annurev.mi.36.100182.001045.

[82] K. Nilsson, S. Birnbaum, S. Flygare, L. Linse, U. Schröder, U. Jeppsson, P.-O. Larsson, K. Mosbach, and P. Brodelius. "A general method for the immobilization of cells with preserved viability". In: *Applied Microbiology and Biotechnology* 17.6 (1983), pp. 319–326. DOI: 10.1007/BF00499497.

[83] K.-D. Vorlop, A. Muscat, and J. Beyersdorf. "Entrapment of microbial cells within polyurethane hydrogel beads with the advantage of low toxicity". In: *Biotechnology Techniques* 6.6 (1992), pp. 483–488. DOI: 10.1007/BF02447818.

[84] A. C. Jen, M. C. Wake, and A. G. Mikos. "Review: Hydrogels for cell immobilization". In: *Biotechnology and Bioengineering* 50.4 (1996), pp. 357–364. DOI: 10.1002/(SICI)1097-0290(19960520)50:4<357::AID-BIT2>3.0.CO;2-K.

[85] S. D. Caras, J. Janata, D. Saupe, and K. Schmitt. "pH-based enzyme potentiometric sensors. Part 1. Theory". In: *Analytical Chemistry* 57.9 (1985), pp. 1917–1920. DOI: 10.1021/ac00286a027.

[86] S. D. Caras, D. Petelenz, and J. Janata. "pH-based enzyme potentiometric sensors. Part 2. Glucose-sensitive field effect transistor". In: *Analytical Chemistry* 57.9 (1985), pp. 1920–1923. DOI: 10.1021/ac00286a028.

[87] S. D. Caras and J. Janata. "pH-based enzyme potentiometric sensors. Part 3. Penicillin-sensitive field effect transistor". In: *Analytical Chemistry* 57.9 (1985), pp. 1924–1925. DOI: 10.1021/ac00286a029.

[88] S. O. Ogundiran, S. Varanasi, and E. Ruckenstein. "Modeling of enzyme-potentiometric sensors involving acid- or base-forming reactions". In: *Biotechnology and Bioengineering* 37.2 (1991), pp. 160–176. DOI: 10.1002/bit.260370209.

2 Field-programmable gate array based controller for multi-spot LAPS with integrated signal correction mode

Carl Frederik Werner[a,b], Sebastian Schusser[a,b], Heiko Spelthahn[a,b], Torsten Wagner[c], Tatsuo Yoshinobu[c], Michael J. Schöning[a,b]

[a] *Institute of Nano- and Biotechnologies, Aachen University of Applied Sciences, Jülich, Germany*
[b] *Institute of Bio- and Nanosystems (IBN-2), Research Centre Jülich, Jülich, Germany*
[c] *Department of Biomedical Engineering, Tohoku University, Sendai, Japan*

Published in: *Electrochimica Acta*, Vol. 56, pp. 9656–9660, DOI: 10.1016/j.electacta.2011.03.012

Submitted: 2010-11-19; Accepted: 2011-03-03; Published: 2011-03-11

Abstract:

A light-addressable potentiometric sensor (LAPS) can measure the concentration of one or several analytes at the sensor surface simultaneously in a spatially resolved manner. A modulated light pointer stimulates the semiconductor structure at the area of interest and a responding photocurrent can be read out. By simultaneous stimulation of several areas with light pointers of different modulation frequencies, the read out can be performed at the same time. With the new proposed controller electronic based on a field-programmable gate array (FPGA), it is possible to control the modulation frequencies, phase shifts, and light brightness of multiple light pointers independently and simultaneously. Thus, it is possible to investigate the frequency response of the sensor, and to examine the analyte concentration by the determination of the surface potential with the help of current/voltage curves and phase/voltage curves. Additionally, the ability to individually change the light intensities of each light pointer is used to perform signal correction.

Zusätzliche Information für die Gutachter: Dieses Kapitel basiert teilweise auf Arbeiten aus meiner Diplomarbeit (Programmierung des VHDL Codes). Allerdings wurde hier der Code für einen andern FPGA eines anderen Herstellers umgeschrieben, sowie die Möglichkeit implementiert, zusätzlich die Phasenverschiebung des Fotostroms zu bestimmen.

2.1 Introduction

A light-addressable potentiometric sensor (LAPS) is a potentiometric semiconductor-based chemical sensor. It is used to determine the concentration of an analyte in a liquid solution on the sensor surface in a spatially resolved manner [1–3]. The sensor consists of a semiconductor/insulator/transducer-layered structure, which is in contact with the analyte solution (Figure 2.1). An external bias voltage V_{bias} is applied between the rear-side contact and the electrolyte with the help of a reference electrode. This bias voltage generates a depletion region inside the semiconductor, which is affected by the surface potential, generated at the transducer/electrolyte interface depending on the concentration of the analyte. With the help of a modulated light source, a photocurrent I_{ph} is generated. The amplitude and the phase of the photocurrent depends on the width of the local depletion region and hence, on the local concentration of the analyte at the sensor surface. This technique allows electrochemical, spatially resolved measurements e.g., for chemical images [4, 5], detection of multiple analytes with the help of different modified transducer layers [5, 6], or determination of the metabolic activity of microorganisms by investigation of the local acidification rate [2, 6–8].

Usually, lasers or light-emitting diodes (LEDs) are utilised as light sources. Two different measurement methods are introduced: The sensor structure is scanned by a moving single light source in a raster-like manner [7] or an array of light sources define a fixed array of measurement spots [6, 9, 10]. The combination of both methods is presented in [11]. By using an array of light sources, the measurement spots, defined by the illuminated area, can be read out concurrently, by modulating each light source with a different frequency. Subsequently, the frequency components of the resulting photocurrent can be separated [6, 9, 10] e.g., with a fast Fourier transform (FFT) algorithm. For a large number of light sources, however, a set-up consisting of individual frequency generators becomes difficult and expensive.

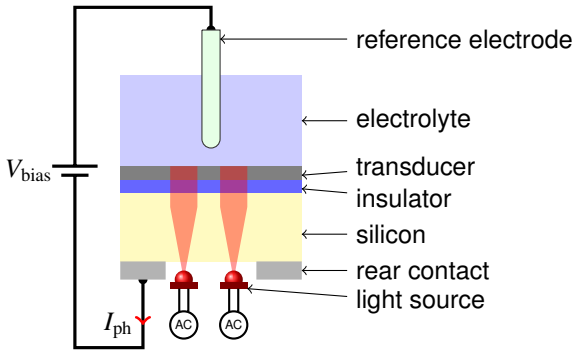

Figure 2.1: Schematic drawing of the LAPS principle.

In this work, the authors introduce a field-programmable gate array (FPGA) as a new method to address a light-addressable potentiometric sensor. In this case, the frequency generators synthesised in the FPGA and the light sources can be contacted directly to the high number of available general purpose input/output (GPIO) pins. By this, a limitation to a certain number of light sources is no more given.

With this FPGA implementation, it is possible to configure the frequency, amplitude, offset and starting phase of the modulation signal individually for each light source. The adjustment of the amplitude of the modulated signal enables to control the light brightness and hence, create the possibility to compensate for variations in brightness due to manufacturing tolerances of the LEDs, frequency behaviour of the photocurrent, tilt between the light-source array and the sensor chip and defects in the semiconductor substrate, as described in [12]. Therefore, a method is introduced to adjust the light brightness of each light source. This new signal correction mode can be applied to the beginning of a measurement cycle for correction of systematically introduced errors.

2.2 Experimental

2.2.1 LAPS set-up

The light-source array consists of a 4×4 infrared-LED array, with a wavelength of $\lambda = 950\,\mathrm{nm}$. The illuminated area of a single infrared LED (measurement spot) is a circle with 2 mm in diameter. The LAPS chip has a size of $2\,\mathrm{cm} \times 2\,\mathrm{cm}$ from which an area of $1.5\,\mathrm{cm} \times 1.5\,\mathrm{cm}$ is in contact with the electrolyte. The LAPS chip consists of thin films of: 60 nm Ta_2O_5, 30 nm SiO_2, 450 µm *p*-doped silicon with 1–10 Ω cm and 300 nm Al for the rear-side contact. The LED array illuminates the silicon from the rear side where the Al is partially removed. A Ag/AgCl-reference electrode from Mettler Toledo is used for the contact to the analyte solution. More information about the LAPS set-up can be found in [6].

A self-made transimpedance amplifier with an amplification factor of $10^6\,\mathrm{V\,A^{-1}}$ is used to amplify the photocurrent and a data-acquisition card (DAQmx PCI-6259 from National Instruments) is used to record the amplified photocurrent and to produce the bias voltage. The photocurrent was sampled with 10^6 samples/s, controlled by a sample clock provided by the FPGA. Final data processing is performed by a self-made software which is written in LabVIEW (National Instruments). Figure 2.2 depicts the signal paths of the LAPS set-up.

2.2.2 FPGA program

To control the 16 infrared LEDs, a FPGA Spartan 3A (XC3S400A) from Xilinx was programmed in very high-speed integrated circuit hardware description language (VHDL). The VHDL code was similar to that described in [11], with the additional ability to configure the starting phase shift. A trigger signal synchronised all frequency generators.

For each infrared LED a signal generator is implemented and synthesised in the FPGA. Each frequency generator generates a square wave (Figure 2.3a) at the configured frequency by dividing the internal clock signal. The generated square wave controls

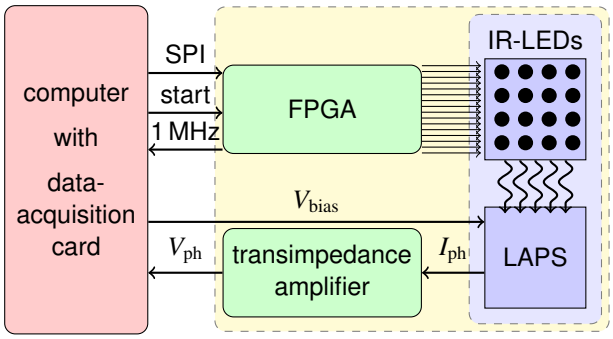

Figure 2.2: Schematic drawing of the presented LAPS set-up with PC, FPGA, light sources, LAPS structure, transimpedance amplifier and data-acquisition card.

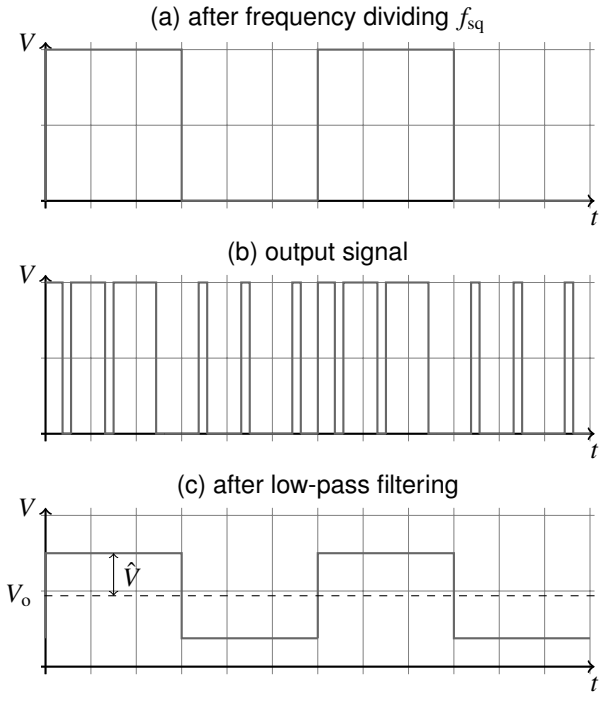

Figure 2.3: Generated signals to modulate the light brightness. The clock signal is divided to the specified frequency (a). With this signal the input of a PDM is changed between two values and two different PDM signals are periodically generated (b). A low-pass filtering of this signal results in a square wave with the specified frequency, amplitude $\hat{V}$ and offset V_o (c).

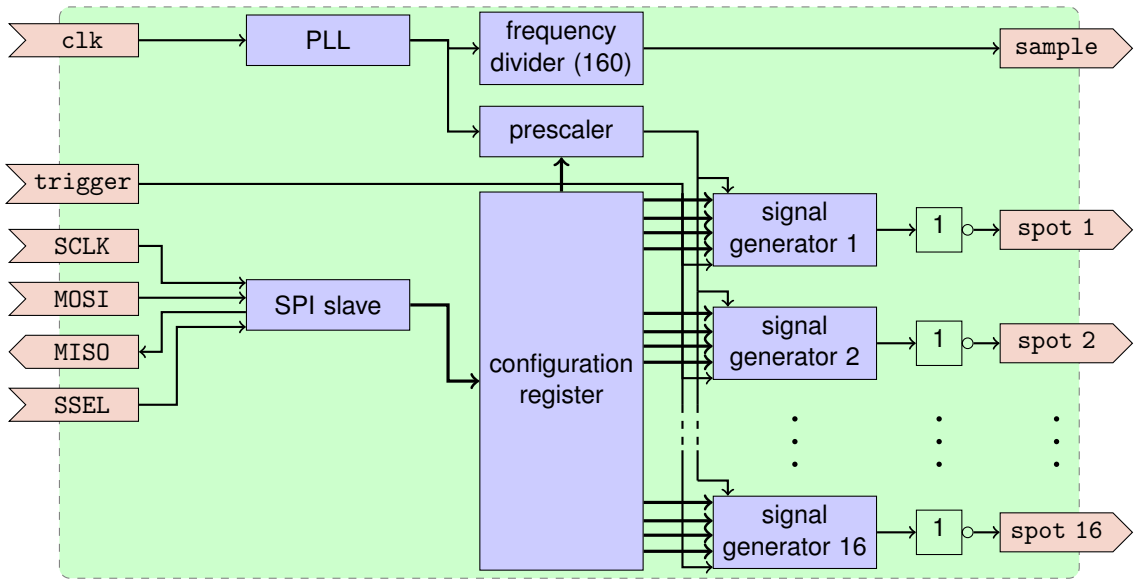

Figure 2.4: Sketch of the architecture of the FPGA. For each infrared LED a signal generator is implemented in the FPGA. Via the SPI interface the parameters (frequency, starting phase and brightness values) of each signal generator can be configured separately during run time.

the selection of one of two pulse-density modulator (PDM) signals (Figure 2.3b). The selected PDM signal, with a minimal pulse length of 12.5 ns, is directly applied to one GPIO of the FPGA, at which the infrared LED in series to a resistor is connected. Applying a low-pass filter results in a signal with the configured modulation frequency, amplitude and offset as depicted in Figure 2.3c. Due to the band-pass filtering characteristic of the LAPS chip itself (as shown in [9, 13, 14]) an additional low-pass filter is not necessary.

The parameters (frequency, starting phase and both PDM values) for each signal generator can be configured during run time via the implemented serial peripheral interface (SPI). The divider and the starting phase are 16 bit long registers, the PDM registers are 10 bit long. These parameters are stored in the configuration register and are assigned to the signal generators. Figure 2.4 shows the architecture of the VHDL code. A phase-locked loop (PLL) generates the main clock of 160 MHz used by the entire design as reference clock. A configureable prescaler reduced the main clock frequency for the frequency generators. By this way, modulating frequencies between 5 mHz and 40 MHz can be generated. That is, for a prescaler of two, the clock signal for the signal generators is 80 MHz, which will be divided by each generator by a value between 2 and 131 072. Therewith, frequencies between 40 MHz and 610 Hz can be generated. At 1 kHz there is a resolution of 12.5 mHz. With the help of an additional frequency divider with a constant value of 160 the main clock is divided to a 1 MHz

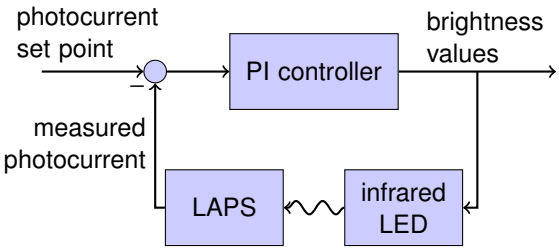

Figure 2.5: Control loop for the brightness control. The photocurrent set point is given by the user or calculated by an average of all measurement spots. This loop is started for each measurement spot to determine the brightness values.

signal, that is utilised as a sampling signal. A trigger input is used to start all signal generators at the same time.

2.2.3 Brightness control

With the brightness-control mode the brightness of each infrared LED can be automatically determined, to equalise all the resulting photocurrents of all measurement spots with respect to a defined bias voltage. At the beginning of a measurement series, this mode has to be run under equal and steady calibration conditions for each measurement spot. The resulting brightness value for each infrared LED can be saved and used for the subsequent measurements.

This mode is realised by a controller loop, presented in Figure 2.5. After the selection of the frequency of each infrared LED and the bias voltage at which the photocurrents should be measured, the photocurrent set point can be set manually or is calculated by the average photocurrent of all measurement spots. After that, the control loop is performed for each measurement spot successively until the brightness value is determined for each measurement spot. The determined brightness values can be stored for future measurements.

2.3 Results and discussion

2.3.1 Frequency response

With regard to validating the new system, the frequency response of a LAPS structure was measured for pH values between pH 5 and pH 9. The bias voltage was set at $V_{\text{bias}} = -0.5\,\text{V}$ in the depletion region. The current/voltage curve and the phase/voltage curve will be shifted along the horizontal axis corresponding to the electrochemical potential at the electrolyte/insulator interface. Infrared LED number 9 out of an array of 16 LEDs was modulated within minimum and maximum brightness. Each decade of

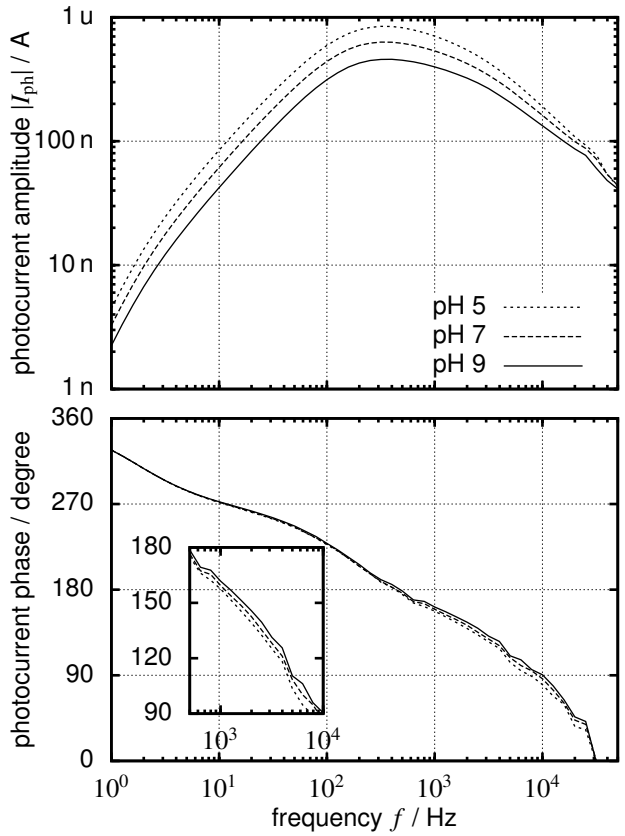

Figure 2.6: Measured amplitude (top) and phase (bottom) of a LAPS structure at pH values of pH 5, pH 7 and pH 9 at different modulation frequencies. The bias voltage was set to $V_{\text{bias}} = -0.5\,\text{V}$ (depletion region). The inlet shows details of the phase in the region of 1 kHz.

frequency was measured by 10 data points. The frequency-response behaviour of the transimpedance amplifier is not compensated, and hence, a phase shift of 180° is added by it, because of the inverting amplifier characteristic.

The results, summarised in Figure 2.6, show a typical band-pass characteristic of a LAPS structure [9, 13, 14] with reduced sensitivity at frequencies above 4 kHz and maximum photocurrents at 400 Hz. In the phase mode, the shift of the phase instead of the amplitude is analysed, described in [15, 16], a higher sensitivity can be found at frequencies around 1 kHz. Hence, subsequent measurements were performed using a modulation frequency of 1 kHz.

2.3.2 pH sensitivity

The pH sensitivity was evaluated by measurements of current/voltage curves and phase/voltage curves of pH 5, pH 7 and pH 9 buffer solution. In a first measurement series, only a single LED of the array was modulated at 1 kHz whereas all others were disabled. For each bias voltage, the resulting photocurrent was measured over a period of 100 ms. Amplitude and phase of the measured signal were calculated by means of an FFT for the preset modulation frequency of 1 kHz. Exemplary, the results of measurement spot 1 are depicted in Figure 2.7a.

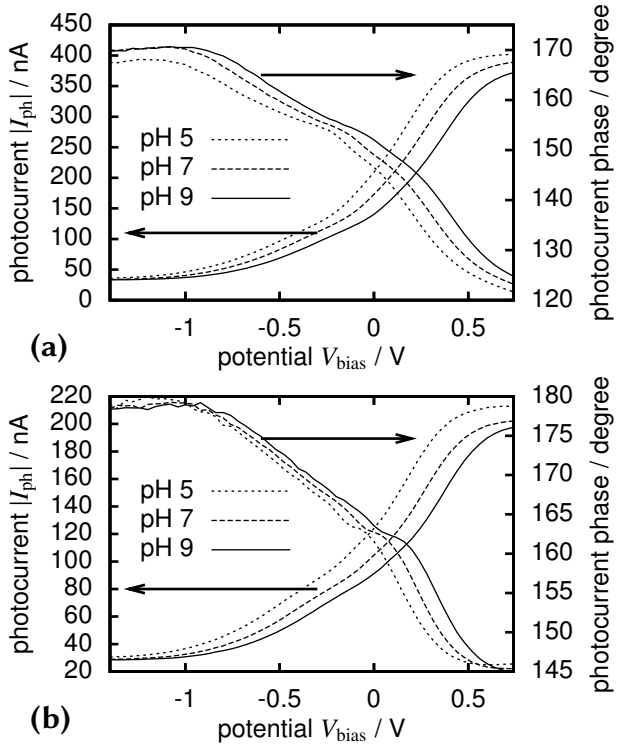

Figure 2.7: Current/voltage and phase/voltage curves of different pH values (pH 5, pH 7 and pH 9) exemplary shown for measurement spot 1 using a single measurement spot modulation at 1 kHz (a). Current/voltage and phase/voltage curve for measurement spot 1 when all other measurement spots are operating simultaneously (b).

In a second series, all 16 measurement spots were modulated concurrently but with different modulation frequencies. Since the FPGA generates signals of square-wave shape, the signal includes second harmonics ($3 \cdot f_0$ and higher). To avoid interferences between the photocurrent of two LEDs, the measurement spot 1 was set to a modulation frequency of 1 kHz and the frequencies of the following measurement spots were increased by 50 Hz, resulting in a modulation of 1.75 kHz for measurement spot 16. The photocurrent was measured for a period of 200 ms and therefore, with a frequency resolution of 5 Hz. The resulting current/voltage and phase/voltage curves at measurement spot 1, when all other measurement spots are illuminated, too, are depicted in Figure 2.7b.

From Figure 2.7, a pH-dependent shift of the photocurrent amplitude and phase can be seen. It is also conspicuous that the amplitude of the photocurrent in case of the concurrent use of all LEDs (Figure 2.7b) is only about 51 % of that in the sequential mode (Figure 2.7a). This might be explained by the increase of the conductance of the space-charge region due to additionally generated charged carriers.

The pH sensitivity of all measurement spots in the concurrent mode was estimated for the current/voltage and the phase/voltage curves. The voltage of the current/voltage and phase/voltage curves of each measured pH value has been determined by a working point of 140 nA and 155°, respectively. Then, the sensitivity has been established by means of linear regression of these voltages against the corresponding pH values.

The sensitivity of the current/voltage mode between pH 5 and pH 9 was calculated to be $(57 \pm 3)\,\mathrm{mV\,pH^{-1}}$, which is close to the theoretical value of $59\,\mathrm{mV\,pH^{-1}}$ and similar to values given in literature [17, 18]. The sensitivity of the phase/voltage mode is $(50.4 \pm 0.6)\,\mathrm{mV\,pH^{-1}}$. Such a reduced sensitivity of the phase shift has also been noted by Miyamoto et al. in [15, 16].

2.3.3 Brightness control

Figure 2.8a depicts the current/voltage curves of all 16 measurement spots measured successively at 1 kHz for pH 7. Typically, the current/voltage curves are diverse, because of several effects to the amplitude of the photocurrent:

- Brightness variations of the infrared LEDs due to manufacturing variances of the used resistors and LEDs.
- Difference in distances or a tilt between the light array and the LAPS structure [19].
- Defects in the semiconductor substrate, as described in [12] as stripe shadows.
- Frequency behaviour of the LAPS (see Figure 2.6) by measurements at different frequencies.

Figure 2.8b depicts the current/voltage curves after the brightness-control method at a bias voltage of −0.25 V. It can be seen, that the current/voltage curves of the 16

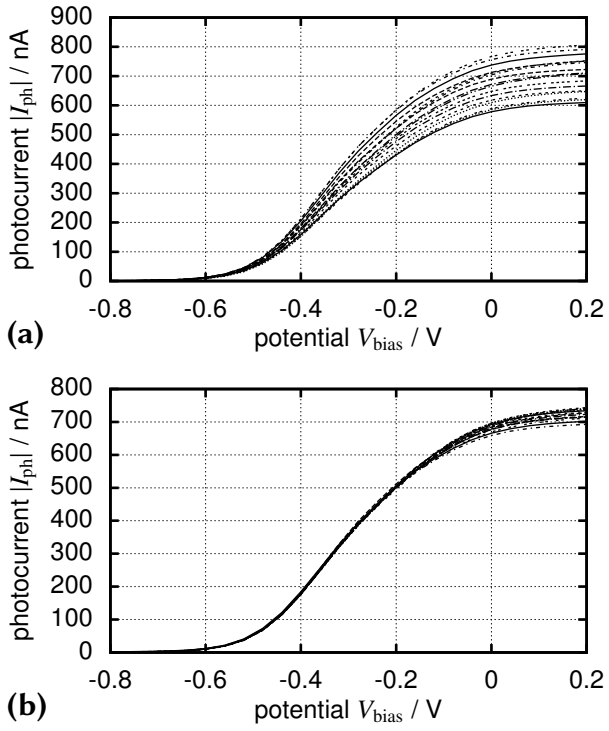

Figure 2.8: Current/voltage curves of all 16 measurement spots measured successively with pH 7. Measurement without calibration of the brightness for all infrared LEDs (a). Measurement after processing the brightness-control method at a bias voltage of −0.25 V (b).

measurements spots are now more equal. Only in the inversion region the curves diverse slightly. This could be an effect of distribution of the flat-band potential [12], which cannot be compensated by the proposed method. By determining the bias voltage at a photocurrent for 500 nA of both measurements, the standard deviation of the determined bias voltage is 41 mV and 2 mV for the measurement without and with brightness-control method, respectively, which would result in a deviation of 0.7 pH and 0.03 pH, for a theoretical sensitivity of 59 mV pH^{-1}.

2.4 Conclusions

A new electronic control unit for LAPS-based chemical sensors using an FPGA has been developed. This technique allows to control the frequency, phase and brightness of each measurement spot of an array of light sources individually and to operate for light sources concurrently. Due to the implementation by an FPGA, it could be easily extended to a larger number of light sources.

The developed system enables to modify modulation parameters during run time, to adapt to a large amount of LAPS structures simultaneously with regard to their individual frequency responses. The new controller technique can perform the well-proven current/voltage as well as the phase/voltage mode, in which the phase shift due to the change of the surface potential is determined. In both modes, concurrent modulation of all light sources of the array at different frequencies is possible.

The brightness control mode was developed and it was demonstrated by characteristics that the current/voltage curves of all measurement spots could be equalised by adjusting the light brightness of each LED.

In further work, this technique can be extended to a larger number of LEDs to distinctly increase the number of sensor spots on the sensor array. Also, an analog-to-digital converter to record the photocurrent and a digital-to-analog converter to produce the bias voltage can be connected to the FPGA to build up an embedded handheld LAPS measurement device for in-field applications.

Acknowledgments

The authors thank the German Federal Ministry of Food, Agriculture and Consumer Protection (BMELV) and the “Fachagentur Nachwachsende Rohstoffe e.V.” (FNR) for financial support of this work (Bio-LAPS).

References

[1] D. G. Hafeman, J. W. Parce, and H. M. McConnell. "Light-addressable potentiometric sensor for biochemical systems". In: *Science* 240.4856 (1988), pp. 1182–1185. DOI: 10.1126/science.3375810.

[2] J. C. Owicki, L. J. Bousse, D. G. Hafeman, G. L. Kirk, J. D. Olson, H. G. Wada, and J. W. Parce. "The light-addressable potentiometric sensor: Principles and biological applications". In: *Annual Review of Biophysics and Biomolecular Structure* 23 (1994), pp. 87–113. DOI: 10.1146/annurev.bb.23.060194.000511.

[3] T. Wagner and M. J. Schöning. "Light-addressable potentiometric sensors (LAPS): recent trends and applications". In: *Electrochemical Sensor Analysis*. Ed. by S. Alegret and A. Merkoci. Vol. 49. Amsterdam: Elesevier, 2007, pp. 87–128.

[4] M. Nakao, T. Yoshinobu, and H. Iwasaki. "Scanning-laser-beam semiconductor pH-imaging sensor". In: *Sensors and Actuators, B: Chemical* 20.2-3 (1994), pp. 119–123. DOI: 10.1016/0925-4005(93)01199-E.

[5] T. Yoshinobu, H. Iwasaki, Y. Ui, K. Furuichi, Y. Ermolenko, Y. Mourzina, T. Wagner, N. Näther, and M. J. Schöning. "The light-addressable potentiometric sensor for multi-ion sensing and imaging". In: *Methods* 37.1 (2005), pp. 94–102. DOI: 10.1016/j.ymeth.2005.05.020.

[6] T. Wagner, R. Molina, T. Yoshinobu, J. P. Kloock, M. Biselli, M. Canzoneri, T. Schnitzler, and M. J. Schöning. "Handheld multi-channel LAPS device as a transducer platform for possible biological and chemical multi-sensor applications". In: *Electrochimica Acta* 53.2 (2007), pp. 305–311. DOI: 10.1016/j.electacta.2007.04.006.

[7] T. Yoshinobu, H. Ecken, A. B. M. Ismail, H. Iwasaki, H. Lüth, and M. J. Schöning. "Chemical imaging sensor and its application to biological systems". In: *Electrochimica Acta* 47.1-2 (2001), pp. 259–263. DOI: 10.1016/S0013-4686(01)00564-3.

[8] B. Stein, M. George, H. E. Gaub, J. C. Behrends, and W. J. Parak. "Spatially resolved monitoring of cellular metabolic activity with a semiconductor-based biosensor". In: *Biosensors & Bioelectronics* 18.1 (2003), pp. 31–41. DOI: 10.1016/S0956-5663(02)00109-4.

[9] Z. Qintao, W. Ping, W. J. Parak, M. George, and G. Zhang. "A novel design of multi-light LAPS based on digital compensation of frequency domain". In: *Sensors and Actuators, B: Chemical* 73.2-3 (2001), pp. 152–156. DOI: 10.1016/S0925-4005(00)00696-1.

[10] K. Miyamoto, Y. Kuwabara, S. Kanoh, T. Yoshinobu, T. Wagner, and M. J. Schöning. "Chemical image scanner based on FDM-LAPS". In: *Sensors and Actuators, B: Chemical* 137.2 (2009), pp. 533–538. DOI: 10.1016/j.snb.2008.12.008.

[11] T. Wagner, C. F. Werner, K. Miyamoto, H.-J. Ackermann, T. Yoshinobu, and M. J. Schöning. "FPGA-based LAPS device for the flexible design of sensing sites on functional interfaces". In: *Physica Status Solidi A: Applications and Materials Science* 207.4 (2010), pp. 844–849. DOI: 10.1002/pssa.200983320.

[12] K. Miyamoto, Y. Sugawara, S. Kanoh, T. Yoshinobu, T. Wagner, and M. J. Schöning. "Image correction method for the chemical imaging sensor". In: *Sensors and Actuators, B: Chemical* 144.2 (2010), pp. 344–348. DOI: 10.1016/j.snb.2008.10.069.

[13] L. Bousse, S. Mostarshed, D. Hafeman, M. Sartore, M. Adami, and C. Nicolini. "Investigation of carrier transport through silicon wafers by photocurrent measurements". In: *Journal of Applied Physics* 75.8 (1994), pp. 4000–4008. DOI: 10.1063/1.356022.

[14] G. Verzellesi, L. Colalongo, D. Passeri, B. Margesin, M. Rudan, G. Soncini, and P. Ciampolini. "Numerical analysis of ISFET and LAPS devices". In: *Sensors and Actuators, B: Chemical* 44.1-3 (1997), pp. 402–408. DOI: 10.1016/S0925-4005(97)00233-5.

[15] K. Miyamoto, T. Wagner, T. Yoshinobu, S. Kanoh, and M. J. Schöning. "Phase-mode LAPS and its application to chemical imaging". In: *Sensors and Actuators, B: Chemical* 154.1 (2011), pp. 28–32. DOI: 10.1016/j.snb.2009.12.022.

[16] K. Miyamoto, T. Wagner, S. Mimura, S. Kanoh, T. Yoshinobu, and M. J. Schöning. "Constant-phase-mode operation of the light-addressable potentiometric sensor". In: *Sensors and Actuators, B: Chemical* 154.2 (2011), pp. 119–123. DOI: 10.1016/j.snb.2010.01.004.

[17] M. J. Schöning, D. Brinkmann, D. Rolka, C. Demuth, and A. Poghossian. "CIP (cleaning-in-place) suitable "non-glass" pH sensor based on a Ta_2O_5-gate EIS structure". In: *Sensors and Actuators B: Chemical* 111–112 (2005), pp. 423–429. DOI: 10.1016/j.snb.2005.03.053.

[18] A. Poghossian and M. J. Schöning. "Silicon-based chemical and biological field-effect sensors". In: *Encyclopedia of Sensors*. Ed. by C. A. Grimes, E. C. Dickey, and M. V. Pishko. Vol. X. Santa Clarita, California, USA: American Scientific Publishers, 2006, pp. 1–71.

[19] T. Wagner, T. Yoshinobu, C. Rao, R. Otto, and M. J. Schöning. ""All-in-one" solid-state device based on a light-addressable potentiometric sensor platform". In: *Sensors and Actuators B: Chemical* 117.2 (2006), pp. 472–479. DOI: 10.1016/j.snb.2005.12.056.

3 Frequency behaviour of light-addressable potentiometric sensors

Carl Frederik Werner[a,b], Torsten Wagner[c], Tatsuo Yoshinobu[c], Michael Keusgen[d], Michael J. Schöning[a,b]

[a] *Institute of Nano- and Biotechnologies, Aachen University of Applied Sciences, Jülich, Germany*
[b] *Peter Grünberg Institute (PGI-8), Research Centre Jülich, Jülich, Germany*
[c] *Department of Biomedical Engineering, Tohoku University, Sendai, Japan*
[d] *Institute of Pharmaceutical Chemistry, Philipps University Marburg, Marburg, Germany*

Published in: *Physica Status Solidi A: Applications and Materials Science*, Vol. 210, pp. 884–891, DOI: 10.1002/pssa.201200929

Submitted: 2012-11-07; Accepted: 2013-02-18; Published: 2013-03-29

Abstract:

Light-addressable potentiometric sensors (LAPS) are semiconductor-based potentiometric sensors, with the advantage to detect the concentration of a chemical species in a liquid solution above the sensor surface in a spatially resolved manner. The addressing is achieved by a modulated and focused light source illuminating the semiconductor and generating a concentration-depending photocurrent. This work introduces a LAPS set-up that is able to monitor the electrical impedance in addition to the photocurrent. The impedance spectra of a LAPS structure, with and without illumination, as well as the frequency behaviour of the LAPS measurement are investigated. The measurements are supported by electrical equivalent circuits to explain the impedance and the LAPS-frequency behaviour. The work investigates the influence of different parameters on the frequency behaviour of the LAPS. Furthermore, the phase shift of the photocurrent, the influence of the surface potential as well as the changes of the sensor impedance will be discussed.

3.1 Introduction

Light-addressable potentiometric sensors (LAPS) are semiconductor-based potentiometric sensors. They have the advantage to detect the concentration of one or more chemical or biological species in a liquid solution with a spatially resolved manner at the sensor surface [1, 2]. This enables LAPS to investigate, e.g., concentration distributions (chemical images) [3–6], detection of multiple analytes by means of different modified transducer layers [6–10], or the determination of the metabolic activity of microorganisms by investigation of the local acidification rate [2, 4, 5, 9, 11–17].

The LAPS consists of an electrolyte/insulator/semiconductor (EIS)-layered structure as depicted in Fig. 3.1. With the help of a reference electrode and a rear-side contact, a bias voltage V_{bias} will be applied across the sensor structure. An additional concentration-dependent surface potential at the electrolyte/insulator interface will be superimposed to the bias voltage. This will cause a space-charge region at the insulator/semiconductor interface. Thus, the local width of the space-charge region depends on the local surface concentration. Utilising a modulated and focused light source illuminating the semiconductor, electron-hole pairs will be generated. These will induce a compensatory capacitively coupled photocurrent I that can be measured in an external circuitry. The amplitude of the photocurrent depends on the local surface potential of the illuminated area and thus, on their analyte concentration. Recently, it was shown that also the phase shift between the observed photocurrent and the light signal will be influenced by the local surface concentration of the analyte [18–20].

The response of the photocurrent will be also influenced by the modulation frequency of the light source. The typical frequency behaviour of the photocurrent amplitude possesses a bandpass characteristic [21–23]. There are some models in the literature, which describe the relation between the stimulated light and the detected photocurrent [22–24]. Those predict that the electrical impedance of the sensor structure and the external circuit, like the resistance of the reference electrode, will affect the photocurrent response. In addition, they discuss the importance whether the illumination appears from the front or rear side. At rear-side illumination, the absorption coefficient of the silicon at the wave length of the light as well as the lifetime of the minority carriers in the bulk silicon are important. Nevertheless, these models only describe the behaviour of the photocurrent amplitude with respect to the modulation frequency, impedance and analyte concentration, but do not address the changes of the phase shift of the photocurrent. In ref. [19], the changes of the phase shift have been discussed due to changes in the impedance of the space-charge region, influenced by the surface potential; nonetheless, these impedance changes were not measured and compared, so far.

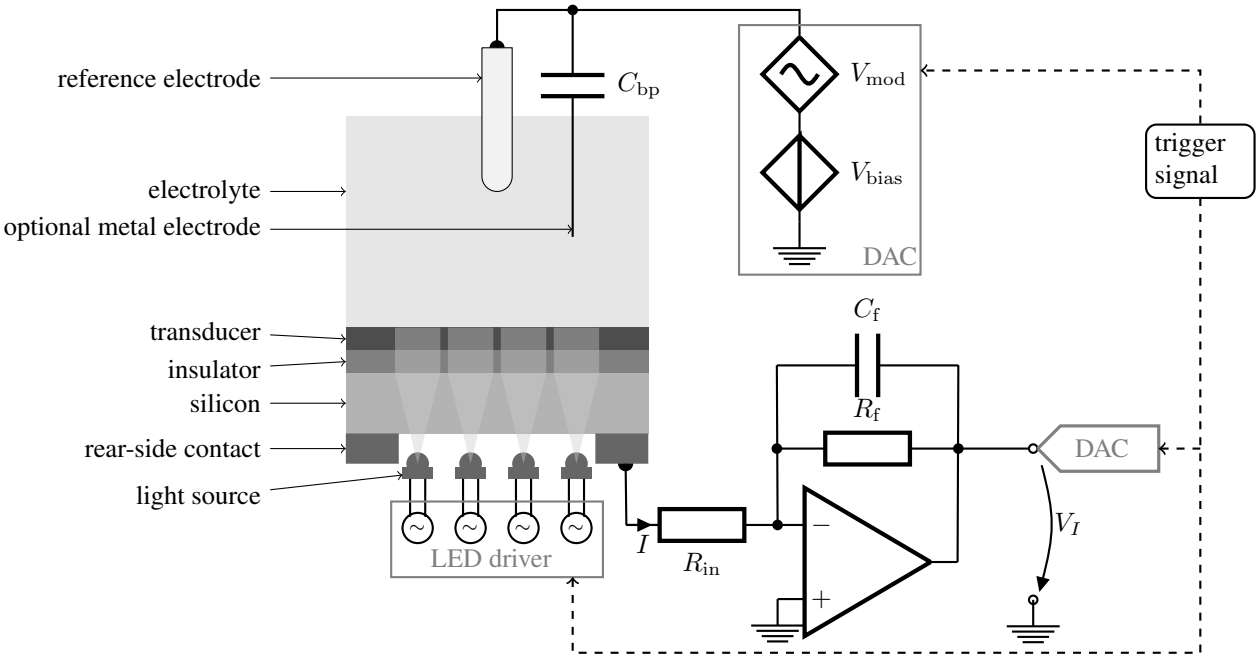

Figure 3.1: Schematic drawing of the LAPS principle with external circuitry. A bias voltage V_{bias} is applied across the sensor structure. By utilising a modulated light source, a concentration-dependent alternating photocurrent I is generated. The current is amplified by a transimpedance amplifier with the elements $R_{\mathrm{f}} = 1\,\mathrm{M\Omega}$, $C_{\mathrm{f}} = 1.4\,\mathrm{nF}$ and $R_{\mathrm{in}} = 1\,\mathrm{k\Omega}$. With the optional modulation voltage V_{mod} the electrical impedance of the sensor structure can be measured. The trigger signal is necessary to determine the correct phase shift of I with respect to the stimulation signal (light source or V_{mod}). An optional metal electrode is capacitively coupled utilising a bypass capacitor C_{bp} to reduce the ohmic resistance of the reference electrode.

3.2 Method and set-up

The authors developed a LAPS set-up to measure the electrical impedance of the LAPS structure by stimulation with an additionally modulated voltage source, similar to the read-out method for capacitive EIS sensors [25], as well as the complex photocurrent at different light-modulation frequencies in one single device. With this device they studied the correlation between the electrical impedance and the photocurrent response (amplitude and phase shift). Therefore, simplified electrical equivalent circuits for the sensor-impedance measurement (see Fig. 3.2a) and the LAPS measurement (see Fig. 3.2b) are used. These equivalent circuits consist of components that can be easily fitted and described by the main physical parameters when operating the sensor in the depletion region. This should help to determine the optimal operation parameters for the LAPS chips and to investigate the principles of LAPS.

The equivalent circuit for the sensor impedance (Fig. 3.2a) is build up of a resistor R including the resistivity of the electrolyte, the resistance of the reference electrode and a possible resistance of the amperemeter. In addition, the resistance of the bias-voltage source and the semiconductor can also be included, but usually they can be

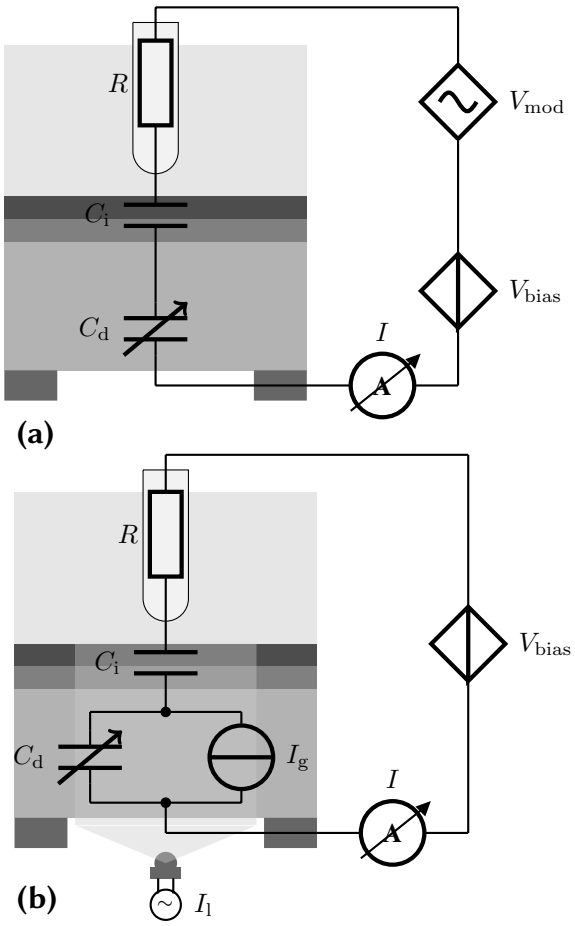

Figure 3.2: Simplified electrical equivalent circuits for the sensor-impedance measurement (a) and the LAPS measurement (b). R includes, e.g., the resistivity of the electrolyte, the resistance of the reference electrode and a possible resistance of the amperemeter. C_{i} is the capacitance of the insulator, C_{d} describes the capacitance of the space-charge region, V_{bias} is the bias voltage, V_{mod} is the modulated voltage to monitor the sensor impedance, I_{g} is the generated photocurrent inside the semiconductor and I_{l} is the current that drives the light source.

neglected. The capacitance C_i is the capacitance of the insulator of the LAPS. It can also consider the double-layer capacitance at the electrolyte/insulator interface, but by using electrolyte solutions with ionic strengths higher than 10^{-4} M it can be neglected [25]. C_d describes the capacitance of the space-charge region and depends on the bias voltage and the surface potential. Thus, the impedance Z of the whole sensor structure is approximated to

$$Z = \frac{V_{mod}}{I} = R + \frac{1}{j\omega C} \tag{3.1}$$

with j as the imaginary number, V_{mod} as the amplitude of the modulated voltage, ω the angular frequency, I the measured current and

$$C = \frac{C_i C_d}{C_i + C_d} \tag{3.2}$$

the series capacitance of C_i and C_d.

The equivalent circuit of the LAPS (Fig. 3.2b) includes the same components and in addition a current source I_g, which describes the compensatory capacitively coupled photocurrent inside the semiconductor. By driving a current I_l through the light source, e.g., a light-emitting diode (LED), light with a defined intensity is emitted depending on the efficiency of the light source. Mainly, most of the light will be focused to the rear side of the semiconductor where the light will be absorbed, depending on the absorption coefficient. By rear-side illumination and wafer thicknesses larger than the penetration depth of the light, almost all of the light is absorbed in the bulk of the semiconductor and will generate electron-holes pairs. A part of these charge carriers recombine and another part diffuses towards the space-charge region, at which they will be separated and induce the photocurrent I_g. According to this behaviour, one can assume the following relation between I_g and I_l:

$$\frac{I_g}{I_l} = \frac{j\omega k}{1 + j\omega\tau_n} \tag{3.3}$$

Equation (3.3) describes the alternating current steady-state diffusion equation, including recombination [22, 24]. Here, $k < 1$ is a factor that includes the efficiency of the LED, the absorption coefficient of the light, the generation of electron-hole pairs and their diffusion. Due to the fact that the photocurrent I_g depends on the width of the space-charge region, because for a higher width more charge carriers are separated, k is also a function of the applied bias voltage and surface potential. The time constant τ_n is the minority-carrier bulk-recombination lifetime. The transfer function of I_l and I,

according to Fig. 3.2b and Eq. (3.3), is

$$\frac{I}{I_\mathrm{l}} = \frac{j\omega k}{1 + j\omega\tau_\mathrm{n}} \cdot \frac{C/C_\mathrm{d}}{1 + j\omega RC} \tag{3.4}$$

whereas k, C and C_d is affected by the bias voltage. Hence, the measured photocurrent I depends on V_bias due to the current generation inside the semiconductor and in addition, due to the change of the capacitance of the space-charge region.

3.3 Experimental

The measurements were performed with a LAPS set-up of a 4×4 infrared light-emitting diode (IR-LED) array, illuminating the LAPS chip from the rear side. The wavelength of the IR-LEDs is 950 nm. The LEDs are driven by a field-programmable gate array (FPGA), which is able to operate all 16 LEDs simultaneously with different modulation frequencies. Each LED can be driven with a maximum current of 35 mA and emits about 6.3 mW. More information about the LAPS set-up can be found in [26]. The amplification circuit to measure the current I is depicted in Fig. 3.1. It is a transimpedance amplifier (TIA) to convert the current I in a measureable voltage V_I. This circuit consists of an operation amplifier TL072A from STMicroelectronics and the feedback elements R_f and C_f. The TL072A behaves in the expected frequency range up to 50 kHz, like an ideal operation amplifier. Therefore, the transfer function of the TIA is:

$$\frac{V_I}{I} = -\frac{R_\mathrm{f}}{1 + j\omega R_\mathrm{f} C_\mathrm{f}} \tag{3.5}$$

The resistor R_in is used to stabilise the sensor set-up for low sensor capacities.

The recording of the output voltage V_I is done by a data acquisition card (DAQmx PCI-6259 from National Instruments) with a sampling rate of 10^6 samples s^{-1}. To determine the correct phase shift the sampling of V_I and the modulation of the LEDs is started simultaneously by a separated trigger signal. After sampling of V_I a Fourier transformation is performed by a fast Fourier transform (FFT) algorithm to determine the complex value of V_I at the frequency of the stimulation signal (either V_mod or I_l). Then, the complex value of I is calculated with the help of the reverse function of Eq. (3.5) and is used for further calculations, e.g., to determine the magnitude and phase shift.

To measure the impedance of the sensor structure, a modulation voltage V_mod is added to the bias voltage V_bias. The sum of both voltages V_bias+V_mod will be applied by the DAQ card. The modulation voltage is a cosine wave voltage with an amplitude of 5 mV and a selectable frequency. V_mod will also be started by the trigger signal. The current I is measured and calculated as described above. To determine the capacitance

C, Eq. (3.1) and the imaginary part of the measured current $\Im(I)$ are used:

$$C = -\frac{\Im(I)}{\omega V_{\text{mod}}} \tag{3.6}$$

The investigated sensor structure is a LAPS chip with a size of 20 mm × 20 mm. It has an active area with contact to the electrolyte of 15 mm × 15 mm. The structure is build up of 60 nm Ta_2O_5, 30 nm SiO_2, about 400 µm p-doped Si (5–10 Ω cm) and a 300 nm Al rear-side contact. The rear-side contact is partly removed at the active area to provide illumination from the rear side. The bias voltage is applied by a Ag/AgCl-reference electrode with a resistance of about 10 kΩ. To achieve a low contact resistance towards the electrolyte, in addition to the reference electrode, a gold electrode is used for the following measurements. The gold electrode is capacitively coupled by a unipolar bypass transistor $C_{\text{bp}} = 10\,\mu\text{F}$ (see Fig. 3.1). Due to the bypass transistor the potential at the gold electrode will not influence the potentiometric measurement. The relatively high capacitance of $C_{\text{bp}} = 10\,\mu\text{F}$ is chosen to achieve impedances that are much lower than the resistance of the reference electrode, thus their resistance can be neglected. In addition, C_{bp} is significantly higher than C_{i}, therefore C_{bp} can be neglected in a series circuit.

3.4 Results and discussion

To validate the measurement set-up, i.e., the determination of the impedance as well as the correct phase shift and the calculation of the current, different combinations of RC circuits were tested. Two different capacitors C with 100 nF and 330 nF and three resistors R with 0 kΩ, 1 kΩ and 10 kΩ were used. These values are in the range of the expected values of the LAPS structure. The measurements were performed at frequencies between 10 Hz and 50 kHz. Figure 3.3 depicts the measured values as well as the calculated impedances (dashed lines) according to Eq. (3.1) and taking the values of R_{in}, R and C into account. The measured values fit the theoretical values of the impedance and phase shift. At low frequencies ($f < 80\,\text{Hz}$) the measured current I and thus, the signal-to-noise ratio is low due to the high impedance; as a result, the determined phase has some deviations from the ideal curve behaviour. The same behaviour can be found at high frequencies ($f > 10\,\text{kHz}$), possible reasons could be additional parasitic impedances and a too low sample rate.

To characterise the LAPS chip in electrochemical environment, measurements with pH 7 buffer solutions were performed. At a modulation frequency of 80 Hz of V_{mod} and bias voltages V_{bias} from −1.5 V to 0.5 V, impedance measurements were carried out. The capacitance voltage (C/V) curves are shown in Fig. 3.4a, with and without

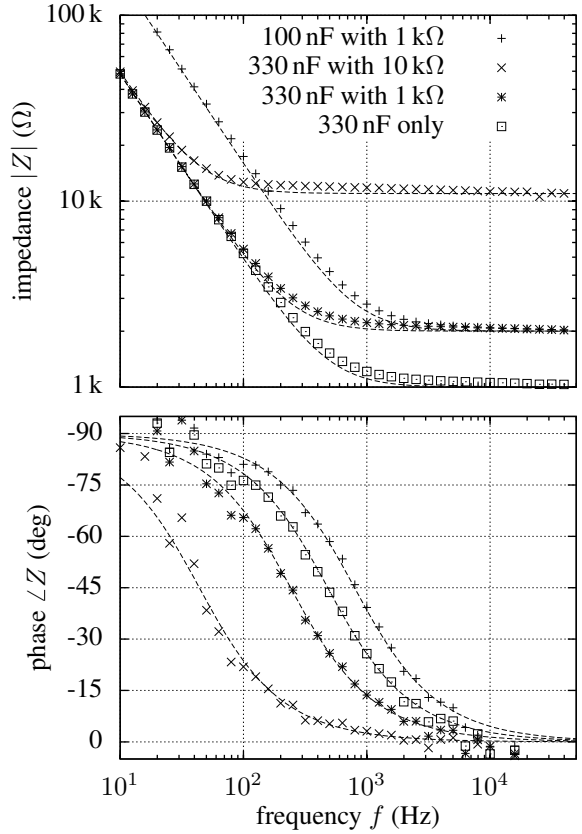

Figure 3.3: Validation of the impedance measurements of the LAPS set-up with different RC series circuits. The symbols indicate the measured values by using the elements of R and C as described in the legend. The dashed lines are the calculated impedances according to Eq. (3.1) considering an additional input resistor $R_{\text{in}} = 1\,\text{k}\Omega$ of the amperemeter.

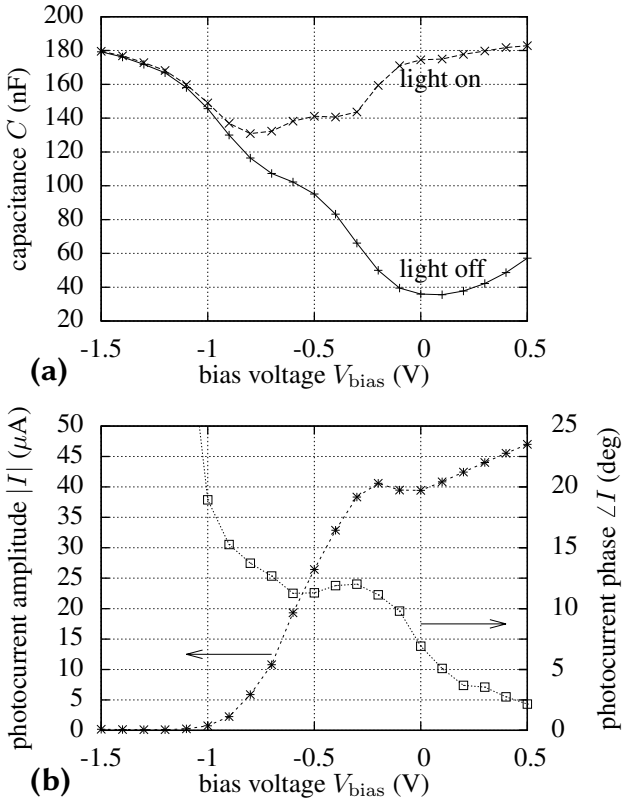

Figure 3.4: C/V curves (a), and I/V curve with phase shift (b) of the same LAPS structure measured with a pH 7 buffer solution. The C/V curves are recorded by determination of the impedance values at $f = 80\,\text{Hz}$ and calculation of the capacitance according to Eq. (3.6). C/V measurements have been performed once with operation of all IR-LEDs and once with all IR-LEDs switched off. The I/V-curve measurement is performed by operating all IR-LEDs at 2 kHz simultaneously.

illumination. In case of illumination, all 16 IR-LEDs were operated without modulation during the C/V cycle. The measurement without light shows a typical C/V curve of an EIS sensor. At $V_{\text{bias}} = -1.5\,\text{V}$ accumulation occurs and no space-charge region exists, thus one can assume that the insulator capacitance is equal to the measured capacitance $C_{\text{i}} = 180\,\text{nF}$. In case of illumination, the change of the C/V curves is smaller because of the additionally generated charge carriers inside the silicon due to the illumination.

Figure 3.4b presents the photocurrent voltage (I/V) curve of the same LAPS structure at the same bias-voltage range as for the C/V measurement. Here, all IR-LEDs were operated at 2 kHz simultaneously. With increasing bias voltage, the amplitude of the photocurrent $|I|$ increases and the phase shift decreases. At about $V_{\text{bias}} = -0.5\,\text{V}$ the slope of the phase curve is low. By considering that the phase-shift change is induced by a change of the capacitance of the space-charge region [19], this behaviour can be described by the C/V curve with illumination, which also has a low slope in this voltage range. The depletion occurs linearly within a range from −0.9 V to −0.3 V. Therefore, the bias voltages −0.9 V, −0.7 V, −0.5 V and −0.3 V are selected for the following impedance and LAPS-frequency behaviour measurements.

Figure 3.5 shows the impedance measurements without illumination and Fig. 3.6 with illumination. The dashed lines are representing fittings of Eq. (3.1) to the measured values by utilising a nonlinear least-squares Marquardt-Levenberg algorithm. Without illumination, a V_{bias}-dependent change of the capacitive part of the impedance can be found. The fitted parameters of Fig. 3.5 are summarised in Tab. 3.1. The fitted value of the resistor R is equal to 1.2 kΩ for all bias voltages, whereas the capacitance C changes from 116 nF to 43.2 nF. This is a typical behaviour of a capacitive EIS sensor and can be also observed in the C/V measurement of Fig. 3.4.

In case of illumination, the impedance will not change significantly, which is also in accordance with the observed C/V curves (Fig. 3.4). The fitted parameters of Fig. 3.6 are summarised in Tab. 3.2. The value of the resistor R is also equal to 1.2 kΩ and shows that the resistor is not influenced by the light or the bias voltage. The capacitance C changes from 121 nF to 113 nF according to the bias-voltage changes. This shows that the additionally generated charge carriers, due to the illumination, will influence the capacitance of the space-charge region significantly. In comparison, the capacitance of the space-charge region, according to Eq. (3.2), at $V_{\text{bias}} = -0.3\,\text{V}$, without illumination is 56.7 nF and with illumination it is 307 nF.

The frequency behaviour of the LAPS by operating all LEDs simultaneously with the particular frequency and applying different bias voltages over the sensor structure is overviewed in Fig. 3.7. The amplitude and the phase shift show a bandpass characteristic. The dashed lines represent fits according to Eq. (3.4), using the parameters obtained from Fig. 3.6 (see also Tab. 3.2). A dependency of the photocurrent amplitude with

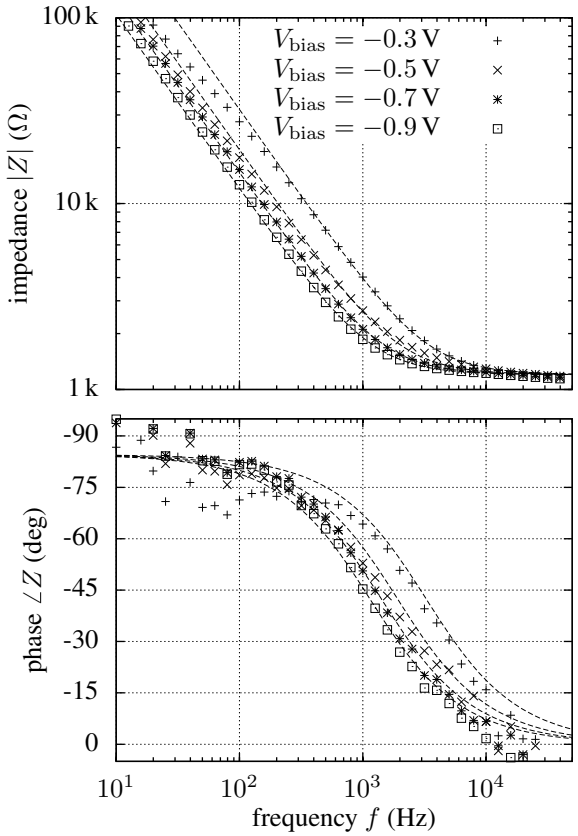

Figure 3.5: Impedance measurements of the LAPS structure at different bias voltages, driving the LAPS structure in the depletion region. The dashed lines are fittings of Eq. (3.1) compared to the measured values. The fitted parameters are summarised in Tab. 3.1.

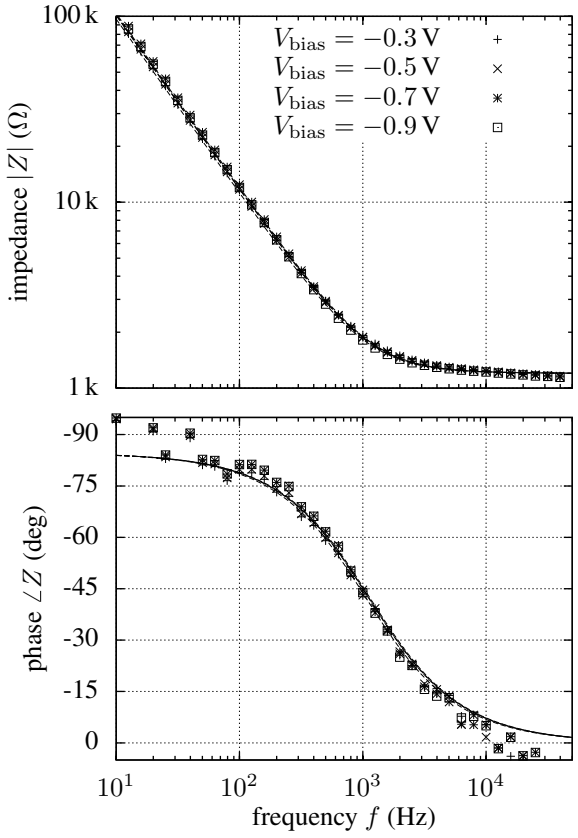

Figure 3.6: Impedance measurements of the LAPS structure at different bias voltages, driving the LAPS structure in the depletion region. In addition, all IR-LEDs of the array are turned on. The dashed lines are fittings of Eq. (3.1) compared to the measured values. The fitted parameters are summarised in Tab. 3.2.

Table 3.1: Fitted parameters with uncertainties from Eq. (3.1) to the impedance measurements of Fig. 3.5.

V_{bias} (V)	C (nF)	C_{d} (nF)	R (kΩ)
−0.9	116 ± 2	324 ± 5	1.20 ± 0.02
−0.7	95 ± 2	200 ± 3	1.20 ± 0.02
−0.5	71 ± 2	118 ± 3	1.20 ± 0.03
−0.3	43.2 ± 0.5	56.7 ± 0.6	1.20 ± 0.03

Table 3.2: Fitted parameters with uncertainties from Eq. (3.1) to the impedance measurements of Fig. 3.6 and Eq. (3.4) to the LAPS measurements of Fig. 3.7.

	impedance measurement			LAPS measurement	
V_{bias} (V)	C (nF)	C_{d} (nF)	R (kΩ)	k (10^{-9})	τ_{n} (µs)
−0.9	121 ± 2	369 ± 7	1.20 ± 0.02	2.10 ± 0.03	12 ± 8
−0.7	115 ± 2	321 ± 6	1.20 ± 0.02	9.2 ± 0.3	12 ± 7
−0.5	116 ± 3	327 ± 6	1.20 ± 0.02	22.9 ± 0.7	12 ± 5
−0.3	113 ± 3	307 ± 6	1.20 ± 0.02	32 ± 1	12 ± 9

respect to the bias voltage is recognisable, however, the change of the phase is low. The maximal photocurrents are at about 3 kHz. The highest changes of the phase shift according to these bias voltage can be observed in the range of 30 Hz to 200 Hz. These changes cannot be described by Eq. (3.4), one reason might be interfaces' trapped charges at the insulator/semiconductor interface, which are not described therein.

The frequency behaviour can be divided into three parts that are bounded by the time constants RC and τ_{n}: In the part for $f < \frac{1}{2\pi RC}$ the photocurrent amplitudes will increase, at $\frac{1}{2\pi RC} < f < \frac{1}{2\pi\tau_{\text{n}}}$ they will be at maximum, and at $f > \frac{1}{2\pi\tau_{\text{n}}}$ the photocurrent decreases. The minority-carrier bulk-recombination lifetime τ_{n} depends on the doping of the silicon and is approximated from the diagram to be about $\tau_{\text{n}} = (12 \pm 4)$ µs, which is a realistic value according to [22], where values between 7.2 µs and 82.6 µs have been observed. The time constant RC includes the capacitance C (including the insulator and the space-charge region capacitance) as well as the input resistor, the resistance of the reference electrode and of the electrolyte (R). For measurements with electrolytes with different conductivities, it is advisable to use low measurement frequencies or an input resistance that is much higher than the resistance of the electrolyte.

Considering the dependence of the bias voltage or the surface potential to the measurable photocurrent amplitude I, there are two mechanisms described in Eq. (3.4) that have influences: One is the generation of the photocurrent I_{g} inside the semiconductor described by the parameter k. The second mechanism is the change of the capacitance described by the parameters C and C_{d}. The value of k varies from 2.1×10^{-9}

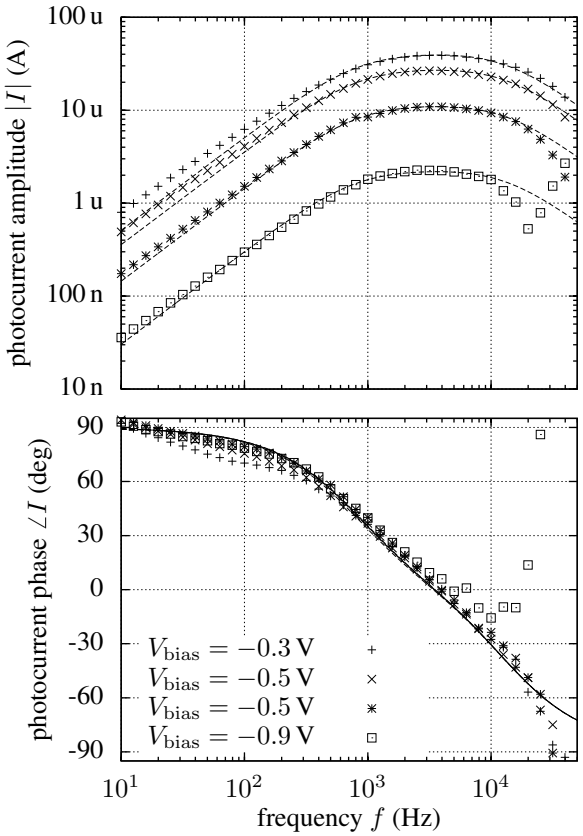

Figure 3.7: Frequency behaviour of the LAPS structure by operating all LEDs simultaneously with different frequencies and applying different bias voltages across the LAPS structure (all in depletion). The dashed lines are fittings of Eq. (3.4) compared to the measured values considering obtained parameters from Fig. 3.6. The fitted parameters are summarised in Tab. 3.2, too.

to 32×10^{-9} in the observed voltage range of $V_{\text{bias}} = -0.9\,\text{V}$ to $V_{\text{bias}} = -0.3\,\text{V}$. This is a change of factor 15. When looking to the change of the capacitance, two cases have to be considered: The fraction $\frac{C}{C_d}$ is interesting at frequencies of $\omega \ll \frac{1}{RC}$ and the fraction $\frac{1}{C_d}$ at frequencies of $\omega \gg \frac{1}{RC}$. In the observed voltage range $\frac{C}{C_d}$ and $\frac{1}{C_d}$ will change by a factor of 1.1 and 1.2, respectively. This shows that the dependence of the photocurrent amplitude by the bias voltage is much more affected by the generation of the photocurrent than by the change of the capacitance.

Considering the phase shift of the photocurrent I, there are the two time constants τ_n and RC, described in Eq. (3.4), that have influences. Since the recombination lifetime τ_n and the components combined in the resistor R are not influenced by the bias voltage or the surface potential, the voltage-depending changes of the phase shift are only affected by changes of the capacitance C and could be measured at frequencies $f > \frac{1}{2\pi RC}$.

3.5 Conclusions

A LAPS set-up with the additional feature to determine the electrical impedance of the sensor structure was developed. The LAPS and impedance measurements can be performed at different frequencies in the range of 10 Hz to 50 kHz and for different

bias voltages. The measured signal is corrected by the frequency behaviour of the transimpedance amplifier to determine the "correct" phase shift and amplitude of the current. Thus, the impedance spectra, i.e., the LAPS-frequency behaviour as well as electrochemical characterisation, like C/V and I/V curves, can be investigated with the same sensor chip within the same set-up simultaneously.

The measurements of the LAPS impedance and the frequency behaviour at different bias voltages (driven in the depletion region) were compared by using electrical equivalent circuits. Thus, the frequency-determining parameters were investigated with regard to the bias voltage. With these results and the help of Eq. (3.4) it was observed that

- the LAPS-frequency behaviour depends on the two time constants τ_n and RC,
- the maximal photocurrent amplitude can be observed in the frequency range of $\frac{1}{2\pi RC}$ to $\frac{1}{2\pi\tau_n}$,
- at frequencies $f > \frac{1}{2\pi RC}$ a dependence towards the electrolyte conductivity must be taken into account,
- changes of the phase shift according to the bias voltage or the surface potential are induced by changes of the capacitance of the space-charge region and can be observed at frequencies $f > \frac{1}{2\pi RC}$,
- the capacitance of the space-charge region is influenced by the illumination; the voltage-depending change of this capacitance is about 5 times lower with illumination,
- the photocurrent amplitude is influenced by the voltage-depending photocurrent generation and capacitance of the space-charge region, whereas the change induced by the photocurrent generation is about 12 times higher.

The demonstrated methods help to characterise and optimise LAPS structures as well as to find the optimised frequency range for I/V measurements. In addition, impedance measurements allow to simultaneous study the intrinsic sensor performance as well as charge changes at the interface sensor/analyte. Particular interest for future applications is devoted to investigate and optimise, respectively, the spot size with respect to the simultaneous I/V and impedance measurement.

Future improvements of this LAPS set-up could be the increasing of the signal-to-noise ratio and the frequency-band width. This could be done with a three-electrode configuration, a gain-scaling network to maximise the input towards the data-acquisition card and the usage of a better operation amplifier with a better noise performance and a higher bandwidth. In order to improve the performance as electrochemical imaging sensor it is important to minimise the influence of the electrolyte conductivity and to decrease the measurement time. To reduce the measurement time, a high photocurrent amplitude (for a good signal-to-noise ratio) and a high measurement frequency is

advantageous. Since the maximal photocurrent amplitude was observed between $\frac{1}{2\pi RC}$ and $\frac{1}{2\pi\tau_n}$ it is advisable to chose these parameters to achieve a high bandwidth at high frequencies, as far as the semiconductor chip fabrication makes it possible.

Acknowledgements

The authors thank the German Federal Ministry of Food, Agriculture and Consumer Protection (BMELV) and the "Fachagentur Nachwachsende Rohstoffe e.V." (FNR) for financial support of this work (Bio-LAPS).

References

[1] D. G. Hafeman, J. W. Parce, and H. M. McConnell. "Light-addressable potentiometric sensor for biochemical systems". In: *Science* 240.4856 (1988), pp. 1182–1185. DOI: 10.1126/science.3375810.

[2] J. C. Owicki, L. J. Bousse, D. G. Hafeman, G. L. Kirk, J. D. Olson, H. G. Wada, and J. W. Parce. "The light-addressable potentiometric sensor: Principles and biological applications". In: *Annual Review of Biophysics and Biomolecular Structure* 23 (1994), pp. 87–113. DOI: 10.1146/annurev.bb.23.060194.000511.

[3] M. Nakao, T. Yoshinobu, and H. Iwasaki. "Scanning-laser-beam semiconductor pH-imaging sensor". In: *Sensors and Actuators, B: Chemical* 20.2-3 (1994), pp. 119–123. DOI: 10.1016/0925-4005(93)01199-E.

[4] M. Nakao, S. Inoue, T. Yoshinobu, and H. Iwasaki. "High-resolution pH imaging sensor for microscopic observation of microorganisms". In: *Sensors and Actuators B: Chemical* 34.1-3 (1996), pp. 234–239. DOI: 10.1016/S0925-4005(96)01903-X.

[5] T. Yoshinobu, H. Ecken, A. B. M. Ismail, H. Iwasaki, H. Lüth, and M. J. Schöning. "Chemical imaging sensor and its application to biological systems". In: *Electrochimica Acta* 47.1-2 (2001), pp. 259–263. DOI: 10.1016/S0013-4686(01)00564-3.

[6] T. Yoshinobu, H. Iwasaki, Y. Ui, K. Furuichi, Y. Ermolenko, Y. Mourzina, T. Wagner, N. Näther, and M. J. Schöning. "The light-addressable potentiometric sensor for multi-ion sensing and imaging". In: *Methods* 37.1 (2005), pp. 94–102. DOI: 10.1016/j.ymeth.2005.05.020.

[7] Y. Ermolenko, T. Yoshinobu, Y. Mourzina, S. Levichev, K. Furuichi, Y. Vlasov, M. Schöning, and H. Iwasaki. "Photocurable membranes for ion-selective light-addressable potentiometric sensor". In: *Sensors and Actuators, B: Chemical* 85.1–2 (2002), pp. 79–85. DOI: 10.1016/S0925-4005(02)00056-4.

[8] T. Yoshinobu, M. J. Schöning, R. Otto, K. Furuichi, Y. Mourzina, Y. Ermolenko, and H. Iwasaki. "Portable light-addressable potentiometric sensor (LAPS) for multisensor applications". In: *Sensors and Actuators, B: Chemical* 95.1-3 (2003), pp. 352–356. DOI: 10.1016/S0925-4005(03)00437-4.

[9] T. Wagner, R. Molina, T. Yoshinobu, J. P. Kloock, M. Biselli, M. Canzoneri, T. Schnitzler, and M. J. Schöning. "Handheld multi-channel LAPS device as a transducer platform for possible biological and chemical multi-sensor applications". In: *Electrochimica Acta* 53.2 (2007), pp. 305–311. DOI: 10.1016/j.electacta.2007.04.006.

[10] J. R. Siqueira, R. M. Maki, F. V. Paulovich, C. F. Werner, A. Poghossian, M. C. F. de Oliveira, V. Zucolotto, O. N. Oliveira, and M. J. Schöning. "Use of information visualization methods eliminating cross talk in multiple sensing units investigated for a light-addressable potentiometric sensor". In: *Analytical Chemistry* 82.1 (2010), pp. 61–65. DOI: 10.1021/ac9024076.

[11] J. W. Parce, J. C. Owicki, K. M. Kercso, G. B. Sigal, H. G. Wada, V. C. Muir, L. J. Bousse, K. L. Ross, B. I. Sikic, and H. M. McConnell. "Detection of cell-affecting agents with a silicon biosensor". In: *Science* 246.4927 (1989), pp. 243–247. DOI: 10.1126/science.2799384.

[12] J. C. Owicki and J. W. Parce. "Biosensors based on the energy metabolism of living cells: The physical chemistry and cell biology of extracellular acidification". In: *Biosensors & Bioelectronics* 7.4 (1992), pp. 255–272. DOI: 10.1016/0956-5663(92)87004-9.

[13] B. Stein, M. George, H. E. Gaub, J. C. Behrends, and W. J. Parak. "Spatially resolved monitoring of cellular metabolic activity with a semiconductor-based biosensor". In: *Biosensors & Bioelectronics* 18.1 (2003), pp. 31–41. DOI: 10.1016/S0956-5663(02)00109-4.

[14] A. Poghossian, S. Ingebrandt, A. Offenhäusser, and M. J. Schöning. "Field-effect devices for detecting cellular signals". In: *Seminars in Cell & Developmental Biology* 20.1 (2009), pp. 41–48. DOI: 10.1016/j.semcdb.2009.01.014.

[15] H. Yu, H. Cai, W. Zhang, L. Xiao, Q. Liu, and P. Wang. "A novel design of multifunctional integrated cell-based biosensors for simultaneously detecting cell acidification and extracellular potential". In: *Biosensors & Bioelectronics* 24.5 (2009), pp. 1462–1468. DOI: 10.1016/j.bios.2008.08.045.

[16] C. F. Werner, C. Krumbe, K. Schumacher, S. Groebel, H. Spelthahn, M. Stellberg, T. Wagner, T. Yoshinobu, T. Selmer, M. Keusgen, M. E. M. Baumann, and M. J. Schöning. "Determination of the extracellular acidification of *Escherichia coli* by a

light-addressable potentiometric sensor". In: *physica status solidi (a)* 208.6 (2011), pp. 1340–1344. DOI: 10.1002/pssa.201001141.

[17] C. F. Werner, S. Groebel, C. Krumbe, T. Wagner, T. Selmer, T. Yoshinobu, M. E. M. Baumann, M. Keusgen, and M. J. Schöning. "Nutrient concentration-sensitive microorganism-based biosensor". In: *physica status solidi (a)* 209.5 (2012), pp. 900–904. DOI: 10.1002/pssa.201100801.

[18] K. Miyamoto, T. Wagner, S. Mimura, S. Kanoh, T. Yoshinobu, and M. J. Schöning. "Constant-phase-mode operation of the light-addressable potentiometric sensor". In: *Procedia Chemistry* 1.1 (2009). Ed. by J. Brugger and D. Briand, pp. 1487–1490. DOI: 10.1016/j.proche.2009.07.371.

[19] K. Miyamoto, T. Wagner, T. Yoshinobu, S. Kanoh, and M. J. Schöning. "Phase-mode LAPS and its application to chemical imaging". In: *Sensors and Actuators, B: Chemical* 154.1 (2011), pp. 28–32. DOI: 10.1016/j.snb.2009.12.022.

[20] K. Miyamoto, T. Wagner, S. Mimura, S. Kanoh, T. Yoshinobu, and M. J. Schöning. "Constant-phase-mode operation of the light-addressable potentiometric sensor". In: *Sensors and Actuators, B: Chemical* 154.2 (2011), pp. 119–123. DOI: 10.1016/j.snb.2010.01.004.

[21] Z. Qintao, W. Ping, W. J. Parak, M. George, and G. Zhang. "A novel design of multi-light LAPS based on digital compensation of frequency domain". In: *Sensors and Actuators, B: Chemical* 73.2-3 (2001), pp. 152–156. DOI: 10.1016/S0925-4005(00)00696-1.

[22] L. Bousse, S. Mostarshed, D. Hafeman, M. Sartore, M. Adami, and C. Nicolini. "Investigation of carrier transport through silicon wafers by photocurrent measurements". In: *Journal of Applied Physics* 75.8 (1994), pp. 4000–4008. DOI: 10.1063/1.356022.

[23] G. Verzellesi, L. Colalongo, D. Passeri, B. Margesin, M. Rudan, G. Soncini, and P. Ciampolini. "Numerical analysis of ISFET and LAPS devices". In: *Sensors and Actuators, B: Chemical* 44.1-3 (1997), pp. 402–408. DOI: 10.1016/S0925-4005(97)00233-5.

[24] G. Massobrio, S. Martinoia, and M. Grattarola. "Light-addressable chemical sensors: Modelling and computer simulations". In: *Sensors and Actuators, B: Chemical* 7.1-3 (1992), pp. 484–487. DOI: 10.1016/0925-4005(92)80348-2.

[25] A. Poghossian and M. J. Schöning. "Silicon-based chemical and biological field-effect sensors". In: *Encyclopedia of Sensors*. Ed. by C. A. Grimes, E. C. Dickey, and M. V. Pishko. Vol. X. Santa Clarita, California, USA: American Scientific Publishers, 2006, pp. 1–71.

[26] C. F. Werner, S. Schusser, H. Spelthahn, T. Wagner, T. Yoshinobu, and M. J. Schöning. "Field-programmable gate array based controller for multi spot light-addressable potentiometric sensors with integrated signal correction mode". In: *Electrochimica Acta* 56.26 (2011), pp. 9656–9660. DOI: 10.1016/j.electacta.2011.03.012.

4 High speed and high resolution chemical imaging based on a new type of OLED-LAPS set-up

Carl Frederik Werner[a,b], Torsten Wagner[c], Ko-ichiro Miyamoto[c], Tatsuo Yoshinobu[c], Michael J. Schöning[a,b]

[a] *Institute of Nano- and Biotechnologies, Aachen University of Applied Sciences, Jülich, Germany*
[b] *Peter Grünberg Institute (PGI-8), Research Centre Jülich, Jülich, Germany*
[c] *Department of Electronic Engineering, Tohoku University, Sendai, Japan*

Published in: *Sensors and Actuators B: Chemical*, Vol. 175, pp. 118-122, DOI: 10.1016/j.snb.2011.12.102

Submitted: 2011-10-18; Accepted: 2011-12-29; Published: 2012-04-12

Abstract:

Light-addressable potentiometric sensors (LAPS) are field-effect-based sensors. A modulated light source is used to define the particular measurement spot to perform spatially resolved measurements of chemical species and to generate chemical images. In this work, an organic light-emitting diode (OLED) display has been chosen as a light source. This allows high measurement resolution and miniaturisation of the system. A new developed driving method for the OLED display optimised for LAPS-based measurements is demonstrated. The new method enables to define modulation frequencies between 1 kHz and 16 kHz and hence, reduces the measurement time of a chemical image by a factor of 40 compared to the traditional addressing of an OLED display.

4.1 Introduction

With a light-addressable potentiometric sensor (LAPS) spatially resolved measurements of chemical species in a liquid solution on the sensor surface can be performed [1–3] and chemical images [4–7] can be generated. LAPS is a field-effect-based potentiometric sensor [8]. As depicted in Fig. 4.1, it consists of a semiconductor/insulator/transducer structure that is in contact with the analyte solution. A reference electrode and a rear-side contact are used to apply a bias voltage V_{bias} across the sensor structure. Due to the applied bias voltage a field effect will occur in the semiconductor at the semiconductor/insulator interface. The local width of the depletion region also depends on the surface potential at the transducer/electrolyte interface. This surface potential is influenced by the local concentration of the analyte on the sensor surface. With a modulated light beam, the local width of the depletion region can be read out. The photons, which penetrate into the semiconductor, generate electron-hole pairs. In presence of the depletion region this electrons and holes are separated and an external detectable photocurrent I_{ph} arises. Thus, the amplitude and phase of the generated photocurrent will change depending on the analyte concentration at the sensor surface, above the illuminated region. More detailed information about the measurement principle of LAPS can be found elsewhere [2, 3].

An important component of the LAPS set-up is the light source, since it defines the measurement resolution, the scanning range, the measurement speed and the signal amplitude. In the past, different light sources for LAPS have been proposed in literature. Conventional set-ups use a single focused laser on a mechanical XY-stage [4, 7, 9]. Typically, these set-ups have a rather high spatial resolution, however, they are rather slow due to the required mechanical movement. Another approach is the use of a fixed array of light sources, e.g., by light-emitting diodes (LEDs) [10–14]. These set-ups are faster, but are limited in their spatial resolution because of the geometrical size of the LEDs. The combinations of both methods is presented in [15]. Recently, the use of commercial imaging techniques, like a digital light processing (DLP) video projector

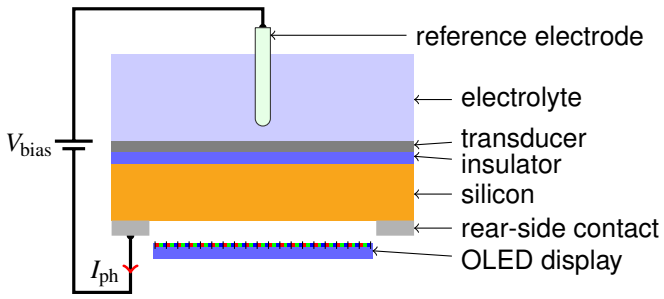

Figure 4.1: Schematic drawing of the OLED-LAPS principle.

[16] or an organic light-emitting diode (OLED) display [17] were presented as possible light sources for LAPS. These techniques allow to design LAPS systems that are free from mechanical movements and can define free measurement areas by customising the size of the illuminated area. OLED and DLP set-ups are mainly utilised for video applications. This applications require only low refresh rates (typical 25 frames s^{-1}). Consequently, both techniques can only generate modulation frequencies below 1 kHz.

Usually, the light modulation is fixed at a refresh rate of e.g., 135 Hz for OLED displays [17]. The rather small size and high resolution of commercially available OLED panels enables miniaturised LAPS systems. On the other hand, the usage of higher modulation frequencies for LAPS measurements is needed in order to perform faster measurement times. The optimal modulation frequency with respect to the signal-to-noise ratio is determined by the frequency behaviour of the LAPS structure [10, 14, 18, 19] and is typically in the kHz range. For this, in the present work a different driving method for the OLED display has been developed to achieve higher modulation frequencies.

4.2 Methods

4.2.1 OLED display

An OLED display DD-9664FC-2A from Densitron was used. It has an integrated driver chip SSD1331 from Solomon Systech. The display is a full-colour display with a diagonal size of 0.95" and an active area of 20.1 mm × 13.2 mm. It consists of $c_{max} = 96$ columns and $r_{max} = 64$ rows. The size of a full-colour pixel is 200 µm × 200 µm. As shown in Fig. 4.1 the OLED panel can be directly mounted below the LAPS structure.

In the normal display mode all 64 rows will be driven consecutively, with a refresh rate of 135 Hz to generate the desired picture on the display. Thereby, each of the 64 rows are driven for about 115 µs. During this time all 96 pixels of a row are addressed simultaneously. When a rectangle with the width of c columns and a height of r rows is illuminated, like in [17], then the integral light intensity overall the display is modulated with the refresh rate of 135 Hz. Increasing the number of columns c increases the light intensity due to more simultaneously illuminated pixels. However, the height r of the rectangle does not increase the light intensity, because the rows are driven consecutively. Increasing the height r changes the duty cycle D according to equation (4.1).

$$D = \frac{r}{r_{max}} \tag{4.1}$$

This behaviour is depicted in Fig. 4.2a schematically by means of an example with a 6 × 4 display and a 2 × 1 rectangle. It shows the illuminated pixels at each cycle (left),

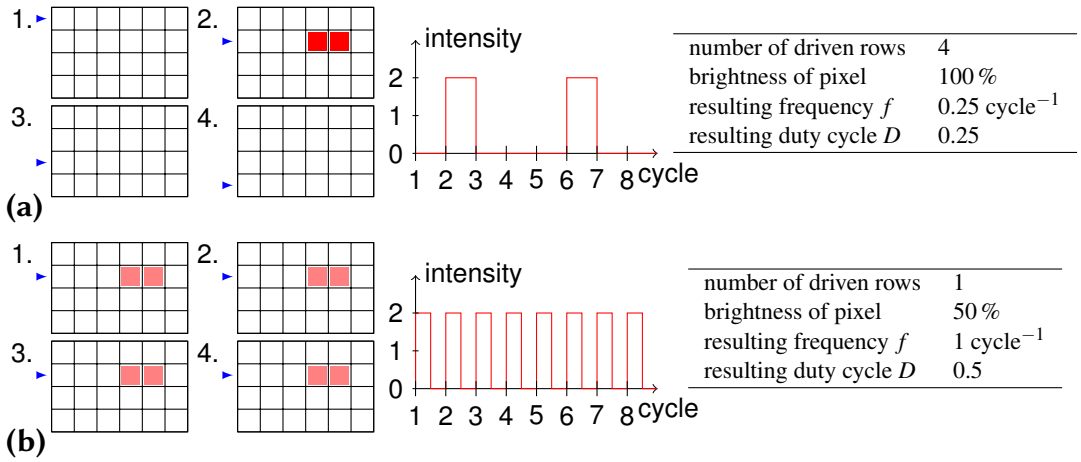

Figure 4.2: Controlling of the OLED display by the driving circuit for a theoretical display with $r_{max} = 4$ rows and $c_{max} = 6$ columns. The arrow indicates the addressed row of the current cycle. A filled box indicates the illuminated pixels. The graph in the middle depicts the light output over the refresh cycle. The intensity is normalised to the intensity of one pixel. In normal display mode, all rows will driven consecutively (a). The new developed driving method only drives one row continuously with 50 % of brightness (b).

the integral light intensity overall the display (middle) and the resulting frequency and duty cycle (right). To achieve higher modulation frequencies and a duty cycle of $D = 0.5$, as desired for LAPS measurements, this method is unsuitable.

With the driver circuit of the OLED display it is possible to limit the number of rows that are addressed consecutively. Decreasing the number of rows, increases the refresh rate and the duty cycle. By choosing only one row, it will be driven continuously and the refresh rate is maximal. The brightness of a pixel is changed by the grey-scale parameter of the display, which is realised by pulse-width modulation. At a grey scale of 50 % the ratio between on and off will become $D = 0.5$, as schematically visualised in Fig. 4.2b. The addressed row, as well as the pixels on this row can be chosen freely. Thus, rectangles with a height of $r = 1$ and a free width of c can be generated at every position on the display without modifying the modulation frequency or the duty cycle. By using more than one row ($r > 1$), the rows will be driven row by row again and the light intensity of the rectangle will not increase.

The modulation frequency is calculated by the clock frequency of the OLED driver $f_{clk} = 1024\,\text{kHz}$, a divider k (range of 1 to 16) and the driving time for one row out of 64 clock cycles:

$$f = \frac{f_{clk}}{64k} \tag{4.2}$$

With this, modulation frequencies in the range of 1 kHz to 16 kHz with a duty cycle

$D = 0.5$ can be generated.

To scan along the sensor plane, a measurement spot consisting of at least one pixel must be moved in a raster-like manner over the display and for each position the photocurrent will be recorded. Therefore, the needed rectangle will be activated at the starting position. Then, the activated row will be moved. After addressing all rows of the first column the same measurement procedure will start for the next column. This order of directions was chosen, because moving the row needs fewer commands, that have to be send to the driver chip; then, changing the column, yields a faster scanning.

4.2.2 Measurements

To characterise the OLED-LAPS set-up a pH-sensitive LAPS structure (Al/n-Si/SiO_2/Si_3N_4) was used. The active LAPS area was defined by the opening window of the rear-side contact, that is 28 mm × 28 mm. All measurements were performed at a modulation frequency of 1.74 kHz with a white measurement spot. To calculate the amplitude of the photocurrent, 23.6 ms per measurement spot are sampled, which corresponds to 41 periods. To obtain a photocurrent/voltage (I/V) curve the bias voltage V_{bias} was swept between −1.8 V and 0 V. The chemical image was performed at pH 7 and a bias voltage of $V_{\text{bias}} = -1.1$ V. For the chemical image the word "LAPS" was written with a polymer resist on the sensor surface.

4.3 Results and discussion

Figure 4.3 presents the waveform of the photocurrent, generated by a light spot of 10 × 1 pixels at a modulation frequency of 1.74 kHz. Due to the frequency behaviour

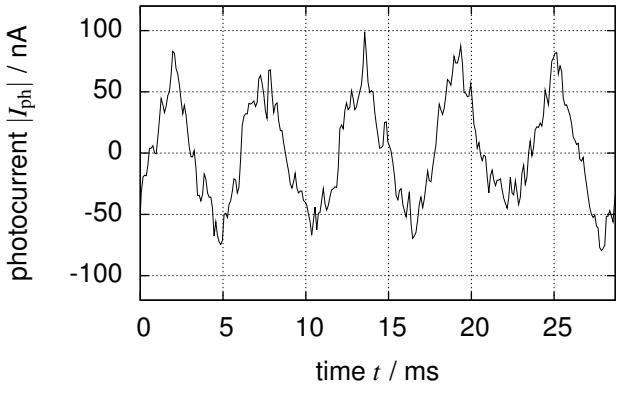

Figure 4.3: Waveform of the photocurrent with a modulation frequency of 1.74 kHz for a measurement spot size of 10 × 1 pixels.

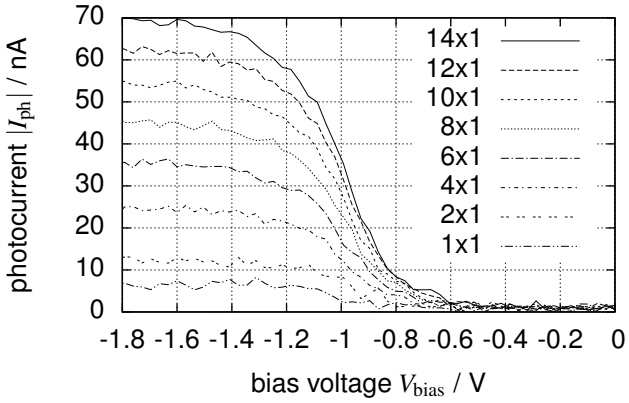

Figure 4.4: Photocurrent/voltage curves for different measurement spot sizes at pH 7.

of the LAPS structure [10, 14, 18, 19], the almost square-wave excitation light signal results in an almost sinusoidal photocurrent waveform.

The amplitude of the photocurrent at the modulation frequency of 1.74 kHz with respect to the applied bias voltage is shown in Fig. 4.4. The figure depicts the I/V curves for different measurement spot sizes between 1×1 and 14×1 pixels. By increasing the measurement spot size the photocurrent amplitude and consequently, the signal-to-noise ratio will increase. The maximum photocurrent in the depletion region varied from 70 nA (14×1 pixels) down to 7 nA (1×1 pixel).

The influence of the measurement spot's wavelength on the photocurrent is demonstrated in Fig. 4.5. Here, the I/V curves have been investigated by a measurement spot with a size of 10×1 pixels at the primary colours red, green and blue as well as for a white measurement spot. With the white measurement spot, where all three primary colour sub-pixels are illuminated, the maximum photocurrent is 50 nA. At red, green and blue the maximum photocurrents are 27 nA, 13 nA and 10 nA, respectively. This confirms that the sum of the photocurrents from the three primary colours will result in the photocurrent of the white measurement spot. The results underline that a shorter wavelength will decrease the photocurrent. By illuminating the rear side of the LAPS structure, photons of a longer wavelength can penetrate deeper into the semiconductor yielding more electron-hole pairs close to the depletion area. As reported in literature, light in the infrared range results in higher photocurrents and a better spatial resolution [4, 20, 21]. As can be seen from Fig. 4.5, the red sub-pixel produces more than 50 % of the photocurrent from the white measurement spot; an OLED display with an entire red pixel of the same size (200 µm × 200 µm) could increase the photocurrent by a factor of 4/3.

Figure 4.6 exemplary illustrates the pH sensitivity in the concentration range of pH 5 to pH 9 for a measurement with a spot size of 10×1 pixels. The I/V curves are shifted

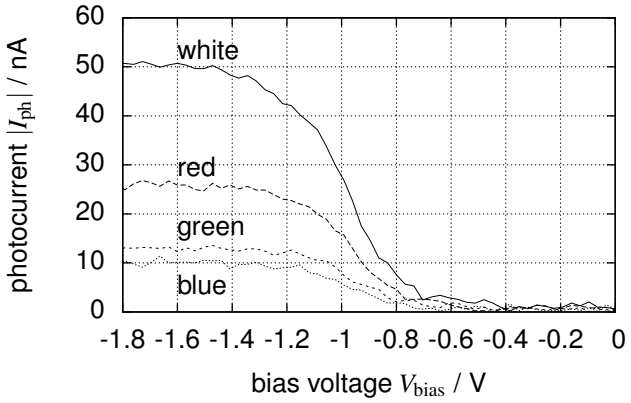

Figure 4.5: Photocurrent/voltage curves of different colours of a measurement spot with the sizes of 10 × 1 pixels at pH 7.

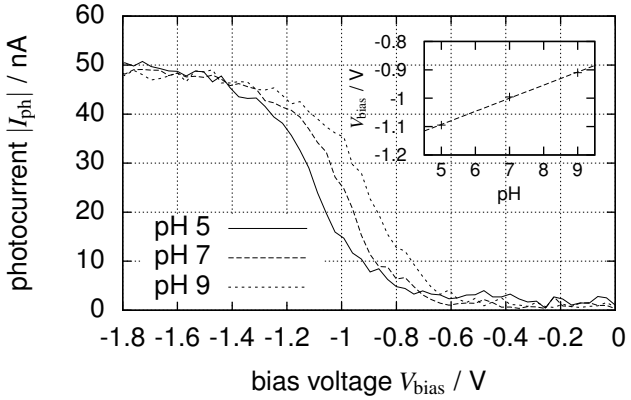

Figure 4.6: Photocurrent/voltage curves for a measurement spot size of 10 × 1 pixels at different pH values. The inlet depicts the calibration plot at a working point of 25 nA.

along the voltage axis depending on the change of the pH value. The pH sensitivity at a working point of 25 nA is about 50 mV pH^{-1}, which corresponds in good agreement with the pH sensitivity of Si_3N_4, discussed in literature (46–58 mV pH^{-1} [8]).

Figure 4.7 depicts an example of a chemical image with the word "LAPS", manually written with a polymer resist on the LAPS surface and recorded by a measurement with a spot size of 2 × 1 pixels with a modulation frequency of 1.74 kHz. To perform the scan, the measurement spot was moved by one pixel in each direction. The polymer resist structure can be detected in the chemical image due to an increase in the photocurrent. An additional layer of polymer resist at the surface results in an additional impedance that decreases the photocurrent. The total measurement time to acquire the chemical image was about 2.5 min. Due to the use of the higher modulation frequencies, the

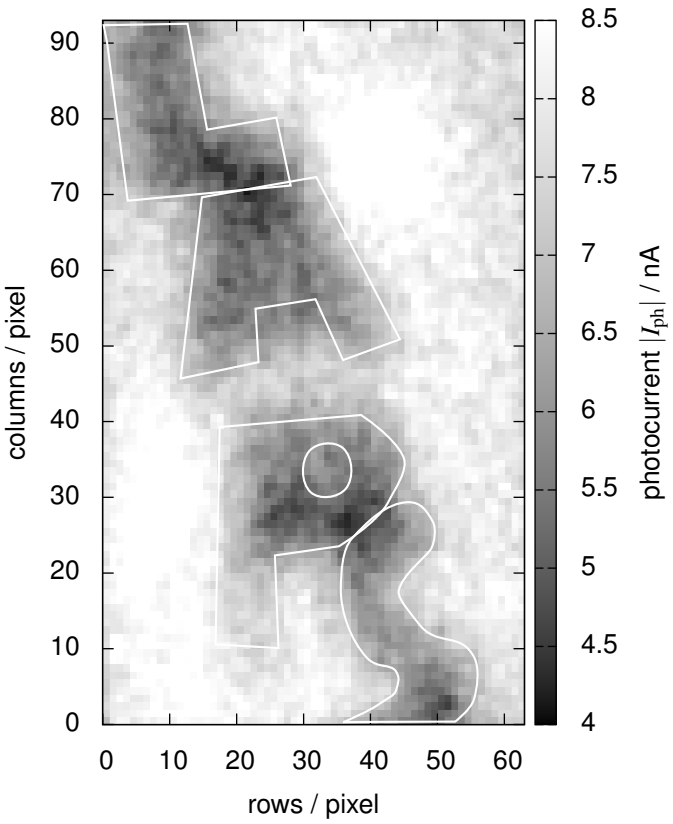

Figure 4.7: Chemical image recorded with a measurement spot size of 2 × 1 pixels and a modulation frequency of 1.74 kHz. On the sensor surface the word "LAPS" was written with a polymer resist.

measurement time could be significantly reduced, compared to the previously presented OLED-LAPS set-up [17] with a measurement time of about 100 min.

4.4 Conclusion and outlook

A LAPS set-up with an OLED display as light source was developed. Due to the array size of 96 × 64 pixels on 20.1 mm × 13.2 mm and a thickness of 2 mm, the OLED panel enables a high measurement resolution of 200 µm and a distinct miniaturisation without the need of mechanical movement. By using a new driving method, modulation frequencies in the range of 1 kHz to 16 kHz can be achieved. Multiple pixels in one row can be activated, which will increase the signal-to-noise ratio but will decrease the spatial resolution. With a pH-sensitive Si_3N_4-LAPS structure, the fundamentals of the developed set-up for e.g., pH measurements has been demonstrated. The red sub-pixel, of a full colour pixel with a size of 200 µm × 200 µm, implies the largest fraction of the

photocurrent. A chemical image of the surface was obtained in 2.5 min. This speeds up the measurement and reduces the time of a chemical image by a factor of 40 (see [17]). The average measurement time of a measurement spot with a size of 0.4 mm × 0.2 mm and a step width of 0.2 mm × 0.2 mm is about 25 ms per spot. Compared with a DLP video projector possessing by a spot size of 0.87 mm × 0.87 mm, which takes 151 ms per spot, the OLED-LAPS set-up is about 5 times faster [16]. However, the minimal spot size of the DLP-LAPS is 43 µm × 43 µm.

In combination with a microcontroller, e.g., a Programmable System-on-Chip (PSoC) the OLED display allows to build small and high-integrated LAPS devices. These devices can be employed for multi-ion imaging [7, 12, 22–24], and the screening of cell growth as well as the detection of the metabolism rate of cells [12, 25–27].

Acknowledgement

The authors gratefully thank the Marubun Research Promotion Foundation for the financial support of this work.

References

[1] D. G. Hafeman, J. W. Parce, and H. M. McConnell. "Light-addressable potentiometric sensor for biochemical systems". In: *Science* 240.4856 (1988), pp. 1182–1185. DOI: 10.1126/science.3375810.

[2] J. C. Owicki, L. J. Bousse, D. G. Hafeman, G. L. Kirk, J. D. Olson, H. G. Wada, and J. W. Parce. "The light-addressable potentiometric sensor: Principles and biological applications". In: *Annual Review of Biophysics and Biomolecular Structure* 23 (1994), pp. 87–113. DOI: 10.1146/annurev.bb.23.060194.000511.

[3] T. Wagner and M. J. Schöning. "Light-addressable potentiometric sensors (LAPS): recent trends and applications". In: *Electrochemical Sensor Analysis*. Ed. by S. Alegret and A. Merkoci. Vol. 49. Amsterdam: Elesevier, 2007, pp. 87–128.

[4] M. Nakao, S. Inoue, T. Yoshinobu, and H. Iwasaki. "High-resolution pH imaging sensor for microscopic observation of microorganisms". In: *Sensors and Actuators B: Chemical* 34.1-3 (1996), pp. 234–239. DOI: 10.1016/S0925-4005(96)01903-X.

[5] S. Inoue, M. Nakao, T. Yoshinobu, and H. Iwasaki. "Chemical-imaging sensor using enzyme". In: *Sensors and Actuators, B: Chemical* 32.1 (1996), pp. 23–26. DOI: 10.1016/0925-4005(96)80104-3.

[6] T. Yoshinobu, H. Iwasaki, M. Nakao, S. Nomura, T. Nakanishi, S. Takamatsu, and K. Tomita. "Application of chemical imaging sensor to electro generated pH distribution". In: *Japanese Journal of Applied Physics* 37.3B (1998), pp. L353–L355. DOI: 10.1143/JJAP.37.L353.

[7] T. Yoshinobu, H. Iwasaki, Y. Ui, K. Furuichi, Y. Ermolenko, Y. Mourzina, T. Wagner, N. Näther, and M. J. Schöning. "The light-addressable potentiometric sensor for multi-ion sensing and imaging". In: *Methods* 37.1 (2005), pp. 94–102. DOI: 10.1016/j.ymeth.2005.05.020.

[8] A. Poghossian and M. J. Schöning. "Silicon-based chemical and biological field-effect sensors". In: *Encyclopedia of Sensors*. Ed. by C. A. Grimes, E. C. Dickey, and M. V. Pishko. Vol. X. Santa Clarita, California, USA: American Scientific Publishers, 2006, pp. 1–71.

[9] W. Moritz, I. Gerhardt, D. Roden, M. Xu, and S. Krause. "Photocurrent measurements for laterally resolved interface characterization". In: *Fresenius' Journal of Analytical Chemistry* 367.4 (2000), pp. 329–333. DOI: 10.1007/s002160000409.

[10] Z. Qintao, W. Ping, W. J. Parak, M. George, and G. Zhang. "A novel design of multi-light LAPS based on digital compensation of frequency domain". In: *Sensors and Actuators, B: Chemical* 73.2-3 (2001), pp. 152–156. DOI: 10.1016/S0925-4005(00)00696-1.

[11] T. Yoshinobu, M. J. Schöning, R. Otto, K. Furuichi, Y. Mourzina, Y. Ermolenko, and H. Iwasaki. "Portable light-addressable potentiometric sensor (LAPS) for multisensor applications". In: *Sensors and Actuators, B: Chemical* 95.1-3 (2003), pp. 352–356. DOI: 10.1016/S0925-4005(03)00437-4.

[12] T. Wagner, R. Molina, T. Yoshinobu, J. P. Kloock, M. Biselli, M. Canzoneri, T. Schnitzler, and M. J. Schöning. "Handheld multi-channel LAPS device as a transducer platform for possible biological and chemical multi-sensor applications". In: *Electrochimica Acta* 53.2 (2007), pp. 305–311. DOI: 10.1016/j.electacta.2007.04.006.

[13] K. Miyamoto, Y. Kuwabara, S. Kanoh, T. Yoshinobu, T. Wagner, and M. J. Schöning. "Chemical image scanner based on FDM-LAPS". In: *Sensors and Actuators, B: Chemical* 137.2 (2009), pp. 533–538. DOI: 10.1016/j.snb.2008.12.008.

[14] C. F. Werner, S. Schusser, H. Spelthahn, T. Wagner, T. Yoshinobu, and M. J. Schöning. "Field-programmable gate array based controller for multi spot light-addressable potentiometric sensors with integrated signal correction mode". In: *Electrochimica Acta* 56.26 (2011), pp. 9656–9660. DOI: 10.1016/j.electacta.2011.03.012.

[15] T. Wagner, C. F. Werner, K. Miyamoto, M. J. Schöning, and T. Yoshinobu. "A high-density multi-point LAPS set-up using a VCSEL array and FPGA control". In: *Sensors and Actuators, B: Chemical* 154.2 (2011), pp. 124–128. DOI: 10.1016/j.snb.2010.03.009.

[16] T. Wagner, C. F. Werner, K. Miyamoto, M. J. Schöning, and T. Yoshinobu. "Development and characterisation of a compact light-addressable potentiometric sensor (LAPS) based on the digital light processing (DLP) technology for flexible chemical imaging". In: *Sensors and Actuators, B: Chemical* 170 (2012), pp. 34–39. DOI: 10.1016/j.snb.2010.12.003.

[17] K. Miyamoto, K. Kaneko, A. Matsuo, T. Wagner, S. Kanoh, M. J. Schöning, and T. Yoshinobu. "Miniaturized chemical imaging sensor system using an OLED display panel". In: *Procedia Engineering* 5 (2010), pp. 516–519. DOI: 10.1016/j.proeng.2010.09.160.

[18] L. Bousse, S. Mostarshed, D. Hafeman, M. Sartore, M. Adami, and C. Nicolini. "Investigation of carrier transport through silicon wafers by photocurrent measurements". In: *Journal of Applied Physics* 75.8 (1994), pp. 4000–4008. DOI: 10.1063/1.356022.

[19] G. Verzellesi, L. Colalongo, D. Passeri, B. Margesin, M. Rudan, G. Soncini, and P. Ciampolini. "Numerical analysis of ISFET and LAPS devices". In: *Sensors and Actuators, B: Chemical* 44.1-3 (1997), pp. 402–408. DOI: 10.1016/S0925-4005(97)00233-5.

[20] M. George, W. J. Parak, I. Gerhardt, W. Moritz, F. Kaesen, H. Geiger, I. Eisele, and H. E. Gaub. "Investigation of the spatial resolution of the light-addressable potentiometric sensor". In: *Sensors and Actuators, A: Physical* 86.3 (2000), pp. 187–196. DOI: 10.1016/S0924-4247(00)00455-6.

[21] L. Chen, Y. Zhou, S. Jiang, J. Kunze, P. Schmuki, and S. Krause. "High resolution LAPS and SPIM". In: *Electrochemistry Communications* 12.6 (2010), pp. 758–760. DOI: 10.1016/j.elecom.2010.03.026.

[22] M. J. Schöning, C. Schmidt, J. Schubert, W. Zander, S. Mesters, P. Kordos, H. Lüth, A. Legin, B. Seleznev, and Y. G. Vlasov. "Thin film sensors on the basis of chalcogenide glass materials prepared by pulsed laser deposition technique". In: *Sensors and Actuators, B: Chemical* 68.1-3 (2000), pp. 254–259. DOI: 10.1016/S0925-4005(00)00438-X.

[23] Y. G. Mourzina, M. J. Schöning, J. Schubert, W. Zander, A. V. Legin, Y. G. Vlasov, and H. Lüth. "Copper, cadmium and thallium thin film sensors based on chalcogenide glasses". In: *Analytica Chimica Acta* 433.1 (2001), pp. 103–110. DOI: 10.1016/S0003-2670(00)01384-2.

[24] A. Poghossian and M. J. Schöning. "Detecting both physical and (bio-)chemical parameters by means of ISFET devices". In: *Electroanalysis* 16.22 (2004), pp. 1863–1872. DOI: 10.1002/elan.200403074.

[25] J. C. Owicki and J. W. Parce. "Biosensors based on the energy metabolism of living cells: The physical chemistry and cell biology of extracellular acidification". In: *Biosensors & Bioelectronics* 7.4 (1992), pp. 255–272. DOI: 10.1016/0956-5663(92)87004-9.

[26] T. Yoshinobu, H. Ecken, A. B. M. Ismail, H. Iwasaki, H. Lüth, and M. J. Schöning. "Chemical imaging sensor and its application to biological systems". In: *Electrochimica Acta* 47.1-2 (2001), pp. 259–263. DOI: 10.1016/S0013-4686(01)00564-3.

[27] C. F. Werner, C. Krumbe, K. Schumacher, S. Groebel, H. Spelthahn, M. Stellberg, T. Wagner, T. Yoshinobu, T. Selmer, M. Keusgen, M. E. M. Baumann, and M. J. Schöning. "Determination of the extracellular acidification of *Escherichia coli* by a light-addressable potentiometric sensor". In: *physica status solidi (a)* 208.6 (2011), pp. 1340–1344. DOI: 10.1002/pssa.201001141.

4.5 Supporting information

4.5.1 Scanning LAPS

In order to investigate the physically limited, lateral resolution of the used LAPS chips, a compact LAPS set-up utilising a single laser diode that is movable due to piezo-electric linear motors was developed. The complete work of this section is published as conference proceedings in German language in:

> C. F. Werner, A. Mansour, F.-M. Rateike, S. Schusser, T. Wagner, T. Yoshinobu, M. Keusgen, and M. J. Schöning. "Kompakter Aufbau eines lichtadressierbaren potentiometrischen Sensors mit verfahrbarem Diodenlaser". In: *10. Dresdner Sensor-Symposium: 05.–07. Dezember 2011, Dresden*. Ed. by G. Gerlach and A. Schütze. Dresden: TUDpress, 2011, pp. 277–280.

The chosen light source is a diode laser of the type QL78F6S-A from the company QSI. The diode laser has a maximum output of 10 mW and a wavelength of 780 nm. The laser is focused with a lens to a spot diameter of about 70 µm and is operated by a laser-diode driver IC-WJ from the company "IC Haus". This makes it possible to modulate the laser power up to frequencies of 300 kHz by utilising an input voltage. As depicted in Fig. 4.8, the laser diode is placed on top of two piezo-electric linear motors that are installed in an XY arrangement. The motors are from the company Klocke (Aachen, Germany) and have a range of ±9 mm with a repeatability of 40 nm.

The photocurrent is amplified by a self-made transimpedance amplifier. The transimpedance amplifier utilises the operation amplifier OPA656 (Texas Instrument) and has an amplification of $10^6\,\mathrm{V\,A^{-1}}$ as well as an anti-aliasing filter at 120 kHz. The scanning-LAPS set-up is controlled by a self-made LabVIEW software. A data-acquisition card from National Instruments (PCI MIO 16XE 10) is used to sample the photocurrent, applying the bias voltage and generating the modulation voltage for the laser-diode

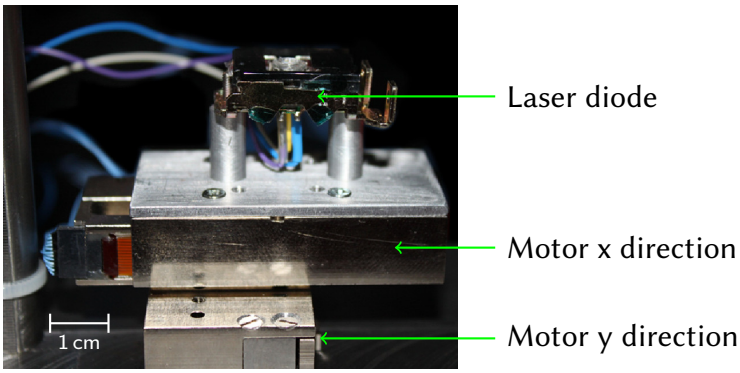

Figure 4.8: Piezo-electric linear motors in XY arrangement with installed laser diode.

driver. By means of the fast Fourier transform (FFT) algorithm, the photocurrent amplitude and phase shift are calculated from the amplified and sampled photocurrent. Thus, the measurement set-up is able to record photocurrent/voltage (I/V) curves at a certain position on the LAPS chip, as well as to record chemical images of the whole sensor surface. To record chemical images, the bias voltage is fixed at a certain value. The LAPS chip is scanned by the laser and the resulting photocurrent at each position is recorded. After that, the photocurrent is plotted in a false-colour image.

Qualitative measurements of the lateral resolution were done with a polymer structure on the LAPS-chip surface. The chemical images were observed at a bias voltage of 0.2 V and a pH-buffer solution with pH 7. The step width of the motors was set to 0.2 mm and the resulting measurement was about 28 min. The results are depicted in Fig. 4.9, with photocurrent amplitude (left) and phase shift (right). The polymeric test structure, which had the shape of a "smiley", can be easily seen. Due to the additional impedance of the polymeric layer, the photocurrent will decrease at the positions with the polymer layer on top. A comparison of the shape sizes shows a good match. The physical diameter of the "nose" is 3.7 mm, whereas it was determined to be 4 mm in the obtained chemical images.

The quantitative investigation of the lateral resolution was done with a LAPS structure with a silicon thickness of 450 µm and an additionally structured gold layer on the sensor surface. In order to achieve line structures with widths of 100 µm, 250 µm, 500 µm, 1 mm and 2 mm, the gold layer was structured by photolithography. The characterisation was done by directly contacting the gold layer, without using any electrolyte or reference electrode. The step width of the motors was set to 0.1 mm and the resulting measurement time for this experiment was about 1 h and 40 min. Figure 4.10 depicts

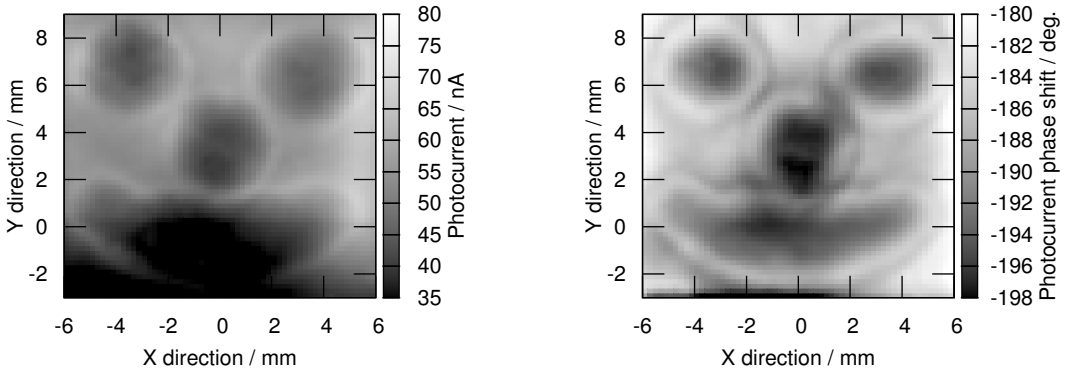

Figure 4.9: Chemical image of a LAPS chip with an additional polymeric structure in shape of a "smiley". The chemical images depict the photocurrent amplitude (left) and the phase shift of the photocurrent (right), referring to their position on the sensor surface.

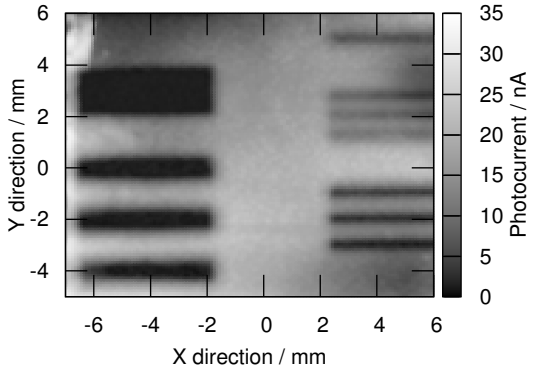

Figure 4.10: Photocurrent amplitude after scanning a LAPS structure with a structured gold layer that consist of different line and space patterns to determine the lateral resolution of the LAPS. The line and space pattern are as followed: 2 mm top left, 1 mm bottom left, 500 µm bottom right, 250 µm middle right and 100 µm top right.

the resulting photocurrent amplitude. The line structures with a width of 500 µm, 1 mm and 2 mm are clearly distinguishable. The 250 µm structures are somewhat fuzzy and the 100 µm lines could no longer be detected. Since the step width and the light-spot diameter is smaller, the physically limited lateral resolution of the LAPS chip can be specified to be about 250 µm, which is in the region of the pixel size of the OLED display.

5 Comparison of label-free ACh-imaging sensors based on CCD and LAPS

Carl Frederik Werner[a,b], Shoko Takenaga[a,c], Hidenori Taki[c], Kazuaki Sawada[c], Michael J. Schöning[a,b]

[a] *Institute of Nano- and Biotechnologies, Aachen University of Applied Sciences, Jülich, Germany*
[b] *Peter Grünberg Institute (PGI-8), Research Centre Jülich, Jülich, Germany*
[c] *Toyohashi University of Technology, Toyohashi, Japan*

Published in: *Sensors and Actuators B: Chemical*, Vol. 177, pp. 745–752, DOI: 10.1016/j.snb.2012.11.012

Submitted: 2012-07-13; Accepted: 2012-11-06; Published: 2012-11-22

Abstract:

Semiconductor-based chemical imaging sensors, like the light-addressable potentiometric sensor (LAPS) or the pH-imaging sensor based on a charge-coupled device (CCD), are becoming a powerful tool for label-free imaging of biological phenomena. We have proposed a polyion-based enzymatic membrane to develop an acetylcholine (ACh) imaging sensor for neural cell-activity observations. In this study, a CCD-type ACh-imaging sensor and a LAPS-type ACh-imaging sensor were fabricated and the prospect of both sensors was clarified by making a comparison of their basic characteristics.

5.1 Introduction

A semiconductor-based chemical sensor provides many advantages such as smaller size, low cost, mass production and multiple integrated functions, for the life-science field. The most familiar semiconductor-based chemical sensor is the ion-sensitive field-effect transistor (ISFET), which was introduced in 1970 for neurophysiological measurements [1], and much fundamental research has been performed for food administration, environmental as well as biological measurements [2, 3]. In biological and medical field, it is getting more important and necessary to achieve 2- or 3-dimensional information of organic activity in human body. Bioimaging tools are an effective way to visualise this. One of them, the fluorescence imaging, allows us to observe the function of ions and chemical species in living cells [4, 5].

On the other hand, the light-addressable potentiometric sensor (LAPS) [6–9] and charge-transfer-type ion-imaging sensor (CCD) [10–12] have been recently developed as semiconductor-based chemical imaging tools. These chemical imaging tools are devices that not only determine quantity, but also acquire label-free images of the local distribution of ions and chemical species in liquid solution with real-time. So far, semiconductor-based chemical imaging sensors are allowed to image not only hydrogen ions but also other ions (e.g., Li^+, Na^+, K^+, Ca^{2+}, Cu^{2+}, Cd^{2+}) [13–19] and chemical species (e.g., glucose and penicillin) [20–25] in solution, by only using an additional selective membrane on the sensor surface.

Due to the semiconductor microfabrication technology and large-scale integration (LSI) technology, semiconductor-based chemical imaging sensors provide a high spacial and time resolution as well as sensitivity. Using a selective membrane (i.e., with enzymes or ionophores), the specific detection of ions or chemical species in solution can be achieved. Semiconductor-based chemical imaging sensors have a potential to be applied in the microbiological and medical field and might help to observe micro-scaled structures such as single cells, cell groups and neuronal networks.

Imaging the instantaneous movement of neurotransmitters is essential for the understanding of neuronal communication [26]. One of the most important neuronal transmitters is acetylcholine (ACh). There is clinical evidence indicating that some neuropsychiatric disorders such as Parkinson disease, Alzheimer disease and myasthenia gravis are correlated with long-term cell degeneration with dysfunctional ACh regulation [27]. However, other studies such as fluorescence imaging have not been achieved to image directly ACh [28].

Recently, we have successfully developed a 32×32 charge-transfer-type ACh-imaging sensor array by immobilising an enzyme membrane (acetylcholine esterase (AChE)) on the sensor [29]. With the help of this membrane we also developed a LAPS-type ACh-imaging sensor. Both sensors are based on the field effect in an elec-

trolyte/insulator/semiconductor (EIS) structure, however, the readout mechanism is different.

Our aim is to compare both sensor types, to observe if they are usable as ACh-imaging sensors and to find their advantages and disadvantages. With these informations we can define useful application fields for each type of sensor and define further improvements.

To compare the response of the used ACh-imaging sensors it is helpful to compare their output with a theoretical model of enzyme-potentiometric sensors. In [30], Ogundiran *et al.* provide a model that describes the complex response of enzyme-potentiometric sensors utilising a pH-sensitive membrane. This model shows that, when the enzyme sensor operates under analyte diffusion-controlled conditions, the response can be predicted by a simplified algebraic equation, which is independent of the actual kinetics of the enzymatic reaction. The equation in case of an enzymatic reaction producing a weak acid is given in equation (5.1).

$$C_{\mathrm{S}}^{\mathrm{b}} = \frac{\left(C_{\mathrm{H^+}}^{0} - \alpha_{\mathrm{H}} C_{\mathrm{H^+}}^{\mathrm{b}}\right)}{\alpha_{\mathrm{S}} \gamma_{\mathrm{A}} \overline{D}_{\mathrm{S}}} \times \left[1 + \frac{\overline{D}_{\mathrm{EH}} \alpha_{\mathrm{E}} C_{\mathrm{TE}}^{\mathrm{b}} K_{\mathrm{E}}}{\left(K_{\mathrm{E}} + \alpha_{\mathrm{H}} C_{\mathrm{H^+}}^{\mathrm{b}}\right)\left(K_{\mathrm{E}} + d_{\mathrm{E}} C_{\mathrm{H^+}}^{0}\right)}\right] \times \left(1 + \frac{\overline{D}_{\mathrm{AH}} C_{\mathrm{H^+}}^{0}}{\left(\overline{D}_{\mathrm{A^-}}\right) K_{\mathrm{A}}}\right) \quad (5.1)$$

This equation describes the relation of the analyte concentration in the bulk solution $C_{\mathrm{S}}^{\mathrm{b}}$ to the measured hydrogen-ion concentration (or pH value) at the sensor surface $C_{\mathrm{H^+}}^{0}$. The total externally added pH-buffer concentration $C_{\mathrm{TE}}^{\mathrm{b}}$ and the H^+ concentration $C_{\mathrm{H^+}}^{\mathrm{b}}$ in the bulk solution will also have an affect to the sensor response. Other parameters are the stoichiometric coefficient of the produced acid γ_{A} in the enzyme reaction, the dissociation constant of the pH buffer K_{E} and the produced weak acid K_{A}, and the partition coefficient between membrane and bulk phases of the hydrogen ions α_{H}, the analyte α_{S} and the buffer α_{E}. Also the diffusion coefficients of all involved species are necessary. They are given as dimensionless diffusion coefficient $\overline{D}_i = D_i / D_{\mathrm{H^+}}$ for the species i (S: analyte, EH: undissociated buffer, AH: undissociated acid and A^-: dissociated acid). The diffusion coefficient of the dissociated buffer is defined by the diffusivity ratio $d_{\mathrm{E}} = D_{\mathrm{EH}} / D_{\mathrm{E^-}}$. Equation (5.1) is valid for a well-stirred solution and diffusion-controlled conditions in the enzymatic film, where the substrate concentration on the sensor surface is negligible compared to $\alpha_{\mathrm{S}} C_{\mathrm{S}}^{\mathrm{b}}$.

5.2 Methods

The two used sensors, namely the LAPS and the charge-coupled device (CCD)-type imaging sensor, are semiconductor-based potentiometric sensors. These kinds of sensors

consist of an EIS structure. Usually, on top of the insulating layer, there is an additional ion- or charge-sensitive layer that serves as a transducer material. At the transducer part of the electrolyte/insulator interface, a concentration-depending potential φ will occur in case of a pH-sensitive transducer, according to the site-binding model [31]. Together with an applied bias voltage, this potential will influence the space-charge region on the insulator/semiconductor interface. The bias voltage is applied across the EIS structure between the rear side and the electrolyte with the help of a reference electrode. Depending on the readout mechanism of the sensor principle, the change of the space-charge region can be determined in different ways: A capacitive EIS sensor will read out the capacitance of the space-charge region [32], whereas the ISFET will monitor the conductivity of the inversion layer [1]. In case of the LAPS, a photocurrent that depends on the width of the space-charge region will be generated by illuminating the semiconductor with a modulated light source [6–9]. For a CCD-type sensor, the depth of the potential well is read out by using a charge-transfer technique (fill and spill). This sensor converts the depth of the potential well into a charge quantity, and the amount of charge is represented as an output voltage by a source-follower circuit [10–12].

5.2.1 LAPS

Figure 5.1a depicts schematically the LAPS principle. The LAPS structure consists of a single EIS structure. Because of illuminating from rear side, the rear-side contact is

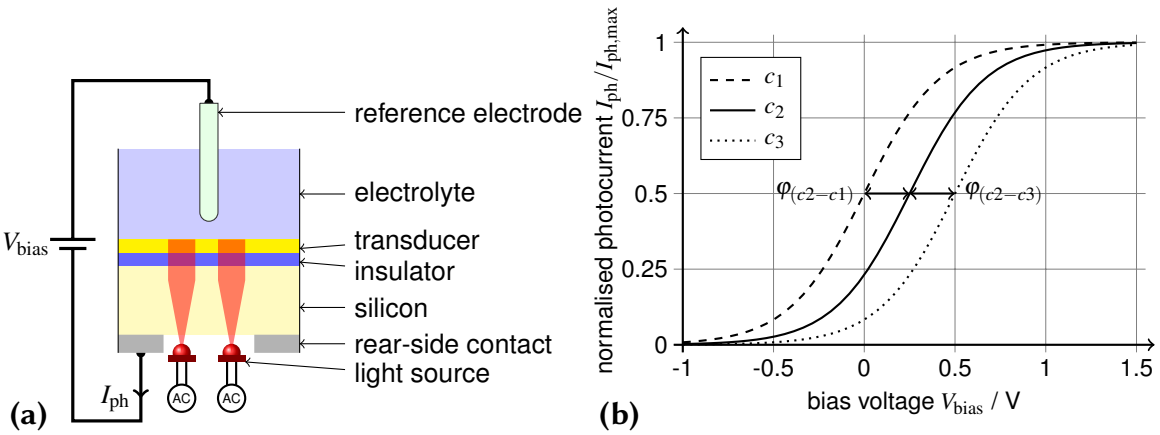

Figure 5.1: Schematic drawing of the LAPS principle (a). A bias voltage V_{bias} is applied across the sensor structure. By utilising a modulated light pointer, a concentration-dependent photocurrent I_{ph} is generated. The relation between I_{ph} and V_{bias} depicts the simulated I/V curve (b) of the LAPS with p-doped silicon. The concentration-dependent potential φ will result in a shift of the I/V curve as shown by different analyte concentrations ($c_1 > c_2 > c_3$).

removed partly. The concentration change of the analyte on the sensor surface influences the space-charge region on the insulator/semiconductor interface locally. With a focused and modulated light pointer shining into the semiconductor, electron-hole pairs are generated. If these electron-hole pairs move to the space-charge region they will be separated, and thus, a measurable photocurrent I_{ph} will occur. The photocurrent I_{ph} depends on the local width of the space-charge region at the illuminated area and consequently, on the local concentration of the analyte of interest on the sensor surface. Measuring the photocurrent amplitude versus the applied bias voltage results in I/V curves as shown in Figure 5.1b. Due to the additional potential a concentration change will cause a shift of the I/V curve along the bias-voltage axis. This voltage shift provides the surface potential and after a calibration, a direct relationship to the analyte concentration on the sensor surface.

As discussed in [33–37], multiple measurement spots can be read out concurrently by using multiple light pointers, driven at different frequencies. Subsequently, the frequency components of the resulting photocurrent can be separated. By mapping the frequencies with the position of the light pointers, the concentration distribution can be determined. In addition, to reduce the measurement time, only at the beginning of a measurement complete I/V curves of all measurement spots were determined simultaneously. After that, the bias voltage is fixed at a constant value. With the help of the reverse functions of the I/V curves from each measurement spot, the surface potential can be calculated from the measured photocurrent amplitudes.

The used LAPS set-up is described in detail in [37]. It consists of a 4×4 infrared light-emitting diode (LED) array that is driven by a field-programmable gate array (FPGA). This results in 16 measurement spots with a diameter of about 3 mm and a pitch width of 3.5 mm. A Ag/AgCl-reference electrode from Metrohm was used to contact the electrolyte. The LAPS chip with an active area of 15 mm $\times$ 15 mm is build up of thin films of: 60 nm Ta_2O_5, 30 nm SiO_2, about 450 µm p-doped silicon and an Al rear-side contact. The LED driver is configured to apply the maximum brightness amplitude for the LEDs. To drive the LEDs concurrently, the modulation frequency of LED 1 was set to 1 kHz and the frequency of the following LEDs were increased by 50 Hz, resulting in a modulation frequency of 1.75 kHz for LED 16 [37]. The photocurrent was sampled for a period of 100 ms and the frequency components were calculated by fast Fourier transform (FFT). For the measurements, the sampling of the photocurrent is repeated each 200 ms.

5.2.2 Charge-transfer-type pH-imaging sensor

A cross section and the operation mechanism of the conventional charge-transfer-type pH sensor are shown in Fig. 5.2. Si_3N_4 is used as transducer layer and the depth of the

potential in the silicon at the sensing areas is varied with hydrogen ions in the solution (Fig. 5.2a). The sensing signals, which are the potential difference between the input control gate and the sensing area (Fig. 5.2c), are output as signal charges using the charge-transfer technique (Fig. 5.2e). The sensor converts the depth of the potential well into a charge amount (Fig. 5.2f), and the amount of charge is represented as an output voltage by a source-follower circuit.

A pH-imaging sensor chip was composed of a 32×32 pixel array and complementary metal-oxide-semiconductor (CMOS) with horizontal and vertical shift registers as read-out circuits. The sensor was fabricated in array form using LSI technology. Therefore, CCD-type sensors have the potential to integrate various kinds of CMOS circuits (e.g., a noise-cancelling circuit and an analog-to-digital (A/D) converter as a signal-processing circuit) onto the chip. The chip size is 8.0 mm $\times$ 7.4 mm. Each pixel is 130 µm $\times$ 130 µm

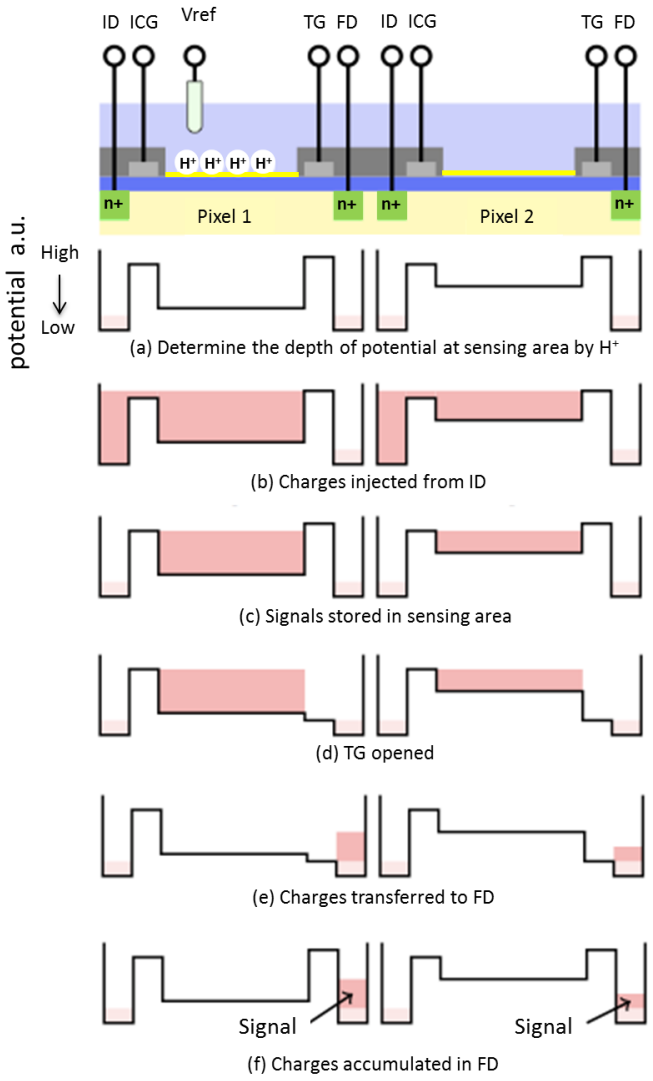

Figure 5.2: Schematic drawing of the CCD principle with an example of two pixels and one reference electrode (Vref). Each pixel consists of a sensing area and four electrodes: input diode (ID), input control gate (ICG), transfer gate (TG) and floating diffusion (FD). Below the schematic, the potential wells of one measurement cycle is shown. In this example, the left pixel has a higher H^+ concentration. (a) Potential well under the pH sensor. (b) Charges are injected from ID. (c) Signal changes determined by H^+ are stored in the sensing area. (d) TG is opened. (e) Signal charges are transferred to FD. (f) Signal charges are accumulated in FD.

with a sensing area of approximately 40 µm². Each pixel has a selection transistor, which turns on the selected signal. The selected signal for each pixel is supplied externally from a pulse generator. The pH signals are output serially after being converted into electrical voltage signals in each pixel. The output signals from the sensors are processed through an external A/D converter before being input to a computer. Computer software converts the signals into a real-time moving image at 5 frames s^{-1}.

5.2.3 Polyion-complex enzyme membrane

The principle of the proposed ACh-imaging sensor is based on the enzyme reaction of AChE, specifically the oxidation of ACh according to the reaction in equation (5.2).

$$\mathrm{ACh} + \mathrm{H_2O} \xrightarrow{\mathrm{AChE}} \text{choline} + \mathrm{CH_3COO^-} + \mathrm{H^+} \tag{5.2}$$

The use of a polyion-complex enzyme membrane is one of the comprehensive methods to immobilise the enzymes on a substrate. AChE is enclosed in the membrane by the electrostatic force of the polycation with a positive charge, poly(L-lysine) hydrobromide (PLL), and the polyanion with a negative charge, poly(sodium-4-styrenesulfonate) (PSS), as shown in Fig. 5.3. The electrostatic force is achieved by the adjustment of numbers of charges into PSS and PLL equivalently. This method has the advantage that the enzyme could be immobilised adjacent to the sensor surface with a high density [38].

All the chemicals used in the experiments were purchased from Sigma-Aldrich. AChE is derived from Electrophorus electricus, PLL (polyanion, molecular weight 70 ku to 150 ku) and PSS (polycation, average molecular weight 70 ku) were used to fabricate the polyion-complex membrane.

Phosphate-buffered solution (PB, pH 7.0, 20 mM) as the supporting electrolyte was prepared by mixing solutions of 20 mM KH_2PO_4 and 20 mM Na_2HPO_4. Three different aqueous solutions were diluted with PB as follows; PLL (60 mM in monomer units), AChE (5 Units μl^{-1}) and PSS (75 mM in monomer units). The three aqueous solutions

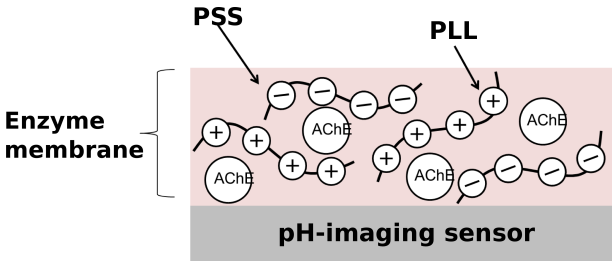

Figure 5.3: Polyion-complex enzyme membrane enclosing AChE by the electrostatic force of PLL and PSS close to the pH-imaging sensor surface.

were mixed and placed on the sensing area of the sensors. For the LAPS, 300 µl of each solution was mixed and for the CCD-type sensor, 20 µl. These quantities of solutions were chosen to achieve the same enzyme density of about 6 Units mm^{-2} on both sensors. After placing these mixtures on the sensors they were allowed to dry overnight at room temperature.

The analyte solutions with different ACh concentrations were prepared by diluting acetylcholinechloride (Sigma-Aldrich) with PB.

5.3 Results and discussion

5.3.1 pH measurements

To confirm the basic characteristics of the LAPS and the CCD-type sensors as pH-imaging sensor, standard buffer solutions with values of pH 4.0, pH 5.0, pH 6.0, pH 7.0, pH 8.0, pH 9.0 for LAPS, and pH 1.68, pH 4.01, pH 6.86, pH 9.18, pH 10.0 for the CCD-type sensor, were used. The calculated mean values for one pixel of the array sensors are shown in Fig. 5.4. For both sensors, a shift in the chemical potential was observed by varying the pH-buffer solutions. It is obvious that the output signal of a single pixel varies linearly with pH. More detailed pH measurements with more pH values can

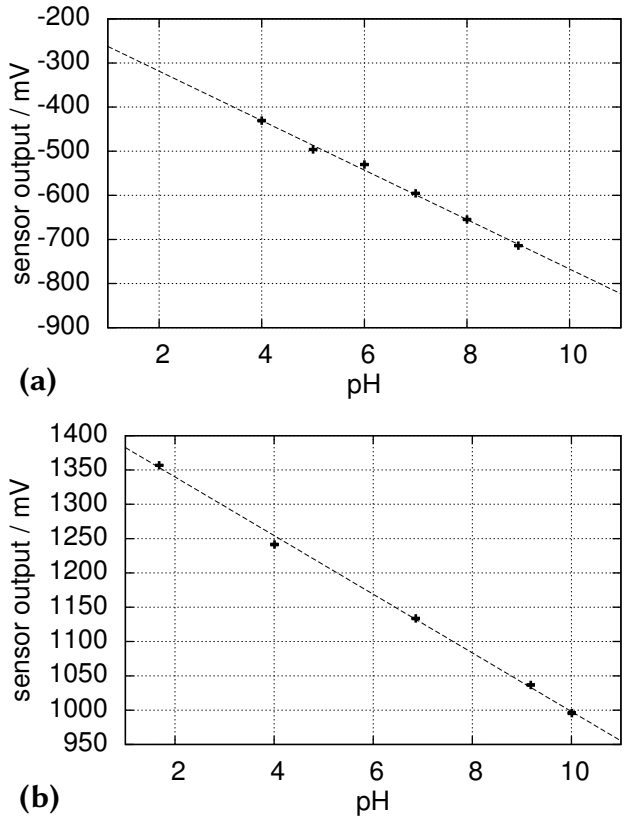

Figure 5.4: Response of the LAPS (a) and CCD (b) set-up to different pH values. For each pH-buffer solution, the output signal was measured 8 times. The mean value and the RMS (error bars) of these measurements are plotted against the pH value. The dashed lines represent the linear regressions.

be found elsewhere [8–11]. The sensitivity was calculated from the plot of Fig. 5.4 by means of linear regression. The error bars show the variation of the measurements and are calculated as root mean square (RMS) voltage. For the LAPS, the sensitivity was 56.0 mV pH^{-1}, which agrees with the reported value of Ta_2O_5 in the range of 55 mV pH^{-1} to 58.5 mV pH^{-1} [32]. By measuring every 200 ms at pH 7 for 60 s a variation of 0.85 mV was achieved and results to a pH resolution of about 0.015 pH.

For the CCD-type sensor, the sensitivity, defined by the sensor-output signal, was 42.7 mV pH^{-1}. Depending on the fabrication conditions of the plasma-enhanced vapour deposition parameters and thus, the number of hydroxyl-group dangling bonds, the sensitivity of the Si_3N_4 transducer surface can vary between about 20 mV pH^{-1} and 45 mV pH^{-1}. In addition, to obtain the "real" sensitivity of the transducer layer, the surface potential must be taken into consideration from the sensor output. This strongly depends on various parameters such as the relative capacitances of the sensing region and the floating diffusion region. From the characteristics of the voltage change on the reference electrode, it is estimated that the sensitivity of the ion-sensitive Si_3N_4 layer is about 52 mV pH^{-1}, which agrees with the reported range of 46 mV pH^{-1} to 58 mV pH^{-1} [32]. By measuring every 200 ms at pH 6.86 for 60 s a variation of 2.4 mV was achieved and results to a pH resolution of about 0.115 pH. We have previously reported a pH resolution of 0.005 pH for a single pixel CCD-based pH sensor without readout circuits [39], which is better than that for the present imaging sensor. The signal variation (i.e., noise source) of the integrated readout circuits in case of the sensor array should therefore be examined in more detail in a further experiment.

5.3.2 ACh measurements

Figure 5.5 shows photographs of the two used sensor chips with immobilised AChE membrane. The enzyme-based LAPS is shown left and the CCD-type enzymatic sensor right, respectively. The enzyme activity of these sensors was about 6 Units mm^{-2}.

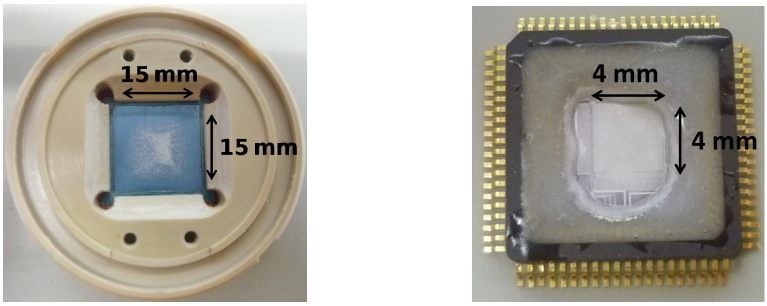

Figure 5.5: Photographs of the ACh-imaging sensor based on LAPS (left) and CCD-type sensor (right) with immobilised polyion-complex AChE membrane.

The response over time of one pixel of each sensor to an ACh-concentration step is presented in Fig. 5.6. At the beginning of the experiment it was measured with phosphate-buffer solution (300 µl for LAPS and 60 µl for CCD-type sensor with pH sensitivities of 56 mV pH^{-1} and 20.5 mV pH^{-1}, respectively). Then, at time $t_0 = 20$ s, a phosphate buffer with 40 mM ACh (100 µl for LAPS and 20 µl for CCD-type sensor) was added and results in a final ACh concentration of 10 mM. The LAPS measurement shows at 20 s a peak-like behaviour ("dip") in the sensor signal. This is mainly induced by opening the measurement (Faraday) cage for adding the ACh solution and originally results from the light sensitivity of the LAPS chip. The dashed line approximates the exponential fit corresponding to equation (5.3).

$$v(t) = \hat{V}\left(1 - \mathrm{e}^{-(t-t_0)/\tau}\right) + V_\mathrm{o} \tag{5.3}$$

Here, $\hat{V}$ is the voltage change, V_o is the offset voltage and τ is the time constant. The response time is $\tau = 13$ s for the LAPS and $\tau = 4.3$ s for the CCD-type sensor. This result indicates that the data of response time is involved in the enzymatically caused reaction time and the time to mix the solutions. To discuss the response time in more detail, further investigations are required by using a fluidic system.

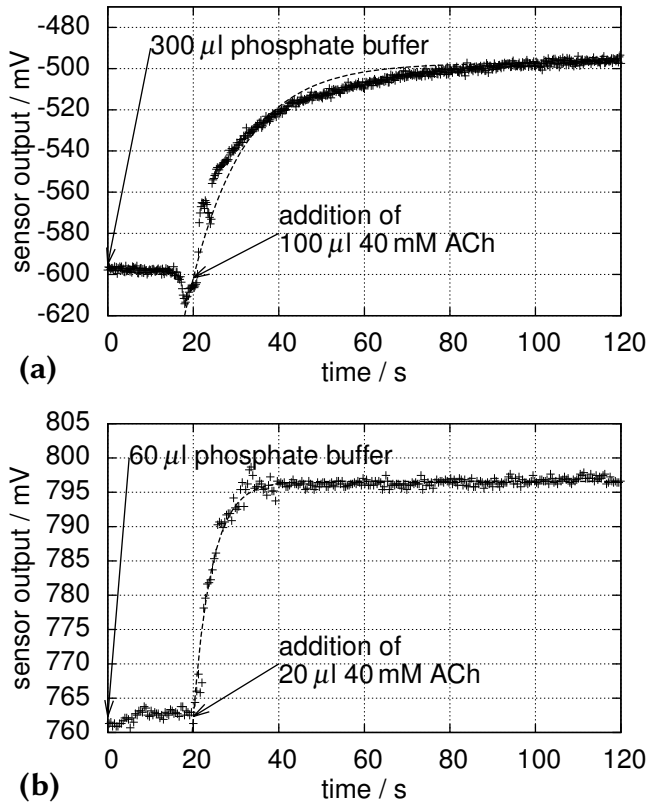

Figure 5.6: Sensor response of LAPS- (a) and CCD-type (b) ACh sensors. At the beginning was measured with phosphate buffer without ACh. Then, at time $t_0 = 20$ s, a phosphate buffer with ACh was added. The dashed line shows the exponential fit.

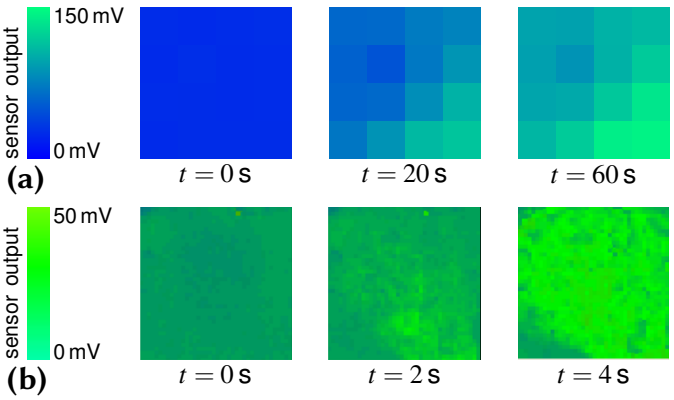

Figure 5.7: Real-time measurement of LAPS (a) and CCD (b) set-up. At the beginning, it was measured with phosphate-buffer solution (300 µl for LAPS and 60 µl for CCD-type sensor). Then, a 40 mM droplet (100 µl for LAPS and 20 µl for CCD-type sensor) was added in the right bottom corner.

Real-time investigations with a measurement time of 200 ms per frame have been performed with both sensor types as shown in Fig. 5.7. Here, the diffusion of a 40 mM ACh-containing droplet added at the right bottom corner in 20 mM PB solution to the particular sensor surface and the subsequent catalytic conversion by the enzyme on top of the sensor surface have been monitored. The results demonstrated the ability of both sensor types to determine those changes spatially and time-resolved.

The response of both sensor types towards different ACh concentrations from 1 µM to 1 M was investigated as calibration measurement in Fig. 5.8, which underlines the expected dependence. In the vertical axis, the sensor-output change with each concentration step was plotted. The sensitivity between 1 mM and 10 mM is 103 mV/p[ACh] in case of the LAPS and 32 mV/p[ACh] in case of the CCD sensor. The different behaviour in the signal amplitude of the sensor-output signal can be explained by the different amplification of the output signal of both sensor types and is in good agreement with the variation of the original pH sensitivity in Fig. 5.4.

In previous work, short-term measurements were performed with a CCD-type ACh-imaging sensor to confirm the activity of the enzyme for repeated measurements [29]. In these experiments, ACh-calibration measurements were performed three times and the resulting repeatability (relative standard deviation) was 8.8 %.

The enzyme membrane on the LAPS sensor possesses a good long-term stability, which is probably due to the absolutely flat sensor surface of the LAPS compared to the more "rougher" surface (caused by the photolithographic patterning) of the CCD-type sensor. Thus, long-term measurements were performed with this sensor after 3 days and 13 days. Between these experiments, the LAPS chip was stored at 4 °C. The results are depicted in Fig. 5.8a, too. The sensitivity of the LAPS chips decreases at higher ACh

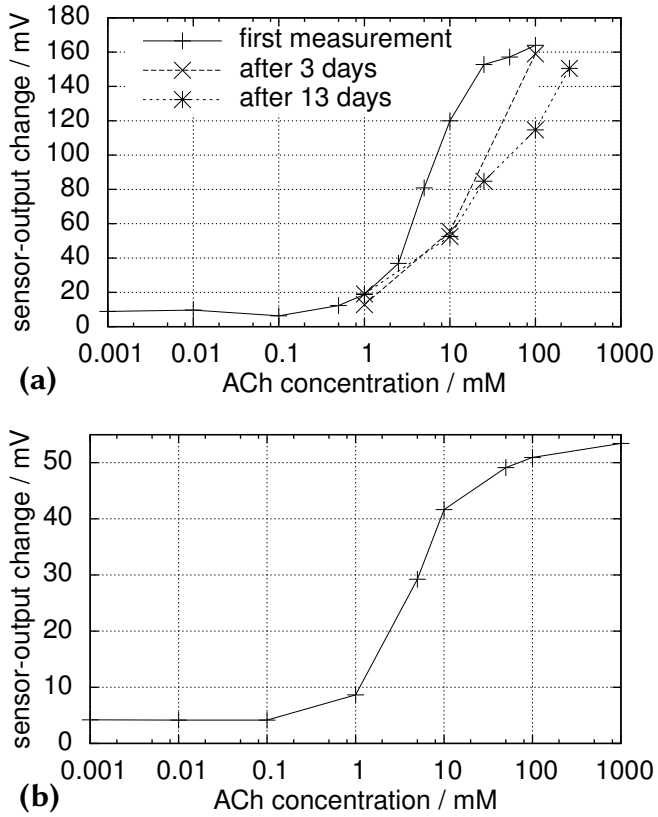

Figure 5.8: Sensor-output change of the LAPS (a) and CCD (b) set-up, respectively, at different ACh concentrations. The measurements were performed, like in Fig. 5.6, and the resulting sensor-signal change is plotted against the ACh concentration.

concentrations over time, which could be explained by a decrease of the enzymatic activity.

To compare the calibration measurements of both ACh sensors, the measured pH value on the sensor surface has been calculated. These calculated pH values are presented in Fig. 5.9 and in addition, the theoretical response by using equation (5.1) has been considered. For this, we used partition coefficients of $\alpha_S = \alpha_H = \alpha_E = 0.5$, the stoichiometric coefficient $\gamma_A = 1$, a diffusivity ratio of $d_E = 1$ and as dimensionless diffusion coefficient $\overline{D}_S = \overline{D}_{EH} = \overline{D}_{AH} = \overline{D}_{A^-} = 0.1$. The dissociation constant for the phosphate buffer and the acetate (CH_3COO^-) is $K_E = 10^{-7.21}$ and $K_A = 10^{-4.7}$, respectively. These values have been also suggested in [30]. The hydrogen-ion concentration of the bulk solution was $C^b_{H^+} = 10^{-7}$ M, and the total concentration of the phosphate buffer was $C^b_{TE} = 20$ mM according to the experimental conditions. For ACh concentrations up to 5 mM, the pH changes of both sensors are nearly the same and up to 3 mM they fit to the theoretically expected response. At higher ACh concentrations, the sensors begin to saturate because here, the sensor responses are no longer diffusion-controlled and thus, equation (5.1) is no more valid. Also, the low pH inside the enzyme layer will inactivate the AChE. According to equation (5.1), a pH change at the sensor surface from pH 7 to pH 6.98 results in a calculated/measured ACh concentration of 0.1 mM

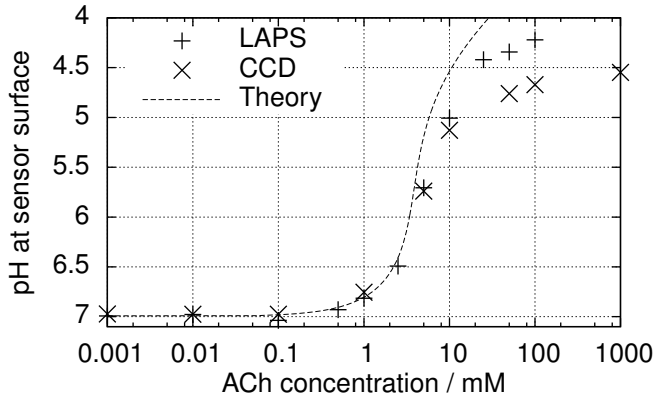

Figure 5.9: Calculated pH value at the sensor surface of the LAPS and CCD-type sensor, respectively, at different ACh concentrations from the measurement routine of Fig. 5.8 and previously determined pH sensitivities. The dashed line depicts the theoretical response of an enzyme-based potentiometric sensor calculated by equation (5.1) with $\alpha_S = \alpha_H = \alpha_E = 0.5$, $\gamma_A = 1$, $K_E = 10^{-7.21}$, $K_A = 10^{-4.7}$, $C^b_{H^+} = 10^{-7}$ M, $C^b_{TE} = 20$ mM, $d_E = 1$ and $\overline{D}_S = \overline{D}_{EH} = \overline{D}_{AH} = \overline{D}_{A^-} = 0.1$.

and represents the lower detection limit of these sensors under given conditions. To detect even lower ACh concentrations, the buffer concentration should be reduced. Another possibility might be to further improve the sensitivity behaviour by choosing a differential sensor set-up, where one part of the chip is covered by AChE and the other serves as a pH reference (without the enzyme). In this way, initial sensor drift, temperature dependence and disturbing light sensitivity can be reduced significantly.

5.4 Conclusions and outlook

The LAPS- and the CCD-type pH-imaging sensor are chemical imaging sensors and able to measure an analyte on their sensor surface spatially and time-resolved. Both sensor types are responding to pH and are able to determine the analyte ACh with the help of the enzyme AChE, immobilised in a polyion-based membrane. The time resolution of both used sensor set-ups is 200 ms resulting in 5 frames s^{-1}. A comparison of the basic characteristics of both sensors is summarised in Tab. 5.1. The fabrication of the CCD-type sensor is rather complex, but all necessary signal-processing circuits (e.g., shift register) are integrated on the sensor chip by CMOS technology. Because of this, CCD-type sensors allow to obtain chemical images in a "microscopic" range and to process small signals. On the other hand, the LAPS chips are easy to fabricate, whereas the driving of the light sources and the signal processing of the photocurrent have to be done externally from the chip itself. Due to the fact that the measurement

Table 5.1: Properties of the ACh-imaging sensor for the CCD- and LAPS-type set-up.

	LAPS	CCD
Image creating	modulated light pointer	array of CCDs
Electronic circuity	external	integrated
Fabrication complexity	low	high
Resolution	4×4 pixels	32×32 pixels
Pixel pitch	3.5 mm	130 µm
Transducer material	Ta_2O_5	Si_3N_4
pH sensitivity[a]	56.5 mV pH^{-1}	20.5 mV pH^{-1}
Response time to ACh	13 s	4.3 s
Long-term stability	high	low

[a] The pH sensitivity is compared to the sensor-output signal.

spots of the LAPS are defined by external light sources, an alignment to an additional micro-fluidic set-up might be possible. Both sensor set-ups show the same pH changes to different ACh concentrations up to a concentration of 5 mM ACh, and these pH changes also fit well to the theoretical model for enzyme-based potentiometric sensors, discussed in [30]. The long-term stability and adhesion of the enzymatic membrane is better on the LAPS surface, which is probably due to the smooth and unstructured surface. We could show that a measurement of an ACh-LAPS sensor is also possible after 13 days. For the CCD-type sensor, the comparison revealed the importance of a flat surface of the sensor for improvement in membrane adhesion and biological measurements. As an example, flattening of CMOS circuit-wiring of the sensor by chemical-mechanical polishing (CMP), which is one of the semiconductor processes, might lead to an improvement of the CCD-type sensor for biological and medical fields.

In this work, a LAPS with a pixel pitch of about 3.5 mm and a CCD-type sensor with a pixel pitch of 130 µm has been used, respectively. In case of achieving spatially resolved measurements, both sensor types are referring on completely different mechanisms. The LAPS is using a single unstructured EIS structure and one or more light pointers to address the position on the sensor surface. The spatial resolution of the LAPS depends on the size of the focused light spot and the diffusion length of the charge carriers inside the semiconductor. Recent works about LAPS have shown spacial resolutions of about 0.8 µm [40]. The CCD-type sensor is utilising an array of CCDs addressed by employing shift registers. High spatial resolution of CCD-type sensors requires a scaling-down of the CMOS-process technology and currently, a CCD-type sensor with a pixel pitch of 24 µm [41] is under investigation.

The resolution of both sensor types is not yet high enough to determine the release of ACh from single cells. For this, a resolution of less than 10 µm would be necessary to visualise single cells. Nevertheless, the detection of cell groups and the

communication in neuronal networks is possible and was shown with the CCD-type sensor [42]. Because of the proof of neuronal cells on the sensor surface, it would be expected that the concentration of released ACh is high enough to be detectable by the ACh-imaging sensor. The stability in case of the ACh-LAPS set-up should make it principally possible to determine long-term cell degradation for investigating diseases, like Alzheimer and myasthenia. For the future, we suggest to improve the spacial resolution of both sensor types without losing sensitivity and time resolution and to tailor the flatness of the CCD-sensor surface. Taking into account the advantages of miniaturised, semiconductor-based sensor chips that can be fabricated by means of silicon planar technology, these sensors might offer potential application fields such as biomedical engineering, pharmaceutical industry as well as biotechnologies, and environmental monitoring purposes.

Acknowledgements

This work was partially supported by the Core Research for Evolutional Science and Technology (CREST) from Japan Science and Technology Agency (JST), an independent public body of the Ministry of Education, Culture, Sports, Science and Technology (MEXT).

The authors also thank the German Federal Ministry of Food, Agriculture and Consumer Protection (BMELV) and the "Fachagentur Nachwachsende Rohstoffe e.V." (FNR) for partial financial support of this work (Bio-LAPS).

References

[1] P. Bergveld. "Development of an ion-sensitive solid-state device for neurophysiological measurements". In: *IEEE Transactions on Biomedical Engineering* BME-17.1 (1970), pp. 70–71. DOI: 10.1109/TBME.1970.4502688.

[2] T. Matsuo and M. Esashi. "Methods of ISFET fabrication". In: *Sensors and Actuators* 1 (1981), pp. 77–96. DOI: 10.1016/0250-6874(81)80006-6.

[3] P. Bergveld. "Future applications of ISFETs". In: *Sensors and Actuators B: Chemical* 4.1–2 (1991), pp. 125–133. DOI: 10.1016/0925-4005(91)80187-0.

[4] V. Vamvakaki, D. Fournier, and N. A. Chaniotakis. "Fluorescence detection of enzymatic activity within a liposome based nano-biosensor". In: *Biosensors and Bioelectronics* 21.2 (2005), pp. 384–388. DOI: 10.1016/j.bios.2004.10.028.

[5] X. Yang, Z. Zhou, D. Xiao, and M. M. Choi. "A fluorescent glucose biosensor based on immobilized glucose oxidase on bamboo inner shell membrane". In: *Biosensors and Bioelectronics* 21.8 (2006), pp. 1613–1620. DOI: 10.1016/j.bios.2005.08.004.

[6] D. G. Hafeman, J. W. Parce, and H. M. McConnell. "Light-addressable potentiometric sensor for biochemical systems". In: *Science* 240.4856 (1988), pp. 1182–1185. DOI: 10.1126/science.3375810.

[7] J. C. Owicki, L. J. Bousse, D. G. Hafeman, G. L. Kirk, J. D. Olson, H. G. Wada, and J. W. Parce. "The light-addressable potentiometric sensor: Principles and biological applications". In: *Annual Review of Biophysics and Biomolecular Structure* 23 (1994), pp. 87–113. DOI: 10.1146/annurev.bb.23.060194.000511.

[8] M. Schöning, T. Wagner, C. Wang, R. Otto, and T. Yoshinobu. "Development of a handheld 16 channel pen-type LAPS for electrochemical sensing". In: *Sensors and Actuators B: Chemical* 108.1–2 (2005), pp. 808–814. DOI: 10.1016/j.snb.2005.01.055.

[9] T. Wagner, T. Yoshinobu, C. Rao, R. Otto, and M. J. Schöning. ""All-in-one" solid-state device based on a light-addressable potentiometric sensor platform". In: *Sensors and Actuators B: Chemical* 117.2 (2006), pp. 472–479. DOI: 10.1016/j.snb.2005.12.056.

[10] T. Hizawa, K. Sawada, H. Takao, and M. Ishida. "Fabrication of a two-dimensional pH image sensor using a charge transfer technique". In: *Sensors and Actuators B: Chemical* 117.2 (2006), pp. 509–515. DOI: 10.1016/j.snb.2006.01.056.

[11] T. Hizawa, K. Sawada, H. Takao, and M. Ishida. "Characteristics of highly sensitive pH sensors with charge accumulation operation". In: *Japanese Journal of Applied Physics* 45.12 (2006), pp. 9259–9263. DOI: 10.1143/JJAP.45.9259.

[12] S. Takenaga, Y. Tamai, M. Ishida, and K. Sawada. "Charge accumulation type hydrogen ion image sensor with high pH resolution". In: *Japanese Journal of Applied Physics* 50.2 (2011), p. 027001. DOI: 10.1143/JJAP.50.027001.

[13] Y. G. Mourzina, M. J. Schöning, J. Schubert, W. Zander, A. V. Legin, Y. G. Vlasov, and H. Lüth. "Copper, cadmium and thallium thin film sensors based on chalcogenide glasses". In: *Analytica Chimica Acta* 433.1 (2001), pp. 103–110. DOI: 10.1016/S0003-2670(00)01384-2.

[14] T. Yoshinobu, M. J. Schöning, R. Otto, K. Furuichi, Y. Mourzina, Y. Ermolenko, and H. Iwasaki. "Portable light-addressable potentiometric sensor (LAPS) for multisensor applications". In: *Sensors and Actuators, B: Chemical* 95.1-3 (2003), pp. 352–356. DOI: 10.1016/S0925-4005(03)00437-4.

[15] T. Yoshinobu, H. Iwasaki, Y. Ui, K. Furuichi, Y. Ermolenko, Y. Mourzina, T. Wagner, N. Näther, and M. J. Schöning. "The light-addressable potentiometric sensor for multi-ion sensing and imaging". In: *Methods* 37.1 (2005), pp. 94–102. DOI: 10.1016/j.ymeth.2005.05.020.

[16] J. Kloock, L. Moreno, A. Bratov, S. Huachupoma, J. Xu, T. Wagner, T. Yoshinobu, Y. Ermolenko, Y. Vlasov, and M. Schöning. "PLD-prepared cadmium sensors based on chalcogenide glasses – ISFET, LAPS and μISE semiconductor structures". In: *Sensors and Actuators B: Chemical* 118.1–2 (2006), pp. 149–155. DOI: 10.1016/j.snb.2006.04.018.

[17] T. Hattori, Y. Masaki, K. Atsumi, R. Kato, and K. Sawada. "Real-time two-dimensional imaging of potassium ion distribution using an ion semiconductor sensor with charged coupled device technology". In: *Analytical Sciences* 26.10 (2010), pp. 1039–1045. DOI: 10.2116/analsci.26.1039.

[18] T. Hattori, M. Yoshitomo, S. Mori, D. Miyamoto, R. Kato, and K. Sawada. "CCD-type sodium ion image sensor: dynamic observation of ion-exchange reactions of a single Na-type cation-exchange resin bead". In: *Electroanalysis* 24.1 (2012), pp. 114–120. DOI: 10.1002/elan.201100442.

[19] T. Hattori, M. Yoshitomo, S. Mori, D. Miyamoto, R. Kato, and K. Sawada. "Development of CCD-type calcium ion image sensor with plasticized PVC membrane contained ionophore". In: *Proc. of the 53rd Chemical Sensor Symposium*. Vol. 28. 2012, p. 29.

[20] A. Seki, S. Ikeda, I. Kubo, and I. Karube. "Biosensors based on light-addressable potentiometric sensors for urea, penicillin and glucose". In: *Analytica Chimica Acta* 373.1 (1998), pp. 9–13. DOI: 10.1016/S0003-2670(98)00364-X.

[21] A. Poghossian, T. Yoshinobu, A. Simonis, H. Ecken, H. Lüth, and M. Schöning. "Penicillin detection by means of field-effect based sensors: EnFET, capacitive EIS sensor or LAPS?" In: *Sensors and Actuators, B: Chemical* 78.1-3 (2001), pp. 237–242. DOI: 10.1016/S0925-4005(01)00819-X.

[22] T. Yoshinobu, H. Ecken, A. Poghossian, A. Simonis, H. Iwasaki, H. Lüth, and M. J. Schöning. "Constant-current-mode LAPS (CLAPS) for the detection of penicillin". In: *Electroanalysis* 13.8-9 (2001), pp. 733–736. DOI: 10.1002/1521-4109(200105)13:8/9<733::AID-ELAN733>3.0.CO;2-N.

[23] S.-R. Lee, K. Sawada, H. Takao, and M. Ishida. "An enhanced glucose biosensor using charge transfer techniques". In: *Biosensors and Bioelectronics* 24.4 (2008), pp. 650–656. DOI: 10.1016/j.bios.2008.06.014.

[24] S.-R. Lee, M. Rahman, K. Sawada, and M. Ishida. "Fabrication of a highly sensitive penicillin sensor based on charge transfer techniques". In: *Biosensors and Bioelectronics* 24.7 (2009), pp. 1877–1882. DOI: 10.1016/j.bios.2008.09.008.

[25] J. R. Siqueira, R. M. Maki, F. V. Paulovich, C. F. Werner, A. Poghossian, M. C. F. de Oliveira, V. Zucolotto, O. N. Oliveira, and M. J. Schöning. "Use of information visualization methods eliminating cross talk in multiple sensing units investigated for a light-addressable potentiometric sensor". In: *Analytical Chemistry* 82.1 (2010), pp. 61–65. DOI: 10.1021/ac9024076.

[26] A. Grace. "Phasic versus tonic dopamine release and the modulation of dopamine system responsivity: A hypothesis for the etiology of schizophrenia". In: *Neuroscience* 41.1 (1991), pp. 1–24. DOI: 10.1016/0306-4522(91)90196-U.

[27] T. Arendt. "Alzheimer's disease as a disorder of mechanisms underlying structural brain self-organization". In: *Neuroscience* 102.4 (2001), pp. 723–765. DOI: 10.1016/S0306-4522(00)00516-9.

[28] R. Li, Q. Lei, G. Song, X. He, and Z. Xie. "Calcium near the release site is essential for basal ACh release in Xenopus". In: *Cell Biology International* 32.9 (2008), pp. 1136–1142. DOI: 10.1016/j.cellbi.2008.05.001.

[29] S. Takenaga, Y. Tamai, K. Okumura, M. Ishida, and K. Sawada. "Label-free acetylcholine image sensor based on charge transfer technology for biological phenomenon tracking". In: *Japanese Journal of Applied Physics* 51 (2012), p. 027001. DOI: 10.1143/JJAP.51.027001.

[30] S. O. Ogundiran, S. Varanasi, and E. Ruckenstein. "Modeling of enzyme-potentiometric sensors involving acid- or base-forming reactions". In: *Biotechnology and Bioengineering* 37.2 (1991), pp. 160–176. DOI: 10.1002/bit.260370209.

[31] D. E. Yates, S. Levine, and T. W. Healy. "Site-binding model of the electrical double layer at the oxide/water interface". In: *Journal of the Chemical Society, Faraday Transactions 1: Physical Chemistry in Condensed Phases* 70 (1974), pp. 1807–1818. DOI: 10.1039/F19747001807.

[32] A. Poghossian and M. J. Schöning. "Silicon-based chemical and biological field-effect sensors". In: *Encyclopedia of Sensors*. Ed. by C. A. Grimes, E. C. Dickey, and M. V. Pishko. Vol. X. Santa Clarita, California, USA: American Scientific Publishers, 2006, pp. 1–71.

[33] Z. Qintao, W. Ping, W. J. Parak, M. George, and G. Zhang. "A novel design of multi-light LAPS based on digital compensation of frequency domain". In: *Sensors and Actuators, B: Chemical* 73.2-3 (2001), pp. 152–156. DOI: 10.1016/S0925-4005(00)00696-1.

[34] T. Wagner, R. Molina, T. Yoshinobu, J. P. Kloock, M. Biselli, M. Canzoneri, T. Schnitzler, and M. J. Schöning. "Handheld multi-channel LAPS device as a transducer platform for possible biological and chemical multi-sensor applications". In: *Electrochimica Acta* 53.2 (2007), pp. 305–311. DOI: 10.1016/j.electacta.2007.04.006.

[35] K. Miyamoto, Y. Kuwabara, S. Kanoh, T. Yoshinobu, T. Wagner, and M. J. Schöning. "Chemical image scanner based on FDM-LAPS". In: *Sensors and Actuators, B: Chemical* 137.2 (2009), pp. 533–538. DOI: 10.1016/j.snb.2008.12.008.

[36] T. Wagner, C. F. Werner, K. Miyamoto, H.-J. Ackermann, T. Yoshinobu, and M. J. Schöning. "FPGA-based LAPS device for the flexible design of sensing sites on functional interfaces". In: *Physica Status Solidi A: Applications and Materials Science* 207.4 (2010), pp. 844–849. DOI: 10.1002/pssa.200983320.

[37] C. F. Werner, S. Schusser, H. Spelthahn, T. Wagner, T. Yoshinobu, and M. J. Schöning. "Field-programmable gate array based controller for multi spot light-addressable potentiometric sensors with integrated signal correction mode". In: *Electrochimica Acta* 56.26 (2011), pp. 9656–9660. DOI: 10.1016/j.electacta.2011.03.012.

[38] F. Mizutani, S. Yabuki, and Y. Hirata. "Amperometric l-lactate-sensing electrode based on a polyion complex layer containing lactate oxidase. Application to serum and milk samples". In: *Analytica Chimica Acta* 314.3 (1995), pp. 233–239. DOI: 10.1016/0003-2670(95)00278-8.

[39] E. Watanabe, T. Hizawa, S. Mimura, T. Ishida, H. Takao, K. Sawada, and M. Ishida. "Low-noise operation of chrage-transfer-type pH sensor using charge accumulation technique". In: *Tech. Dig. 11th Int. Conf. Miniaturized Systems for Chemistry and Life Sciences*. 2007, p. 479.

[40] L. Chen, Y. Zhou, S. Jiang, J. Kunze, P. Schmuki, and S. Krause. "High resolution LAPS and SPIM". In: *Electrochemistry Communications* 12.6 (2010), pp. 758–760. DOI: 10.1016/j.elecom.2010.03.026.

[41] F. Dasai, M. Futagawa, D. Suzuki, R. Otake, M. Ishida, and K. Sawada. "A 128x128 pixels charge transfer type pH and photo image sensor with high density and high frame rate". In: *Proc. of The 6th Asia-Pacific Conference on Transducers and Micro/Nano Technologies (APCOT 2012), Nanjing, China*. 2012.

[42] S. Takenaga, Y. Tamai, K. Hirai, K. Takahashi, T. Sakurai, S. Terakawa, M. Ishida, K. Okumura, and K. Sawada. "Label-free real time imaging of neural communication using acetylcholine image sensor". In: *Solid-State Sensors, Actuators and Microsystems Conference (TRANSDUCERS), 2011 16th International*. 2011, pp. 954–957. DOI: 10.1109/TRANSDUCERS.2011.5969337.

5.5 Supporting information

Figure 5.10 depicts the pH-calibration measurements of the sensor chips used in section 5.3.2, immediately before immobilising the AChE membrane. The resulting pH sensitivities are 56 mV pH^{-1} for the LAPS and 20.5 mV pH^{-1} for the CCD-type set-up. These two calibration curves represent not-published information material.

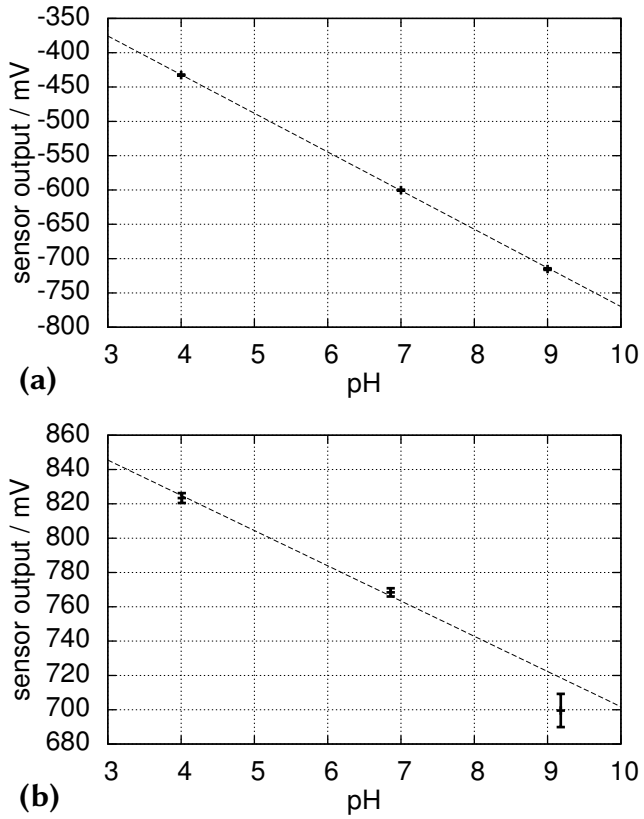

Figure 5.10: Response of the LAPS (a) and CCD (b) set-up to different pH values. For each pH-buffer solution, the output signal was measured for 60 s resulting in 300 single measurements. The mean value and the RMS (error bars) of these measurements are plotted against the pH value. The dashed lines represent the linear regressions.

6 Determination of the extracellular acidification of *Escherichia coli* by a LAPS

Carl Frederik Werner[a,b], Christoph Krumbe[a], Katharina Schumacher[a], Simone Groebel[a], Heiko Spelthahn[a], Michael Stellberg[c], Torsten Wagner[d], Tatsuo Yoshinobu[d], Thorsten Selmer[a], Michael Keusgen[e], Marcus E. M. Baumann[a], Michael J. Schöning[a,b]

[a] *Institute of Nano- and Biotechnologies, Aachen University of Applied Sciences, Jülich, Germany*
[b] *Institute of Bio- and Nanosystems (IBN-2), Research Centre Jülich, Jülich, Germany*
[c] *Laboratory for Product Development, Aachen University of Applied Sciences, Jülich, Germany*
[d] *Department of Biomedical Engineering, Tohoku University, Sendai, Japan*
[e] *Institute of Pharmaceutical Chemistry, Philipps University Marburg, Marburg, Germany*

Published in: *Physica Status Solidi A: Applications and Materials Science*, Vol. 208, pp. 1340–1344, DOI: 10.1002/pssa.201001141

Submitted: 2010-10-08; Accepted: 2010-12-22; Published: 2011-05-12

Abstract:

The monitoring and control of a biogas digester is important to maximise the energy output and to avoid down times. Within the digester process, the metabolic activity of relevant organisms represents a key parameter. A light-addressable potentiometric sensor (LAPS) can be used to determine the extracellular acidification of these organisms. With the developed on-chip differential LAPS set-up, external influences, like sensor drift, temperature fluctuations and external pH changes can be compensated. An immobilisation protocol based on polyacrylamide has been developed to immobilise the organisms on the sensor surface. To validate the system, *Escherichia coli* have been used as a model organism. Measurements with *E. coli* in suspension and measurements with *E. coli* embedded in polyacrylamide gel were performed. It was shown, that the activity of the *E. coli* in the polyacrylamide was as high as in suspension, when determining the effect of the immobilisation towards the extracellular acidification rate.

6.1 Introduction

Biomass is a renewable energy source, like solar and wind energy. One method to produce energy from biomass is the biogas production process by means of anaerobic digestion. The produced biogas can be further transformed, with the help of a cogeneration unit, to heat and electricity. During the anaerobic digestion, many different organisms are involved to finally produce the biogas, which mainly contains methane and carbon dioxide [1]. The process has to be monitored and controlled, to avoid expensive down times and loss in production. Therefore, parameters such as the pH value, the redox potential and the temperature of the digester have to be monitored [2]. However, due to the large size of the digester, changes of the above mentioned parameters might affect later to threaten the sensitive microorganisms. Thus, the metabolic activity of relevant organisms involved in the anaerobic digestion must be controlled directly to determine their "welfare". Within this work, the metabolic activity is investigated by determining their extracellular acidification rate. Microbes produce organic acids (e.g., acetic acid and lactic acid) as metabolic waste product. These acids cause a pH-value change around the microbes, which could be determined by a biosensor setup [3, 4]. A fast acidification would refer on a high activity and a slow acidification might indicate a possible threat of the bio-digestion process.

It has been demonstrated that the extracellular acidification can be detected by a light-addressable potentiometric sensor (LAPS) [5–10]. The LAPS is a potentiometric semiconductor-based chemical sensor [11], with the advantage to detect chemical species on the sensor surface in a spatially resolved manner. It consists of a semiconductor/insulator/transducer-layered structure as shown in Fig. 6.1. An external bias voltage V_{bias} will be applied with the help of a rear-side contact and a reference electrode. This generates a space-charge region in the semiconductor. The local width of this space-charge region depends on the local potential at the sensor surface between the transducer layer and the electrolyte solution. A modulated light pointer is used to

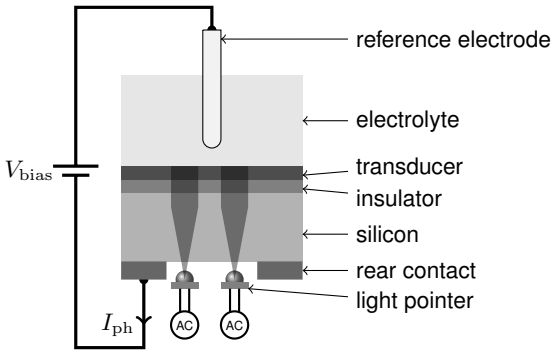

Figure 6.1: Schematic drawing of the LAPS principle.

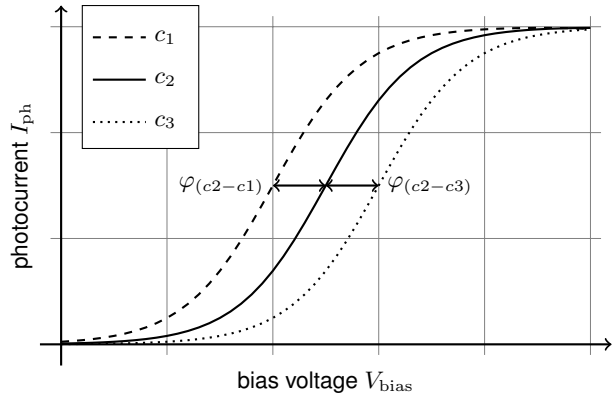

Figure 6.2: Simulated I/V curve of a LAPS with p-doped silicon by different analyte concentrations ($c_1 > c_2 > c_3$).

generate an external photocurrent, which is dependent on the width of the space-charge region. Here, the illuminated area defines the size of the measurement spot on the sensor surface. The I/V curve depicts the correlation between the measured photocurrent I_{ph} and the bias voltage V_{bias} as shown in Fig. 6.2. A change of the ion concentration affects the surface potential φ and hence, moves the I/V curve along the V_{bias} axis. By determining these voltage shifts, the ion concentration can be calculated. More information about the LAPS principle can be found elsewhere [6, 11–13].

The determination of the extracellular acidification of cells by LAPS has been successfully performed for mammalian cells [5, 6, 8–10]. To determine the acidification, the cells are immobilised on the sensor surface and the culture medium is changed periodically. During each cycle, the pH or the surface potential φ is determined at least twice, to calculate the potential-change rate $\dot{\varphi}$ by linear regression. The relation between the potential-change rate $\dot{\varphi}$ and the acidification rate α, is described in [6]. Here, the acidification rate α indicates how many H^+ ions per second and per cell are produced. The acidification rate α is of high interest, because it depicts the metabolic activity per cell and does not depend on the buffer capacity of the used medium. To determine α correctly, the specific pH-buffer capacity β, the volume V of the used medium, the pH sensitivity S and the numbers of cells n are required. Equation (6.1) summarises the relation between these parameters together with the Avogadro constant N_{A}.

$$\dot{\varphi} = S \frac{1}{\beta V} \frac{n\alpha}{N_{\mathrm{A}}} \tag{6.1}$$

Due to the small potential-change rates in this kind of measurements, external influences, like sensor drift, temperature fluctuations and external pH changes could significantly falsify the measurement signal. To compensate for these influences, an on-chip differential set-up was realised. Utilising the addressability of LAPS, two areas

were defined with and without microbes. External influences would affect both areas and thus, could be compensated by differential measurements.

6.2 Experimental

6.2.1 LAPS set-up

The designed LAPS set-up utilises a 4×4 infrared light-emitting diode (LED) array as described in [14]. The addressing of the LED array is performed by a field-programmable gate array (FPGA) described in detail in [15, 16]. The LAPS chip has a size of 20 mm × 20 mm and an active measurement area of 15 mm × 15 mm, which stays in contact with the electrolyte solution. The LAPS chip consists of thin films of: 60 nm Ta_2O_5, 30 nm SiO_2, 450 µm *p*-doped silicon with 1–10 Ω cm and 300 nm Al for the rear side contact, respectively. The aluminium was removed for the area where the LED array should illuminate the silicon from the rear side. The additional Ta_2O_5 layer is known to be a robust transducer with a nearly Nernstian pH sensitivity of $S = 58\,\mathrm{mV\,pH^{-1}}$ [17]. The I/V curves of all 16 measurement spots were measured successively. The potential shift φ was determined by the difference between the initial and the actual I/V curve for each measurement spot.

6.2.2 Measurements with *E. coli* in suspension

The first measurements were performed with *E. coli* in suspension. The *E. coli* were cultivated for 12 h in lysogeny broth (LB) medium (10 g l^{-1} tryptone, 5 g l^{-1} yeast extract and 10 g l^{-1} NaCl) at 37 °C and 180 rpm. The desired cell concentration was established by cell counting, a centrifugation step at 805 g and finally, resuspension with the corresponding amount of LB medium.

The following measurement procedure was utilised: After the first 12 min of measuring within 2 ml LB medium, 1 ml of the *E. coli* suspension, with different numbers of cells (6×10^9, 12×10^9 and 24×10^9), was added to the measurement cell. The used LB medium had a pH-buffer capacity of $\beta = (4.6 \pm 0.2)\,\mathrm{mmol\,l^{-1}\,pH^{-1}}$. For the given values, the acidification rate of *E. coli* under normal conditions, was calculated.

6.2.3 Immobilisation in gel

To determine the acidification rate over time, it is necessary to fix the microbes on the sensor surface. Therefore, the *E. coli* have been immobilised in a polyacrylamide gel on the LAPS chip. A 160 µm thick SU-8 layer was deposited on top of the Ta_2O_5 layer. By photolithography, two wells with a size of 6 mm × 13 mm were created within the SU-8. Figure 6.3 depicts a cross section of the fluidic set-up. The composition of the

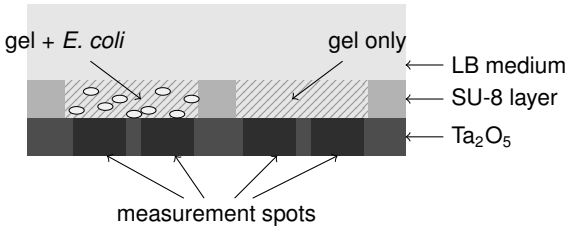

Figure 6.3: Schematic drawing of the immobilised *E. coli* in polyacrylamide gel on the sensor surface. The on-chip differential set-up with one side with *E. coli* in gel and the other side without organisms in gel.

Table 6.1: Composition of the polyacrylamide gel to immobilise the *E. coli* on the sensor surface.

ingredients	volume percentage (%)
E. coli in buffer solution / TRIS	46
acrylamide	4
ammonium persulfate (APS)	0.56
tetramethylethylenediamine (TEMED)	0.44

polyacrylamide gel is shown in Table 6.1. *E. coli* were cultivated as described above, and diluted after harvesting in TRIS buffer. 50 µl of this gel with $n = 1.4 \times 10^9$ *E. coli* were put in the well above the measurement spots 1, 2, 5, 6, 9, 10, 13 and 14. In the well above measurement spots 3, 4, 7, 8, 11, 12, 15 and 16, 50 µl gel without microbes was added. During each measurement cycle for all 16 measurement spots, I/V curves were recorded every 2 min. After 12 min, the measurement cycle was stopped and the complete measurement volume of $V = 500$ µl was replaced with a pipet to start a new measurement cycle; 10 measurement cycles have been performed in total.

6.3 Results and discussion

6.3.1 Measurements with *E. coli* in suspension

The results of the measurements with the *E. coli* in suspension are depicted in Fig. 6.4. The measurements were performed with 6×10^9, 12×10^9 and 24×10^9 *E. coli* cells diluted in 3 ml measurement solution. The continuous decrease of the potential after adding *E. coli*, in contrast to 12 min before, demonstrates the acidification by *E. coli*.

In Table 6.2, rates of the potential change $\dot{\varphi}$ calculated by linear regression are listed. It can be seen that a higher number n of *E. coli* results in a higher potential-change rate $\dot{\varphi}$. However, the correlation is not linear. The calculated acidification rate per cell α,

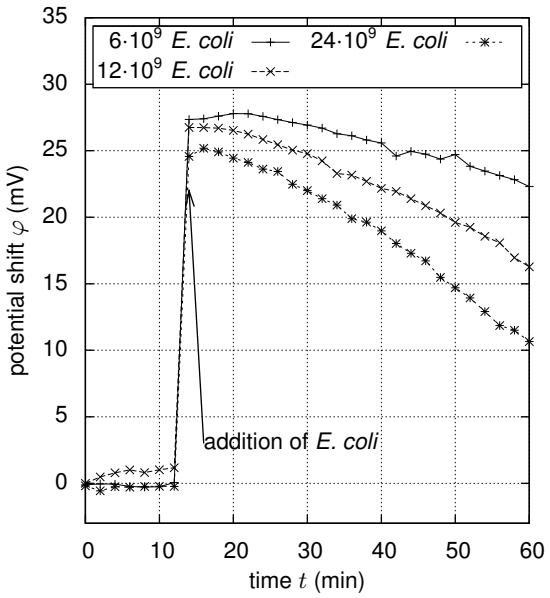

Figure 6.4: Mean potential shift of all 16 measurement spots. Starting 2 ml with LB medium, 1 ml LB medium with the specified amount of *E. coli* was added after 12 min.

Table 6.2: Rates of potential change determined by linear regression from Fig. 6.4. The acidification rate was calculated by equation (6.1).

number of *E. coli* n	potential-change rate $\dot{\varphi}$ ($\mathrm{mV\,min^{-1}}$)	acidification rate α ($10^4\,\mathrm{H^+\,s^{-1}\,cell^{-1}}$)
6×10^9	-0.138 ± 0.004	5.4 ± 0.3
12×10^9	-0.258 ± 0.006	5.0 ± 0.2
24×10^9	-0.365 ± 0.008	3.6 ± 0.2

which should be theoretically equal, decreases with the increase of numbers of *E. coli* cells. This could be because of limited nutrients transport to the cells due to the high cell concentration. An acidification rate of $5 \times 10^4\,\mathrm{H^+\,s^{-1}}$ per cell is low compared to the acidification rate of mammalian cells ($10^8\,\mathrm{H^+\,s^{-1}}$ per cell [4]). One possible reason might be the low volume of a *E. coli* cell, which is 1000 times lower compared to the volume of a mammalian cell [4].

6.3.2 Immobilisation in gel

Figure 6.5 shows the polymerised gel on top of the sensor chip. The high concentration of *E. coli* of $n = 1.4 \times 10^9$ cells in 50 µl gel avoids optical transmission, therefore, the well with *E. coli* appears white, whereas the normal gel is transparent. The gel showed good adhesion to the sensor surface and appears stable over long time in solution.

Figure 6.6 presents the results of the on-chip differential measurements with and without *E. coli* cells. The gel with *E. coli* (measurement spots 1, 5, 9, 13) appears more

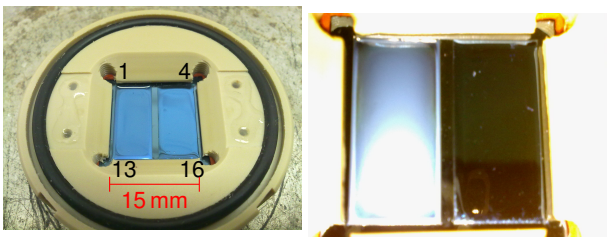

Figure 6.5: Picture of the LAPS measurement cell (left) and polyacrylamide gel on top of the LAPS chip (right). The left well is filled with gel and *E. coli*, the right well contains only gel. The numbers on the left picture indicate the measurement-spot numbers.

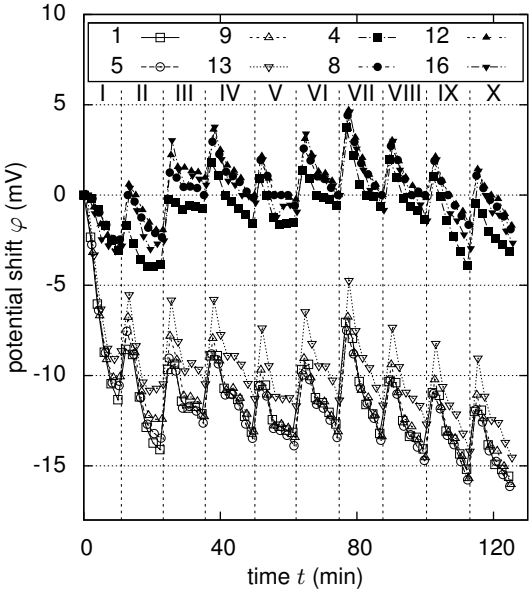

Figure 6.6: Potential shifts for several measurement cycles due to acidification by *E. coli* with the on-chip differential setup. Potential shifts of the well with *E. coli* (measurement spots 1, 5, 9, 13) and the well without bacterias (measurement spots 4, 8, 12, 16) for measurement cycles I to X.

acidic compared to the gel without microbes (measurement spots 4, 8, 12, 16). The difference was about 10 mV, or equivalent to 0.17 pH. The measurement cycles show a higher potential change on the well with *E. coli*. This indicates the acidification by *E. coli*. As an example, the potential-change rates of each measurement spot from measurement cycle IV ($t = 36$ min to $t = 48$ min) are depicted in Fig. 6.7. The well with *E. coli* (measurement spots 1, 2, 5, 6, 9, 10, 13, 14) and without *E. coli* (measurement spots 3, 4, 7, 8, 11, 12, 15, 16), have a mean potential-change rate of $-0.4\,\mathrm{mV\,min^{-1}}$ and $-0.3\,\mathrm{mV\,min^{-1}}$, respectively. Thus, both wells are distinguishable from each other. However, a potential-change rate on the well without microbes is visible too, which can not be described by diffusion or sensor drift. Currently, the authors investigate possible effects of turbulence due to the insertion of the medium. A general increasing trend of the rates of potential change as observed from measurement spots 1, 2, 3, 4 to measurement spots 13, 14, 15, 16. One reason might be the measurement sequence

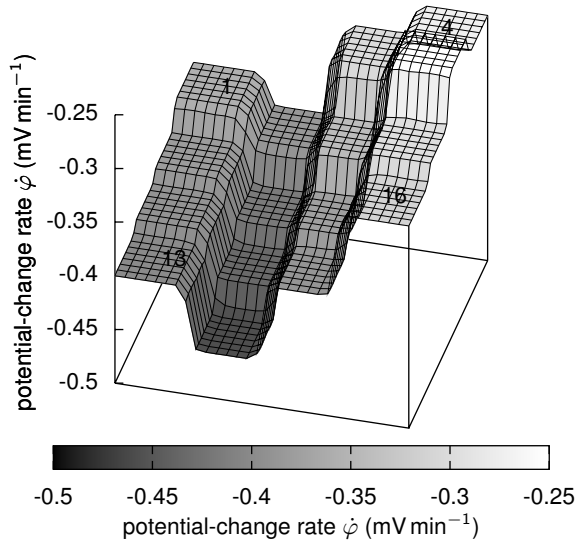

Figure 6.7: Plot of the potential-change rates from measurement cycle IV ($t = 36\,\text{min}$ to $t = 48\,\text{min}$) of the measurement of Figure 6.6. The potential-change rates were determined by linear regression.

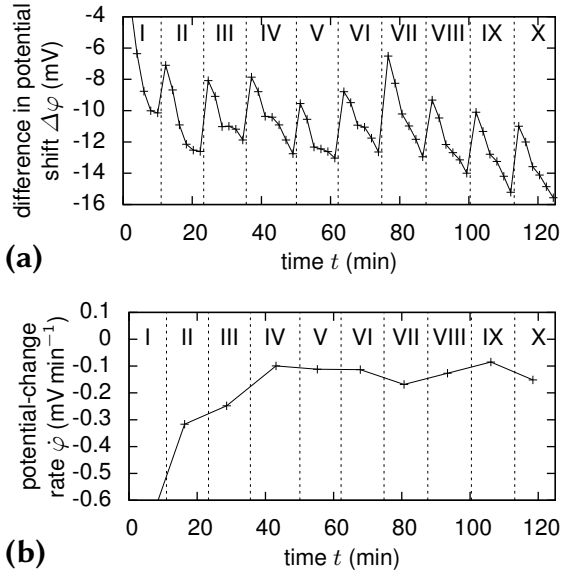

Figure 6.8: (a) Difference between the mean value of measurements spots 1, 5, 9, 13 and the mean value of measurement spots 4, 8, 12, 16 in Fig. 6.6. (b) Potential-change rate of each measurement cycle determined in (a).

from measurement spot 1 to 16. Each measurement takes 5 s per measurement, during which the potential-change rate may increase.

The difference between the mean values of the measurement spots 1, 5, 9, 13 with *E. coli* and the mean value of the measurement spots 4, 8, 12, 16 without *E. coli* are compared in Fig. 6.8. The linear regression of each measurement cycle is shown as potential-change rate. Until cycle IV, a conditioning phase is visible. After that, the potential-change rate is nearly constant and was determined to be $\dot{\varphi} = (0.14 \pm 0.06)\,\text{mV}\,\text{min}^{-1}$. Calculated by equation (6.1), the acidification rate is $\alpha = (4 \pm 2) \times 10^4\,\text{H}^+\,\text{s}^{-1}$ per cell. This is similar to the values of *E. coli* in suspension (Table 6.2). This demonstrates that

the immobilisation in polyacrylamide does not suppress the metabolic activity of the *E. coli*.

6.4 Conclusions

A new protocol to immobilise microbes on a LAPS chip was demonstrated using *E. coli* as model organisms. This allows to place a large number of cells near to the sensor surface without any additional surface-treatment steps. In addition, the organisms are protected against washing steps. The measurement results of the extracellular acidification showed that the metabolic activity of *E. coli* in the polyacrylamide gel is not suppressed compared to measurements with *E. coli* in suspension. An on-chip differential set-up was developed by defining two wells. Thus, external influences such as sensor drift, temperature and external pH changes can be compensated. In future work, the authors plan to integrate the LAPS set-up as online analysis system into a biogas digester for monitoring the activity of anaerobic organisms. Therefore, as a next step, those organisms will be immobilised on the chip. Moreover, the LAPS chip might be extended for additional control of physical parameters (e.g., temperature, conductivity, flow rate) as already discussed for ion-sensitive field-effect transistors (ISFETs) in [18].

Acknowledgements

The authors thank the German Federal Ministry of Food, Agriculture and Consumer Protection (BMELV) and the "Fachagentur Nachwachsende Rohstoffe e.V." (FNR) for financial support of this work (Bio-LAPS).

References

[1] B. K. Ahring. "Perspectives for anaerobic digestion". In: *Biomethanation I*. Ed. by T. Scheper. Vol. 81. Berlin, Heidelberg: Springer-Verlag, 2003, pp. 1–30. DOI: 10.1007/3-540-45839-5_1.

[2] P. Weiland. "Wichtige Messdaten für den Prozessablauf und Stand der Technik in der Praxis". German. In: *Messen, Steuern, Regeln bei der Biogaserzeugung*. Vol. 27. Gülzower Fachgespräche. Gülzow: Fachagentur für Nachwachsende Rohstoffe (FNR), 2007, pp. 17–31. URL: http://www.fnr-server.de/ftp/pdf/literatur/pdf_328-gf_band_27_biogaserzeugung_bf.pdf.

[3] H. M. McConnell, J. C. Owicki, J. W. Parce, D. L. Miller, G. T. Baxter, H. G. Wada, and S. Pitchford. "The cytosensor microphysiometer: biological applications of silicon technology". In: *Science* 257.5078 (1992), pp. 1906–1912. DOI: 10.1126/science.1329199.

[4] J. C. Owicki and J. W. Parce. "Biosensors based on the energy metabolism of living cells: The physical chemistry and cell biology of extracellular acidification". In: *Biosensors & Bioelectronics* 7.4 (1992), pp. 255–272. DOI: 10.1016/0956-5663(92)87004-9.

[5] J. W. Parce, J. C. Owicki, K. M. Kercso, G. B. Sigal, H. G. Wada, V. C. Muir, L. J. Bousse, K. L. Ross, B. I. Sikic, and H. M. McConnell. "Detection of cell-affecting agents with a silicon biosensor". In: *Science* 246.4927 (1989), pp. 243–247. DOI: 10.1126/science.2799384.

[6] J. C. Owicki, L. J. Bousse, D. G. Hafeman, G. L. Kirk, J. D. Olson, H. G. Wada, and J. W. Parce. "The light-addressable potentiometric sensor: Principles and biological applications". In: *Annual Review of Biophysics and Biomolecular Structure* 23 (1994), pp. 87–113. DOI: 10.1146/annurev.bb.23.060194.000511.

[7] M. Nakao, S. Inoue, R. Oishi, T. Yoshinobu, and H. Iwasaki. "Observation of microorganism colonies using a scanning-laser-beam pH-sensing microscope". In: *Journal of Fermentation and Bioengineering* 79.2 (1995), pp. 163–166. DOI: 10.1016/0922-338X(95)94085-6.

[8] T. Yoshinobu, H. Ecken, A. B. M. Ismail, H. Iwasaki, H. Lüth, and M. J. Schöning. "Chemical imaging sensor and its application to biological systems". In: *Electrochimica Acta* 47.1-2 (2001), pp. 259–263. DOI: 10.1016/S0013-4686(01)00564-3.

[9] B. Stein, M. George, H. E. Gaub, J. C. Behrends, and W. J. Parak. "Spatially resolved monitoring of cellular metabolic activity with a semiconductor-based biosensor". In: *Biosensors & Bioelectronics* 18.1 (2003), pp. 31–41. DOI: 10.1016/S0956-5663(02)00109-4.

[10] A. Poghossian, S. Ingebrandt, A. Offenhäusser, and M. J. Schöning. "Field-effect devices for detecting cellular signals". In: *Seminars in Cell & Developmental Biology* 20.1 (2009), pp. 41–48. DOI: 10.1016/j.semcdb.2009.01.014.

[11] T. Wagner and M. J. Schöning. "Light-addressable potentiometric sensors (LAPS): recent trends and applications". In: *Electrochemical Sensor Analysis*. Ed. by S. Alegret and A. Merkoci. Vol. 49. Amsterdam: Elesevier, 2007, pp. 87–128.

[12] D. G. Hafeman, J. W. Parce, and H. M. McConnell. "Light-addressable potentiometric sensor for biochemical systems". In: *Science* 240.4856 (1988), pp. 1182–1185. DOI: 10.1126/science.3375810.

[13] T. Yoshinobu, H. Iwasaki, Y. Ui, K. Furuichi, Y. Ermolenko, Y. Mourzina, T. Wagner, N. Näther, and M. J. Schöning. "The light-addressable potentiometric sensor for multi-ion sensing and imaging". In: *Methods* 37.1 (2005), pp. 94–102. DOI: 10.1016/j.ymeth.2005.05.020.

[14] T. Wagner, R. Molina, T. Yoshinobu, J. P. Kloock, M. Biselli, M. Canzoneri, T. Schnitzler, and M. J. Schöning. "Handheld multi-channel LAPS device as a transducer platform for possible biological and chemical multi-sensor applications". In: *Electrochimica Acta* 53.2 (2007), pp. 305–311. DOI: 10.1016/j.electacta.2007.04.006.

[15] C. F. Werner, H. Spelthahn, M. J. Schöning, C. Krumbe, T. Wagner, T. Yoshinobu, and M. Keusgen. "Neue Ansteuerungselektronik für LAPS-basierte Biosensoren zur gleichzeitigen ortsaufgelösten Messung der pH-Konzentration". German. In: *Sensoren und Messsysteme 2010: Vorträge der 15. ITG-GMA-Fachtagung vom 18. bis 19. Mai 2010 in Nürnberg / ITG-GMA Fachtagung Sensoren und Messsysteme 2010*. Ed. by R. Gerhard. Berlin, Offenbach: VDE Verlag GmBH, 2010, pp. 109–114. URL: http://d-nb.info/1002307023.

[16] T. Wagner, C. F. Werner, K. Miyamoto, H.-J. Ackermann, T. Yoshinobu, and M. J. Schöning. "FPGA-based LAPS device for the flexible design of sensing sites on functional interfaces". In: *Physica Status Solidi A: Applications and Materials Science* 207.4 (2010), pp. 844–849. DOI: 10.1002/pssa.200983320.

[17] M. Schöning, N. Näther, V. Auger, A. Poghossian, and M. Koudelka-Hep. "Miniaturised flow-through cell with integrated capacitive EIS sensor fabricated at wafer level using Si and SU-8 technologies". In: *Sensors and Actuators B: Chemical* 108.1–2 (2005), pp. 986–992. DOI: 10.1016/j.snb.2004.12.029.

[18] A. Poghossian and M. J. Schöning. "Detecting both physical and (bio-)chemical parameters by means of ISFET devices". In: *Electroanalysis* 16.22 (2004), pp. 1863–1872. DOI: 10.1002/elan.200403074.

7 Nutrient concentration sensitive microorganism-based biosensor

Carl Frederik Werner[a,b], Simone Groebel[a], Christoph Krumbe[a], Torsten Wagner[c], Thorsten Selmer[a], Tatsuo Yoshinobu[c], Marcus E. M. Baumann[a], Michael Keusgen[d], Michael J. Schöning[a,b]

[a] *Institute of Nano- and Biotechnologies, Aachen University of Applied Sciences, Jülich, Germany*
[b] *Peter Grünberg Institute (PGI-8), Research Centre Jülich, Jülich, Germany*
[c] *Department of Biomedical Engineering, Tohoku University, Sendai, Japan*
[d] *Institute of Pharmaceutical Chemistry, Philipps University Marburg, Marburg, Germany*

Published in: *Physica Status Solidi A: Applications and Materials Science*, Vol. 209, pp. 900–904, DOI: 10.1002/pssa.201100801

Submitted: 2011-11-21; Accepted: 2012-03-28; Published: 2012-04-18

Abstract:

This work presents a biosensor based on living cells immobilised on a light-addressable potentiometric sensor (LAPS). The set-up is sensitive to the concentrations of nutrients metabolised by bacteria, which results in an extracellular acidification. This is exemplarily demonstrated with glucose as nutrient and *Escherichia coli* as microorganism. The function of this biosensor is comparable to an enzyme-based field-effect sensor when using diffusion limitation. With the help of addressability of the LAPS an on-chip differential set-up was developed. Thus, external influences such as sensor drift, temperature and external pH changes can be minimised.

7.1 Introduction

Biosensors with living cells are under investigation for drug screening, cell-growth observations and environmental monitoring [1–3]. They are often based on the detection of acidification of the cell environment due to the metabolic activity of cells. One interesting application of these biosensors is the monitoring of biogas processes. In a biogas process, biogas will be produced by anaerobic digestion of biomass by several kinds of microorganisms [4, 5]. Biogas mainly consists of methane and carbon dioxide and is used as energy carrier to produce fuel, electricity and heat. To avoid expensive down times and loss in production, the anaerobic digestion must be monitored and controlled. A new approach is to monitor the metabolic activity and thus, the "welfare" of relevant organisms that are involved in the anaerobic digestion [6]. Our aim is to determine whether the relevant organisms are showing a good metabolic activity and are supplied with nutrients in the biogas digester.

A light-addressable potentiometric sensor (LAPS) is an often used sensor device to determine the extracellular acidification [1, 2, 6–9]. LAPS are field-effect-based potentiometric sensors [10] with the advantage to detect chemical species in a liquid solution on its sensor surface in a spatially resolved manner. As shown in Fig. 7.1 (left), the LAPS consists of a semiconductor/insulator/transducer-layered structure. With the help of a reference electrode and a rear-side contact, a bias voltage V_{bias} will be applied along the structure. This will create a depletion region inside the semiconductor. The local width of this depletion region is additionally influenced by the local surface potential φ on the sensor surface, which depends on the local concentration. With a modulated light beam pointing at the semiconductor, a photocurrent I_{ph} will be generated, which depends on the local width of the depletion region in the illuminated area. The illuminated area defines the measurement spot. The I/V curve depicts the correlation between the photocurrent I_{ph} and the applied bias voltage V_{bias} (see Fig.

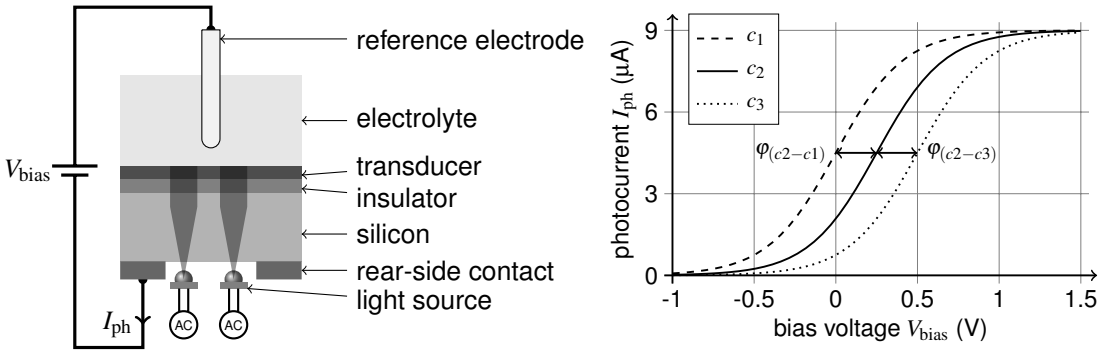

Figure 7.1: Schematic drawing of the LAPS principle (left). Simulated I/V curve of a LAPS with p-doped silicon by different analyte concentrations ($c_1 > c_2 > c_3$) (right).

7.1, right). A change in concentration changes the surface potential φ and causes a shift of the I/V curve along the bias voltage axis. By determination of the voltage shift, the local concentration can be calculated. More information about the measurement principle of LAPS can be found elsewhere [11–13].

To observe the extracellular acidification of living cells with the help of a LAPS, the cells must be immobilised on a pH-sensitive surface. By determining the local pH change, the extracellular acidification can be calculated. According to the metabolic pathway (glycolysis or respiration) the metabolism of one glucose molecule can produce two or six H^+ ions, respectively [1]. The relation between the potential-change rate $\dot{\varphi}$ and the average acidification rate α of one cell is described in Refs. [1, 6] and summarised in Eq. (7.1) as

$$\alpha = \frac{\dot{\varphi}}{S}\frac{N_\mathrm{A}}{n}\beta V. \tag{7.1}$$

Here, S is the pH sensitivity of the LAPS chip, n is the number of immobilised cells, β is the specific pH-buffer capacity, V is the volume of the medium and N_A is the Avogadro constant. The acidification rate α describes how many H^+ ions will be produced in average by one cell in one second.

To compensate external influences, like sensor drift, temperature fluctuations and external pH changes, the addressability of LAPS is utilised for an on-chip differential set-up [6]. Thus, two areas were defined on the sensor surface, one with and one without immobilised cells. The formerly mentioned external influences would affect both areas and consequently, could be compensated by differential measurements.

At a high number of immobilised cells or at low nutrient concentrations, the transport of the nutrient is limited by diffusion. Under this condition the nutrient concentration can be determined, similar to works based on enzyme-based field-effect sensors [14, 15]. For enzyme-based field-effect sensors, the enzymes are immobilised onto a pH-sensitive sensor surface. The substrate concentration is then determined by means of the enzymatic catalysis that typically yields a pH shift [16]. Utilising whole cells or bacteria instead of single enzymes has the advantage to determine all nutrients simultaneously that can be metabolised (under creation of acids or bases) by the immobilised microorganism. In the present work, this is exemplarily shown with *Escherichia coli* as organism and glucose as nutrient.

7.2 Experimental

7.2.1 LAPS set-up

The designed LAPS set-up utilised a 4×4 infrared light-emitting diode (LED) array as described in Ref. [9]. The LED array is driven by a field-programmable gate ar-

ray (FPGA), see Ref. [17]. The LAPS chip consists of thin films of 60 nm Ta_2O_5 and 30 nm SiO_2, a 450 µm p-doped Si and a Al rear-side contact. The contact area with the electrolyte and reference electrode (Ag/AgCl) is 15 mm × 15 mm. Every 2 min, the I/V curves are recorded for all 16 measurement spots successively. To determine the potential shift φ, the difference between the initial and the actual I/V curve were calculated.

7.2.2 Immobilisation and measurement

To realise the differential set-up, two wells on the LAPS-chip surface were created with the help of a photolithographically patterned SU-8 layer. The size of both wells has been 6 mm × 13 mm. One well is located above the measurement spots 1 to 8 and is defined as active area, immobilised with *Escherichia coli* within the polyacrylamide gel. The other well above measurements spots 9 to 16 serves as reference area; here, only gel without microbes is added. To determine the potential shifts, measurement spots 1 to 4 are used to calculate a mean value of the active area and measurement spots 13 to 16 are used for the reference area. The two outer columns have been chosen to obtain the maximal distance and to avoid diffusion effects between both areas.

The cultivation and immobilisation of *E. coli* is similar to that described in Ref. [6]. The *E. coli* were cultivated for 18 h in lysogeny broth (LB) medium at 37 °C and stirred with 180 rpm. The final cell concentration was established by cell counting, centrifugation at 805 g and finally, resuspension in TRIS buffer. After that, the *E. coli* were immobilised by embedding them into the polyacrylamide gel. More information about the gel composition can be found in Ref. [6]. In both wells an amount of 37 µl polyacrylamide gel was added. The gel on the active area contains $n = 1 \times 10^9$ *E. coli* cells.

For the measurement, a volume of $V = 1$ ml phosphate buffered saline (PBS) buffer with a pH-buffer capacity of $\beta = 0.2\,\mathrm{mM\,pH^{-1}}$ was used. At the beginning, PBS buffer without glucose was applied for conditioning. After this, measurements with different glucose concentrations of 0.5 mM, 1.0 mM and 1.5 mM added to the PBS buffer were performed, respectively. Between the measurements, PBS buffer without glucose was utilised as cleaning step of 30 min.

7.3 Results and discussion

Figure 7.2 shows the polymerised polyacrylamide gel on the LAPS-chip surface. Due to the high concentration of $n = 1 \times 10^9$ *E. coli* in 37 µl gel, the active area appears white. The microscopic picture in Fig. 7.3 depicts the high density of cells inside the polyacrylamide gel. Several methods have been discussed in literature to immobilise cells [18]. For the flat LAPS surface, alternatively e.g., the adherent growth [9], covalent

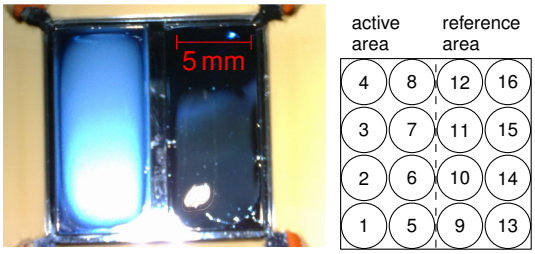

Figure 7.2: The polymerised polyacrylamide gel on the LAPS-chip surface. The left well is filled with the gel and *E. coli* cells, the right well contains only the gel. The numbers explain the measurement-spot locations.

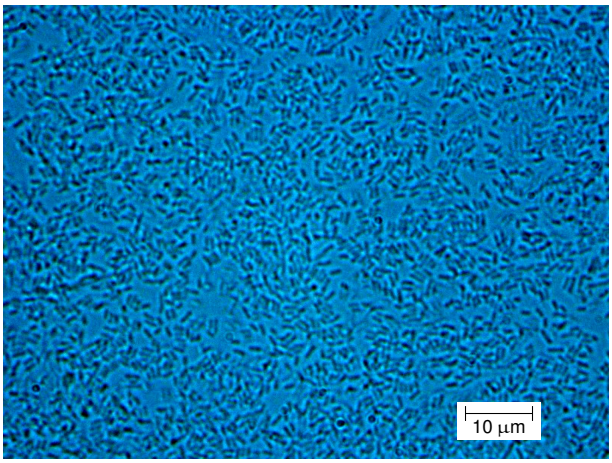

Figure 7.3: Microscopic picture of *E. coli* cells in the polyacrylamide gel.

immobilisation [19] or matrix entrapment in gel [20] have been suggested. *E. coli* and organisms from the biogas process are not growing adherently. Therefore, to guarantee a uniform cell distribution with a high amount of cells, we decided to utilise matrix entrapment in gel, which additionally acts as a physical protection layer. Possible gel matrices are, e.g., alginate, agarose or polyacrylamide gel [6, 20]. In our previous experiments with biogas-fermentation solution, polyacrylamide gel has been shown to be the most stable method. Additional measurements with *E. coli* growing in LB medium suspension have shown an acidification rate α of 5×10^4 H^+ ions per cell and per second, whereas for immobilised *E. coli* in polyacrylamide gel the acidification rate α was 4×10^4 H^+ ions per cell and per second [6]. This showed that the metabolic activity of *E. coli* is not negatively affected by the polyacrylamide gel.

The potential shifts of both measurement areas, with and without *E. coli*, at different glucose concentrations are presented in Fig. 7.4. During the first 45 min, PBS buffer without glucose was measured. A drift can be observed during this time and after a short conditioning the potential shifts are equal. After changing the medium to PBS

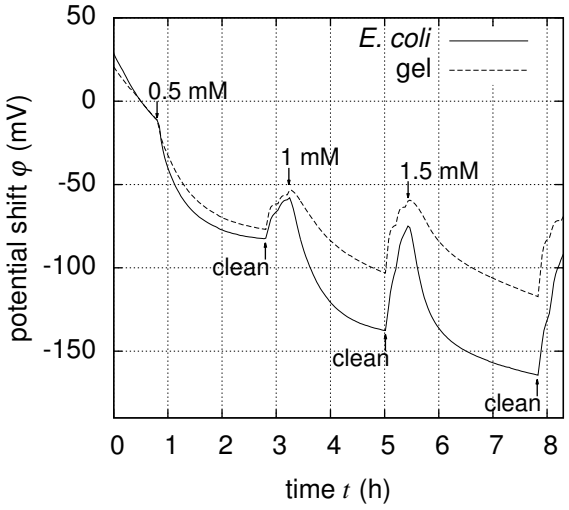

Figure 7.4: Potential shifts of both measurement areas (with and without *E. coli*) at different glucose concentrations. The arrows indicate the time at which the measurement medium was changed; the concentration values indicate the glucose concentration in the PBS buffer.

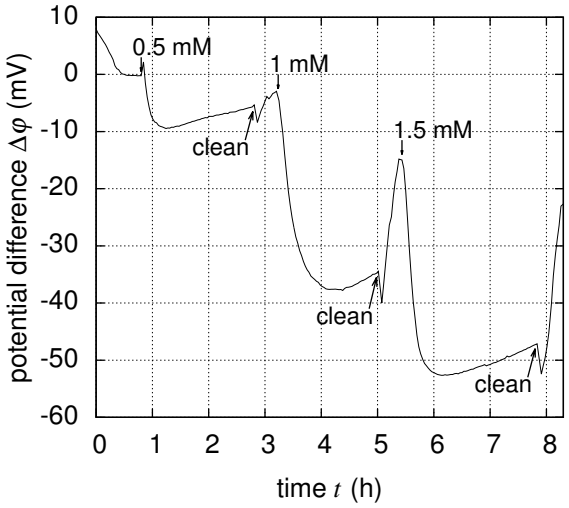

Figure 7.5: Potential difference, calculated by the subtraction of the reference area from the active area, at different glucose concentrations. The arrows indicate the time at which the measurement medium was changed; the concentration values indicate the glucose concentration in the PBS buffer.

buffer with glucose, an increase of the amount of potential shift can be seen. This is due to the extracellular acidification of the *E. coli* bacteria as a result of their metabolism of glucose. The potential shift that belongs to the area with *E. coli* indicates a higher acidification. In addition, a decrease of the reference signal is observable, too, which might be a result of the diffusion of produced acids from the active area to the reference area. During the cleaning steps with PBS buffer the sensor signal is recovering and becoming more positive again. This confirms that the previous potential shifts have been an effect of the extracellular acidification. However, the overall time of the cleaning steps is probably not long enough for a total removal of the produced acids from the gel.

The potential difference, calculated by subtraction of the reference area from the active area, is shown in Fig. 7.5. This difference signal underlines again the conditioning

phase followed by a steady phase during the first 45 min. During this time, PBS buffer without glucose was used. Consequently, without nutrients, the microorganisms have no additional metabolic activity. After the medium change to PBS buffer with glucose, the variation of the potential difference induced by the extracellular acidification can be easily identified. However, the signal behaviour is quite slow; it takes about 30 min to reach a minimum value. One possible explanation therefore is the hindered diffusion of the glucose molecules through the relatively thick polyacrylamide gel of about 470 µm. After the difference signal has reached a minimum it slightly increases. This is probably due to the produced acids, which are diffusing from the active area into the reference area of the LAPS chip: The potential shift in the reference part decreases, too, finally leading to an increase in the difference signal (after subtraction). During the cleaning steps the potential differences nearly – but not completely – originate their original starting values. Also in this case, the exchange (diffusion of the produced acids out of the gel) might be delayed by the thick membrane layer yielding a "hysteric"-type response behaviour of the LAPS.

To distinguish the relatively slow response time of the gel-covered LAPS chip from its hindered diffusion, further experiments with polyacrylamide gel without organisms have been performed. Here, different pH-buffer solutions (between pH 6 and pH 8) have been investigated (see Fig. 7.6). In that case the response time with approximately 30 min is also increased by a factor of about 30 when comparing the signal behaviour to a bare pH-sensitive LAPS set-up, described in literature [9, 21].

A calibration curve that represents the potential difference with respect to the glucose concentration is illustrated in Fig. 7.7. Since the LAPS is a potentiometric sensor, the response to the glucose concentration is calculated in the logarithmic scale. The three "potential difference" values in the diagram correspond to the particular minimum value

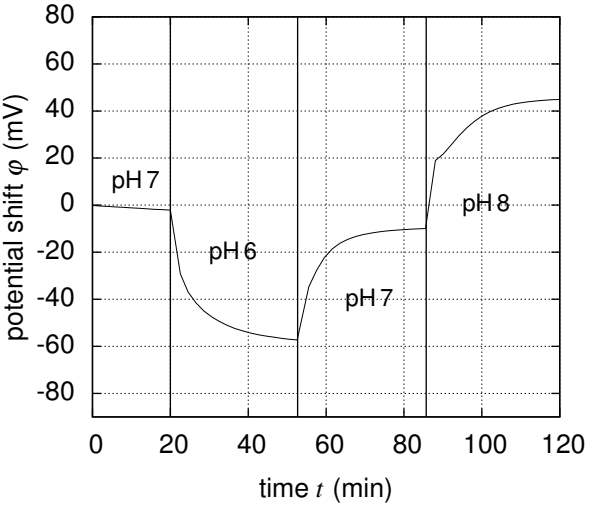

Figure 7.6: Response-time measurement of a LAPS chip with polyacrylamide gel without organisms at different pH-buffer solutions. The arrows indicate the time at which the pH-buffer solutions were changed.

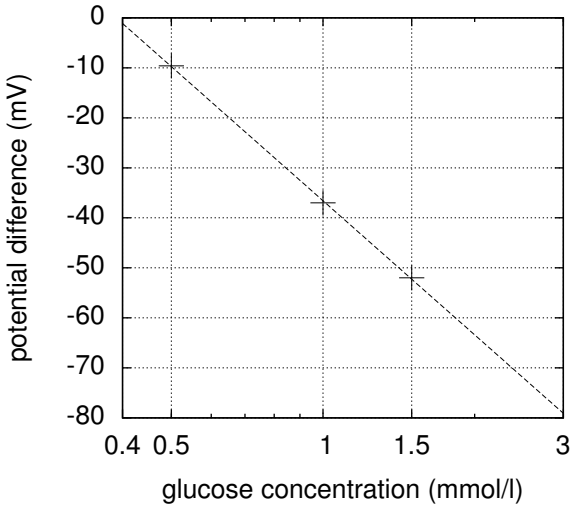

Figure 7.7: Minimum in the potential difference at the glucose concentration from Fig. 7.5 with respect to the glucose concentration.

Table 7.1: Rates of potential changes during the first 14 min after medium change from Fig. 7.5 and acidification rates calculated by Eq. (7.1).

glucose concentration c (mM)	potential-change rate $\dot{\varphi}$ (mV min^{-1})	acidification rate α (10^4 H$^+$ s^{-1} cell^{-1})
0.5	-0.78 ± 0.14	0.60 ± 0.12
1.0	-1.57 ± 0.04	1.30 ± 0.03
1.5	-2.27 ± 0.08	2.00 ± 0.07

of the three glucose concentrations from Fig. 7.5. Moreover, each of these values has been calculated as a mean value of four measurement spots, determining the glucose concentration at the sensor chip at the same time. With the help of a linear regression of these values, the sensitivity is calculated to be (89.0 ± 1.5) mV per decade glucose. Considering the signal-to-noise ratio, the lower detection limit for the present set-up is about 0.4 mM glucose. Nevertheless, more detailed investigations should be performed in further experiments in order to exactly define its value.

To prove, that the transport of glucose is limited by diffusion, the slope in the potential difference during the first 14 min after addition of the particular glucose solution was calculated by linear regression for each glucose concentration from Fig. 7.5. With these potential-change rates, the acidification rates were calculated with the help of Eq. (7.1). Both data are listed in Table 7.1 and are describing the kinetics of the reaction rate from glucose to its acid. The values are correlating linearly with the glucose concentration. The acidification rate α at 1.5 mM glucose is calculated to be $(2.00 \pm 0.07) \times 10^4$ H$^+$ ions per cell and per second. In previous experiments, the acidification rate α of *E. coli* in LB-medium suspension was determined to be about 5×10^4 H$^+$ ions per cell and per second [6]. Both acidification rates are in the same order of magnitude, but the value at

1.5 mM glucose is somewhat lower; this might be a result of the limited diffusion of the glucose through the polyacrylamide membrane.

7.4 Conclusion and outlook

A biosensor based on *E. coli* immobilised on a LAPS chip was developed. This set-up is sensitive to the concentrations of nutrients metabolised by *E. coli* resulting in an extracellular acidification. This has been demonstrated with glucose as nutrient. The set-up has a sensitivity of $(89.0 \pm 1.5)\,\mathrm{mV/p[glucose]}$ and a lower detection limit of about 0.4 mM. The functional principle of this new set-up is comparable to enzyme-based field-effect sensors using diffusion limitation. With the help of the addressability of the LAPS an on-chip differential set-up was developed. Thus, external influences, like sensor drift, temperature and external pH changes can be reduced.

However, the response time of the sensor with about 30 min is rather slow. A decrease of the polyacrylamide gel thickness could improve the response time. Due to the very high cell density inside the polyacrylamide gel, the number of cells can only be increased by a higher gel thickness. An optimal thickness of the gel layer must be found, which balances between the amount of microbes inside the gel to achieve a diffusion limitation and a fast response time. Since biogas fermentation represents a relatively slow process with a hydraulic retention time of 30 to 50 days in conventional biogas plants [5], an on-line monitoring with 30 min to 1 h intervals is sufficiently high enough to perform real-time measurements.

In further investigations, the sensitivity towards other nutrients metabolised by *E. coli* or other microbes by producing acids or bases should be investigated. Examples of other microbes and nutrient combinations are described in [22]. Finally, the presented set-up should be used to monitor biogas processes. For this, a protocol to immobilise a relevant organism of the anaerobic digestion, e.g. *Methanosaeta concilii* is under process.

Besides the monitoring of biogas processes, those microorganism-based biosensors that are sensitive towards nutrient concentration open a wide field of possible applications for e.g., cell growth in fermentation processes. Their ability to be sensitive to all nutrients and also inhibiting substances that are affecting the metabolic activity of the immobilised organisms might serve as an overall indicator to define the status of the fermentation process. This might be also helpful to further optimise cell culturing in fermentation processes in the fields of food or pharmaceutical industry.

Acknowledgements

The authors thank the German Federal Ministry of Food, Agriculture and Consumer Protection (BMELV) and the "Fachagentur Nachwachsende Rohstoffe e.V." (FNR) for financial support of this work (Bio-LAPS).

References

[1] J. C. Owicki and J. W. Parce. "Biosensors based on the energy metabolism of living cells: The physical chemistry and cell biology of extracellular acidification". In: *Biosensors & Bioelectronics* 7.4 (1992), pp. 255–272. DOI: 10.1016/0956-5663(92)87004-9.

[2] T. Yoshinobu, H. Ecken, A. B. M. Ismail, H. Iwasaki, H. Lüth, and M. J. Schöning. "Chemical imaging sensor and its application to biological systems". In: *Electrochimica Acta* 47.1-2 (2001), pp. 259–263. DOI: 10.1016/S0013-4686(01)00564-3.

[3] A. Poghossian, S. Ingebrandt, A. Offenhäusser, and M. J. Schöning. "Field-effect devices for detecting cellular signals". In: *Seminars in Cell & Developmental Biology* 20.1 (2009), pp. 41–48. DOI: 10.1016/j.semcdb.2009.01.014.

[4] B. K. Ahring. "Perspectives for anaerobic digestion". In: *Biomethanation I*. Ed. by T. Scheper. Vol. 81. Berlin, Heidelberg: Springer-Verlag, 2003, pp. 1–30. DOI: 10.1007/3-540-45839-5_1.

[5] Yadvika, Santosh, T. Sreekrishnan, S. Kohli, and V. Rana. "Enhancement of biogas production from solid substrates using different techniques—a review". In: *Bioresource Technology* 95.1 (2004), pp. 1–10. DOI: 10.1016/j.biortech.2004.02.010.

[6] C. F. Werner, C. Krumbe, K. Schumacher, S. Groebel, H. Spelthahn, M. Stellberg, T. Wagner, T. Yoshinobu, T. Selmer, M. Keusgen, M. E. M. Baumann, and M. J. Schöning. "Determination of the extracellular acidification of *Escherichia coli* by a light-addressable potentiometric sensor". In: *physica status solidi (a)* 208.6 (2011), pp. 1340–1344. DOI: 10.1002/pssa.201001141.

[7] M. Nakao, S. Inoue, T. Yoshinobu, and H. Iwasaki. "High-resolution pH imaging sensor for microscopic observation of microorganisms". In: *Sensors and Actuators B: Chemical* 34.1-3 (1996), pp. 234–239. DOI: 10.1016/S0925-4005(96)01903-X.

[8] B. Stein, M. George, H. E. Gaub, J. C. Behrends, and W. J. Parak. "Spatially resolved monitoring of cellular metabolic activity with a semiconductor-based biosensor". In: *Biosensors & Bioelectronics* 18.1 (2003), pp. 31–41. DOI: 10.1016/S0956-5663(02)00109-4.

[9] T. Wagner, R. Molina, T. Yoshinobu, J. P. Kloock, M. Biselli, M. Canzoneri, T. Schnitzler, and M. J. Schöning. "Handheld multi-channel LAPS device as a transducer platform for possible biological and chemical multi-sensor applications". In: *Electrochimica Acta* 53.2 (2007), pp. 305–311. DOI: 10.1016/j.electacta.2007.04.006.

[10] A. Poghossian and M. J. Schöning. "Silicon-based chemical and biological field-effect sensors". In: *Encyclopedia of Sensors*. Ed. by C. A. Grimes, E. C. Dickey, and M. V. Pishko. Vol. X. Santa Clarita, California, USA: American Scientific Publishers, 2006, pp. 1–71.

[11] D. G. Hafeman, J. W. Parce, and H. M. McConnell. "Light-addressable potentiometric sensor for biochemical systems". In: *Science* 240.4856 (1988), pp. 1182–1185. DOI: 10.1126/science.3375810.

[12] J. C. Owicki, L. J. Bousse, D. G. Hafeman, G. L. Kirk, J. D. Olson, H. G. Wada, and J. W. Parce. "The light-addressable potentiometric sensor: Principles and biological applications". In: *Annual Review of Biophysics and Biomolecular Structure* 23 (1994), pp. 87–113. DOI: 10.1146/annurev.bb.23.060194.000511.

[13] T. Wagner and M. J. Schöning. "Light-addressable potentiometric sensors (LAPS): recent trends and applications". In: *Electrochemical Sensor Analysis*. Ed. by S. Alegret and A. Merkoci. Vol. 49. Amsterdam: Elesevier, 2007, pp. 87–128.

[14] A. Poghossian, T. Yoshinobu, A. Simonis, H. Ecken, H. Lüth, and M. Schöning. "Penicillin detection by means of field-effect based sensors: EnFET, capacitive EIS sensor or LAPS?" In: *Sensors and Actuators, B: Chemical* 78.1-3 (2001), pp. 237–242. DOI: 10.1016/S0925-4005(01)00819-X.

[15] J. R. Siqueira Jr., C. F. Werner, M. Bäcker, A. Poghossian, V. Zucolotto, O. N. Oliveira Jr., and M. J. Schöning. "Layer-by-layer assembly of carbon nanotubes incorporated in light-addressable potentiometric sensors". In: *Journal of Physical Chemistry C* 113.33 (2009), pp. 14765–14770. DOI: 10.1021/jp904777t.

[16] S. D. Caras, J. Janata, D. Saupe, and K. Schmitt. "pH-based enzyme potentiometric sensors. Part 1. Theory". In: *Analytical Chemistry* 57.9 (1985), pp. 1917–1920. DOI: 10.1021/ac00286a027.

[17] C. F. Werner, S. Schusser, H. Spelthahn, T. Wagner, T. Yoshinobu, and M. J. Schöning. "Field-programmable gate array based controller for multi spot light-addressable potentiometric sensors with integrated signal correction mode". In: *Electrochimica Acta* 56.26 (2011), pp. 9656–9660. DOI: 10.1016/j.electacta.2011.03.012.

[18] G. A. Dervakos and C. Webb. "On the merits of viable-cell immobilisation". In: *Biotechnology Advances* 9.4 (1991), pp. 559–612. DOI: 10.1016/0734-9750(91)90733-C.

[19] K. S. Siow, L. Britcher, S. Kumar, and H. J. Griesser. "Plasma methods for the generation of chemically reactive surfaces for biomolecule immobilization and cell colonization – a review". In: *Plasma Processes and Polymers* 3.6-7 (2006), pp. 392–418. DOI: 10.1002/ppap.200600021.

[20] A. C. Jen, M. C. Wake, and A. G. Mikos. "Review: Hydrogels for cell immobilization". In: *Biotechnology and Bioengineering* 50.4 (1996), pp. 357–364. DOI: 10.1002/(SICI)1097-0290(19960520)50:4<357::AID-BIT2>3.0.CO;2-K.

[21] T. Wagner, C. Rao, J. Kloock, T. Yoshinobu, R. Otto, M. Keusgen, and M. Schöning. ""LAPS Card" – A novel chip card-based light-addressable potentiometric sensor (LAPS)". In: *Sensors and Actuators, B: Chemical* 118.1–2 (2006), pp. 33–40. DOI: 10.1016/j.snb.2006.04.019.

[22] M. Sole, N. Rius, and J. G. Loren. "Rapid extracellular acidification induced by glucose metabolism in non-proliferating cells of *Serratia marcescens*". In: *International microbiology* 3.1 (2000), pp. 39–43. URL: http://revistes.iec.cat/index.php/IM/article/view/4c457c0c4ac46.002.

7.5 Supporting information

7.5.1 Observing of other nutrients[1]

In addition, the extracellular acidification of *E. coli* to different nutrients was investigated. The acidification measurements were performed with PBS solutions including various concentrations of different saccharides (glucose, fructose, maltose) and glycerol, known to be used by *E. coli* as substrates for growth. The extracellular acidification was determined in suspensions (see Fig. 7.8 and Fig. 7.9) and by in polyacrylamide gel entrapped cells in a differential set-up (see Fig. 7.10 and Fig. 7.11) in order to study the effect of immobilisation.

Interestingly, measurements with glycerol, a substrate exclusively used by *E. coli* under aerobic conditions, showed no acidification in case of the immobilised cells. The lack of signals in presence of glycerol strongly suggests the assumption that the observed acidification is due to anaerobic, mixed-acid fermentation of *E.coli* on the LAPS-chip surface.

[1]The results of this section are not part of the present article and will be published separately.

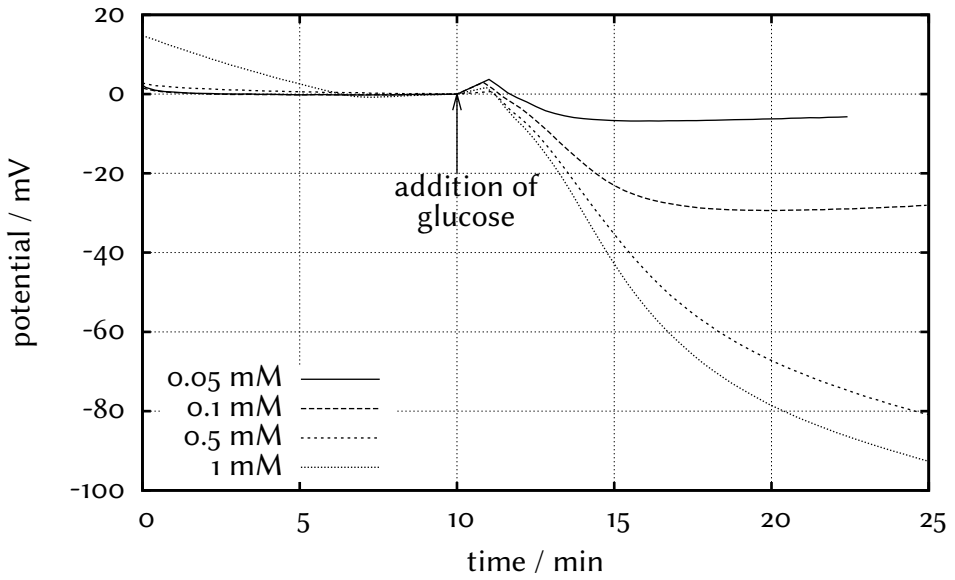

Figure 7.8: Determination of the extracellular acidification of *E. coli* in suspension. Starting with about 10^{10} cells in 2 ml PBS buffer. After 10 min, glucose was added to achieve the specified concentration.

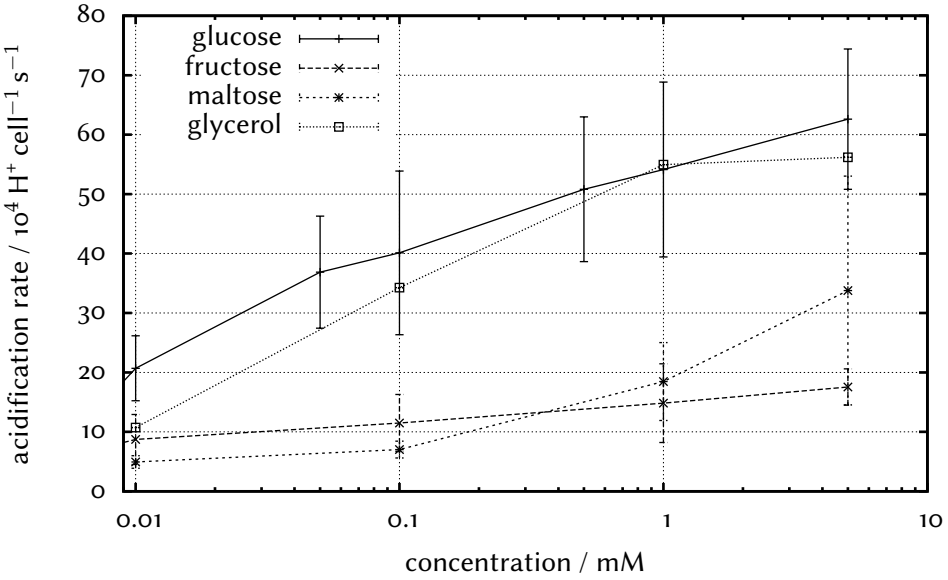

Figure 7.9: Acidification rates at different nutrient concentrations by utilising *E. coli* in suspension. The acidification rates are calculated by Eq. (7.1).

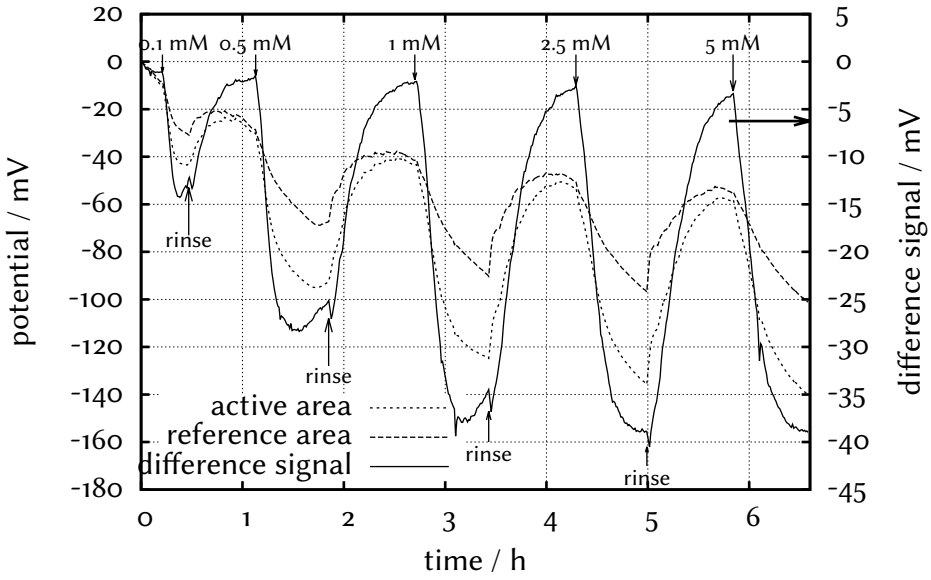

Figure 7.10: Determination of the extracellular acidification of immobilised *E. coli* utilising PBS buffer and different glucose concentrations. Potential shifts of both measurement areas (with and without *E. coli*) as well as the difference signal is shown. The arrows indicate the time at which the measurement medium was changed; the concentration values indicate the glucose concentration in the PBS buffer.

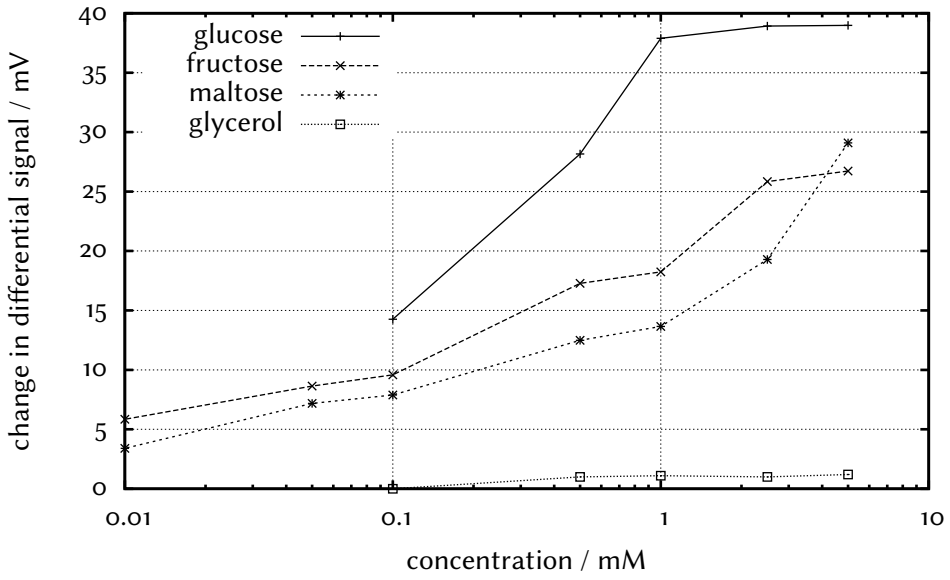

Figure 7.11: Maximal changes in the differential signal at different nutrient concentrations by utilising *E. coli* immobilised in differential arrangement.

7.5.2 Measurements in biogas-digester solution[2]

The same sensor system as described in the chapter 7 was used to observe the extracellular acidification of the immobilised *E. coli* by measuring in slurry that is used as substrate for a biogas digester instead of PBS buffer. The measurements were performed by utilising an anaerobic flow-through cell, to prevent any gas exchange. To achieve an extracellular acidification, glucose was added to the slurry just before the slurry was pumped into the measurement chamber. Figure 7.12 and Fig. 7.13 depict the sensor response of both areas as well as the differential signal for two independent measurements. After adding the 5 mM glucose, the differential signal will change of about −3 mV due to the extracellular acidification of the immobilised *E. coli*. Thereafter, the differentice signal tends to 0 mV, probably caused by the decreasing glucose concentration due to the metabolism by other living microorganisms inside the slurry. An exchange of the slurry with new glucose will result in a further acidification. This demonstrates the ability of this biosensor to be used in a biogas-digester solution and to observe indirectly the metabolic activity of the microorganisms that are involved in the anaerobic digestion.

[2]The results of this section are not part of the present article and will be published separately.

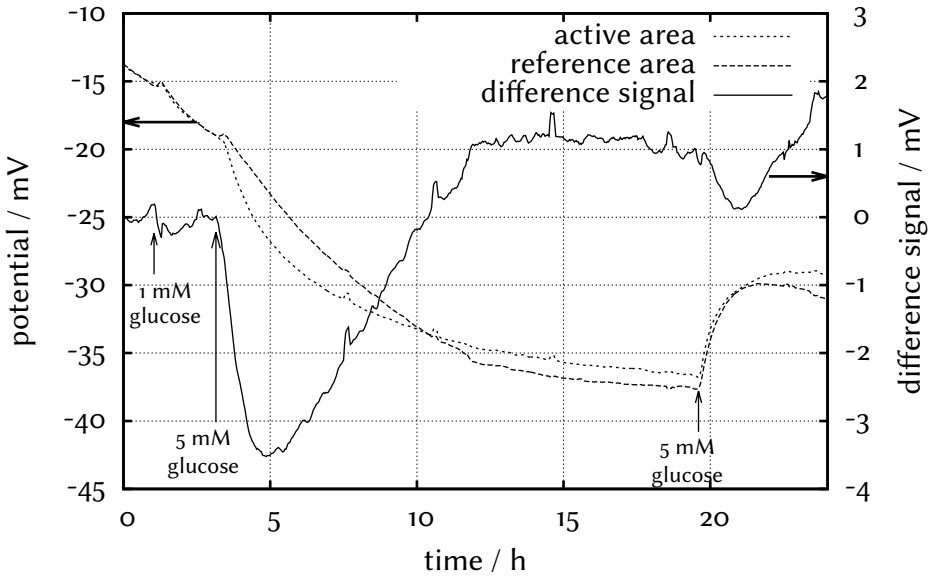

Figure 7.12: Determination of the extracellular acidification of immobilised *E. coli* utilising slurry used as substrate for biogas digesters. Potential shifts of both measurement areas (with and without *E. coli*) as well as the difference signal is shown. The arrows indicate the time at which slurry was exchanged; the concentration values indicate the glucose concentration that was added to the slurry directly before exchanging.

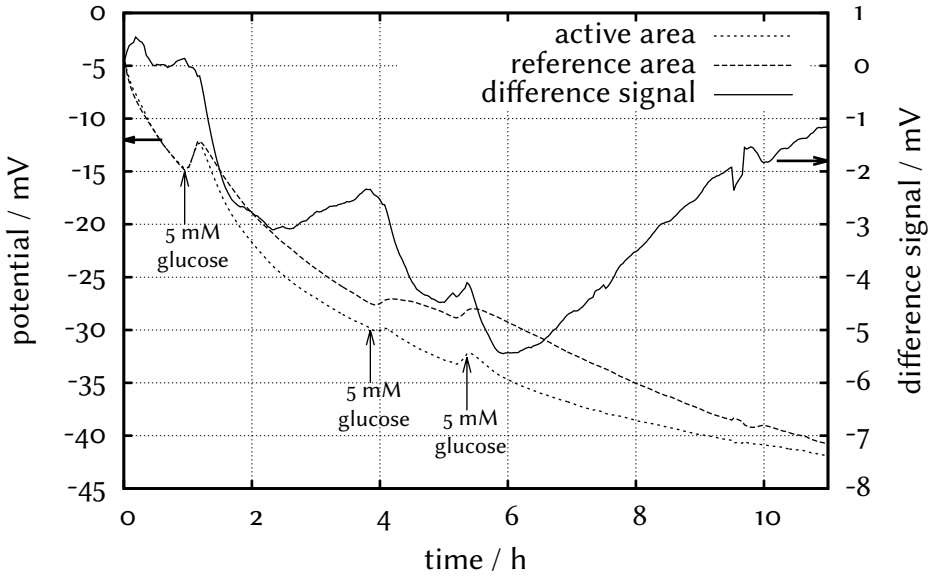

Figure 7.13: Determination of the extracellular acidification of immobilised *E. coli* utilising slurry used as substrate for biogas digesters. Potential shifts of both measurement areas (with and without *E. coli*) as well as the difference signal is shown. The arrows indicate the time at which slurry was exchanged; the concentration values indicate the glucose concentration that was added to the slurry directly before exchanging.

8 Summary and perspectives

Light-addressable potentiometric sensors (LAPS) enable the monitoring of analyte concentrations of aqueous solutions in a spatially resolved manner. Therefore, a light pointer is used to address the region of interest (the measurement spot) on the sensor surface. A concentration-depending photocurrent is generated in the illuminated area. This allows to analyse the two-dimensional concentration distribution as well as its change over time and to visualise them in form of chemical images. Another feature of the LAPS is the possibility to analyse the concentration of multiple analytes with one single sensor chip by utilising different sensitive transducer materials, membranes or complex recognition elements, e.g., enzymes or cells. The ability to determine concentration distributions and multiple analytes with one single sensor chip makes LAPS an interesting tool for observing chemical, biochemical and microbiological processes. Thus, LAPS are attractive for a wide field of applications in the areas of chemistry, biotechnology and pharmacy.

The present thesis aimed to be the successor of the thesis of Dr. Torsten Wagner from 2008 [1], who demonstrated the potential of LAPS for pharmaceutical applications. Furthermore, he developed miniaturised and self-contained LAPS set-ups utilising only commercially available components to demonstrate the practicability of LAPS for an industrial implementation. This present thesis is divided into two parts: The first part was dedicated to further developments of different LAPS set-ups and their characterisation. In detail, the frequency behaviour and the lateral resolution of the used LAPS chips were characterised and discussed. The second part of this present thesis highlights potential application of LAPS. Therefore, enzymes and bacteria were used as complex biological recognition elements to demonstrate the capability of these sensors in the field of process engineering, biology, medicine and pharmacy.

8.1 Development and characterisation of new LAPS set-ups

In **chapter 2** a new electronic control unit for LAPS-based chemical sensors using a field-programmable gate array (FPGA) was presented. This FPGA-based control unit, utilising a Spartan 3A (XC3S400A) FPGA from Xilinx, is used to drive a light-

source array consisting of a 4×4 infrared light-emitting diode (IR-LED) array with a wavelength of 950 nm. With the FPGA implementation, it is possible to configure the frequency, amplitude, offset and starting phase of the modulation signal individually for each light source. Thus, all 16 IR-LEDs can be driven simultaneously and the measurement spots, defined by the illuminated area, can be read out concurrently by modulating each light source with a different frequency. Subsequently, the frequency components of the resulting photocurrent will be separated with a fast Fourier transform (FFT) algorithm and can be mapped to the corresponding measurement spot.

This FPGA-based LAPS represents a further stage of development of the FFT-based LAPS from [1], where the 16 IR-LEDs were driven by 16 discrete electrical circuitries as frequency generators. Utilising the FPGA will bring some further advantages: The frequency generators are synthesised in the FPGA chip and the IR-LEDs can be contacted directly to a large number of available general purpose input/output pins. This way, more compact measurement systems could be achieved and the number of light sources can easily be extended without additional circuitries. The second advantage is the possibility to adjust the amplitude of the modulation signal individually. The adjustment of the amplitude of the modulation signal enables to control the light brightness and hence, makes it possible to compensate variations in brightness due to manufacturing tolerances of the IR-LEDs, to adjust the frequency behaviour of the photocurrent, to equalise tilt between the light-source array and the sensor chip and to compensate defects in the semiconductor substrate. Furthermore, a common clock and a trigger signal for the frequency generators and the photocurrent sampling were introduced to be able to determine the phase shift of the photocurrent compared to the excitation signal.

The developed LAPS system allows to modify modulation parameters during run time. Thus, it was shown that this LAPS set-up provides the possibility to observe the frequency response of LAPS structures with regard to the amplitude and phase shift and to use optimised frequencies for individual LAPS structures. The analyte concentration-depending surface potential can be read out in the well-proven current/voltage as well as the phase/voltage mode, in which the phase shift due to the change of the surface potential is determined. Both modes offer the possibility of concurrent modulation of all light sources of the array at different frequencies. This was demonstrated with a pH-sensitive LAPS chip and different pH-buffer solutions.

In addition, a brightness-control mode was implemented. This way, the brightness of each IR-LED can automatically be adjusted, in order to equalise all the resulting photocurrent amplitudes of the measurement spots with respect to a defined bias voltage. At the beginning of a measurement series, this mode has to be run under equal and steady calibration conditions for each measurement spot. The resulting brightness value

for each IR-LED can be saved and used for the subsequent measurements. Exemplary measurements showed that by using this mode, the variance of the determined surface potential of all 16 measurement spots is reduced by a factor of about 20.

In **chapter 3**, the previously developed FPGA-based LAPS set-up is used to analyse the frequency behaviour and the bias-voltage dependency of a LAPS chip. In order to analyse the frequency behaviour and to determine frequency-depending components of the LAPS set-up, the frequency response was compared with the electrical impedance of the LAPS structure by means of electrical equivalent circuits. To determine the electrical impedance of LAPS structures, the FPGA-based LAPS set-up was modified in such way to enable measurements of the electrical impedance at different frequencies by superimposing a modulated voltage to the bias voltage. This way, the electrical impedance spectra, the LAPS-frequency behaviour as well as the electrochemical characterisation, e.g., C/V and I/V curves, may be investigated with a single set-up simultaneously. Furthermore, the detection of the phase shift of the photocurrent was improved by taking into account the frequency behaviour of the photocurrent amplifier. Thus, the "correct" frequency behaviour of the phase shift of the photocurrent could be determined for the first time.

The newly implemented electrical impedance-measurement mode was validated by means of different RC series connections in the frequency range between 10 Hz and 50 kHz. After that, the C/V and I/V curves of the LAPS structure at pH 7 were measured in order to determine the bias-voltage range, at which depletion occurs. At four different bias voltages in the depletion region, the electrical impedance spectra were measured and fitted to an RC series connection. The evaluated parameter of R describes the resistivity of the electrolyte and the resistance of the reference electrode, whereas the evaluated parameter of C describes the capacitance of the insulator of the LAPS structure and the bias voltage-depending capacitance of the space-charge region. The electrical impedance was measured with and without illumination by the IR-LEDs. Without illumination, the capacitance C decreased with increasing bias voltage, which is a typical behaviour of a capacitive electrolyte/insulator/semiconductor (EIS) sensor, such as LAPS structure, in this measurement mode. However, with illumination, the capacitance C shows a more than 5 times lower dependency of the bias voltage. This demonstrates that the additionally generated charge carriers, due to the illumination, will influence the capacitance of the space-charge region significantly. With the same LAPS structure, the frequency responses of the photocurrent at light-modulation frequencies in the same frequency range and at the same bias voltages, like the electrical impedance measurements, were observed. These frequency responses were fitted to a model, which includes the same parameters such as the RC series connection and in addition, the time constant τ_n, which represents the bulk recombination lifetime

of the minority-charge carriers and a bias voltage-depending factor $k < 1$. The factor k describes the internal generation of the photocurrent and thus, includes the efficiency of the IR-LED, the absorption coefficient of the light, the generation of electron-hole pairs and their diffusion. The frequency responses of the LAPS when utilising the light sources represent a bandpass-like characteristic in terms of amplitude and phase shift of the photocurrent. By utilising the parameters resulting from the electrical-impedance measurement with illumination, the time constants of the bandpass characteristic are RC and τ_n. The highest photocurrent amplitude was found between these time constants. At the same point, the best signal-to-noise ratio could be achieved for electrochemical measurements. For the LAPS structures that were used in this work, the optimal frequency is in the range of about 1 kHz to 10 kHz. Considering the mechanisms how the bias voltage or the surface potential will influence the photocurrent amplitude, it was demonstrated that the photocurrent amplitude is influenced by the voltage-depending photocurrent generation and the capacitance of the space-charge region. The comparison of both mechanisms underlines that the change induced by the photocurrent generation is about 12 times higher. It could be also shown that under some conditions, e.g. modulation frequencies $f > \frac{1}{2\pi RC}$ and low ionic strengths, the photocurrent amplitude and thus the measurement signal could be influenced by the electrolyte conductivity. By utilising the phase shift of the photocurrent instead of the amplitude, the influence of the electrolyte conductivity can be reduced. Overall, the demonstrated methods in **chapter 3** help to characterise and optimise LAPS structures as well as to find the optimised frequency range for I/V measurements. In addition, impedance measurements allow to simultaneously study the intrinsic sensor performance as well as charge changes at the interface sensor/analyte. In order to improve the performance as electrochemical imaging sensor, it is important to minimise the influence of the electrolyte conductivity and to decrease the measurement time. To reduce the measurement time, a high photocurrent amplitude (for a good signal-to-noise ratio) and a high measurement frequency is advantageous. Since the maximal photocurrent amplitude was observed between the time constants RC and τ_n, it is advisable to choose these parameters to achieve a high bandwidth at high frequencies, as far as this is in the range of the possible semiconductor chip-fabrication technologies.

To achieve a higher lateral resolution, more light sources have to be placed in an array with a higher density. Since this requires smaller light-emitting diodes (LEDs) and a more complex circuit board, designing an LED array with a higher number of individual LEDs is not always the practical way to improve lateral resolution. On this account, in **chapter 4**, a commercially available organic light-emitting diode (OLED) display has been chosen as a light source. This OLED display consists of 96×64 pixels on an area of 20.1 mm $\times$ 13.2 mm, which equals in a pixel size of 200 µm $\times$ 200 µm. Thus, this

OLED display allows an over 16 times higher resolution compared to the IR-LED array of the FPGA-based LAPS set-up and, with a thickness of only 2 mm, the OLED panel enables a further miniaturisation of the measuring instruments. Since OLED displays are mainly utilised for video applications, which only require low refresh rates (typical 50 Hz), the refresh rate is fixed at 135 Hz by the integrated driving chip of the used OLED panel. However, the characterisation of the frequency response of the LAPS structures (see chapter 3) showed that the optimal modulation frequency with respect to the signal-to-noise ratio is typically in the kHz range. In addition, the usage of higher modulation frequencies for LAPS measurements is needed in order to perform faster measurements. Therefore, a different driving method for the OLED display has been implemented, in order to achieve higher modulation frequencies. The new method offers the possibility to use modulation frequencies between 1 kHz and 16 kHz and hence, reduces the measurement time of a chemical image compared to the traditional addressing of an OLED display. With the implemented driving method, multiple pixels in a single row can be activated, which will increase the signal-to-noise ratio but will decrease the spatial resolution. Since the used OLED display is a full-colour display, where one pixel consists of three colours (red, green, blue), the fraction of each colour to the resulting photocurrent was analysed. The results underline that a shorter wavelength will decrease the photocurrent, thus the red sub-pixel produces more than 50 % of the photocurrent from the white measurement spot. With a pH-sensitive Si_3N_4-LAPS structure, the fundamentals of the developed set-up for e.g., pH measurements have been demonstrated. A chemical image of the surface was achieved in 2.5 min. The time to obtain a chemical image is thereby reduced by a factor of 40 compared to the traditional addressing of an OLED display (see [2]). A possible application of the OLED-based LAPS set-up is the multi-ion imaging. Therefore, different ion-sensitive membranes could be fabricated periodically line by line on the LAPS-chip surface in a way that they fit to the pixel rows of the OLED display.

The lateral resolution of LAPS is not only specified by the light sources, also the semiconductor layer of the LAPS chip has an impact to its lateral resolution, e.g., its thickness and the bulk-recombination time of electron-hole pairs [3]. To characterise the lateral resolution of the LAPS structures, a scanning-LAPS set-up was developed. The scanning-LAPS set-up is described in **section 4.5.1** It utilises a laser diode that can be moved by an XY stage. The laser is focused to a spot with a diameter of about 70 µm and the XY stage can move it with a repeatability of 40 nm. With line and space pattern of gold on the LAPS surface, the lateral resolution of the LAPS chips was demonstrated to be about 250 µm. This lateral resolution fits to the light density of the OLED panel of the developed OLED-based LAPS set-up. Thus, the OLED-based LAPS can achieve its maximum resolution without redesigning the LAPS structures.

Table 8.1: Properties of the pH-imaging sensor for the LAPS- and CCD-type set-up.

	LAPS	CCD
Image creating	modulated light pointer	array of CCDs
Electronic circuitry	external	integrated
Fabrication complexity	low	high
Resolution	4×4 pixels	32×32 pixels
Pixel pitch	3.5 mm	130 µm
Transducer material	Ta_2O_5	Si_3N_4
pH sensitivity[a]	56.5 mV pH^{-1}	20.5 mV pH^{-1}
Long-term stability	high	low
Signal variation within 60 s	0.015 pH	0.115 pH

[a] The pH sensitivity is compared to the sensor-output signal.

In **chapter 5**, the FPGA-based LAPS set-up is compared to a pH-imaging sensor based on the charge-coupled device (CCD) principle that was developed by the Toyohashi University of Technology in Japan. The properties of both pH-imaging sensors are summarised in Tab. 8.1. The CCD-type sensor consists of an array of 32×32 single CCD-based sensors, arranged in a distance of 130 µm. They are fabricated on one single sensor chip together with an additional circuitry for addressing and signal processing. To compare the dynamic behaviour of the LAPS and the CCD-type sensor, the constant-voltage read-out mode was implemented for the FPGA-based LAPS, where all 16 IR-LEDs are driven simultaneously. To obtain the potential shift of each measurement spot, first, the I/V curves of all 16 measurement spots are recorded concurrently. Then, the bias voltage is fixed to a specific value and only the photocurrents of all 16 measurement spots are recorded periodically. After the measurement, the surface-potential shift of each measurement spot is calculated by utilising the inverse function of the corresponding I/V curve. With this method it is possible to obtain a chemical image within 200 ms, which is equal to 5 frames per second. By observing the diffusion and transformation of analytes by chemical reactions, the ability to measure an analyte distribution on the sensor surface in a spatially and temporal-resolved manner was demonstrated with the LAPS- and the CCD-type pH-imaging sensor. From a comparison of both sensors it was concluded that they, depending on their properties, yield advantage for specific applications. The CCD-based imaging sensor offers a higher resolution that enables to obtain chemical images in a "microscopic" range. However, the FPGA-based LAPS showed, with a pH sensitivity of 56.5 mV pH^{-1} and a signal variation of only 0.015 pH, a better performance for electrochemical measurements. Furthermore, the LAPS provided a better adhesion of enzymatic layers and a better long-term stability, which is probably due to its smooth and unstructured surface. All in all, the LAPS set-up is advantageous for long-term measurements of several hours

Table 8.2: Overview of the developed LAPS set-ups and their properties. Beside of the LAPS chip properties, the resulting lateral resolution of the LAPS set-ups depends on the parameters "distance between the light sources" and "light-spot size diameter"; either of these parameters defines the highest achievable lateral resolution.

Properties	FFT LAPS[a]	FPGA LAPS	OLED LAPS	Scanning LAPS
Number of light sources	4×4	4×4[b]	96×64	1
Light-source type	LED	LED	OLED	Laser diode
Light colour	Infrared	Infrared	Red + green + blue	Red
Light wavelength	950 nm	950 nm	Not specified	780 nm
Distance between light sources	3.5 mm	3.5 mm	210 µm	40 nm
Light-spot size diameter	2.5 mm	2.5 mm	190 µm	70 µm
Addressable area	$14 \times 14\,mm^2$	$14 \times 14\,mm^2$	$20 \times 13\,mm^2$	$18 \times 18\,mm^2$
Maximal light-modulation frequency	12.5 MHz	80 MHz	16 kHz	300 kHz
Photocurrent-sampling rate	1 MHz	1 MHz	100 kHz	100 kHz
Typical duration of chemical image	–	20 ms	2.5 min	1.5 h[c]
Simultaneous measurable spots	All	All	One	One
Able to measure the phase shift of the photocurrent	No	Yes	No	Yes
Able to measure the electrical impedance	No	Yes	No	No
Able to adjust the brightness of the light	No	Yes	No	Yes

[a] Previous LAPS set-up from [1] not developed during this present thesis, listed only for comparison.
[b] Expandable to 36 light sources.
[c] With a resolution of 100 µm and a scanning area of $18 \times 18\,mm^2$.

and days.

In **chapter 2** to **chapter 5** the development and characterisation of three new LAPS set-ups is described. The properties of these set-ups together with the predecessor model are summarised in Tab. 8.2. The FPGA-based and the FFT-based LAPS provide the lowest lateral resolution of 4×4 pixels with a distance of about 3.5 mm. However, the FPGA-based LAPS is able to measure in a wide frequency range and enables to monitor dynamic processes with 5 chemical images per second. Furthermore, the phase shift of the photocurrent and the electrical impedance of the LAPS structure may be determined by means of the FPGA-based LAPS. These features allow to characterise the LAPS chips in detail. In concrete terms, to determine the surface potential by different methods and thus, to check the sensor is working properly. Beside of the LAPS chip properties, the resulting lateral resolution of the LAPS set-ups depends on the parameters distance between the light sources and light-spot size diameter; either of these parameters defines the highest achievable lateral resolution. Since the scanning LAPS provides the highest achievable lateral resolution, the limited lateral resolution of the LAPS chip was observed with this device to be about 250 µm. To achieve better lateral resolutions the LAPS structures have to be improved, e.g., by thinning the silicon layer [4] or using amorphous silicon [5]. Also, by additionally improving the optical properties of the scanning LAPS, a lateral resolution in the range of 10 µm seems to be possible, which would be necessary to observe single cells or cell communications. By means of the OLED-based LAPS, the possibility to use commercially available OLED panels as light source for LAPS was demonstrated. A new implemented driving method allows to set modulation frequencies from 1 kHz to 16 kHz, which is the optimal range for the LAPS structures. The lateral resolution of 96×64 pixels with a distance of 210 µm also is in a good agreement with many applications of LAPS and due to a thickness of the OLED panel of only about 2 mm, a further miniaturisation of LAPS set-ups is realisable.

8.2 Applications of LAPS as biosensor

One possibility for LAPS-based biosensors is the usage of enzymes as complex biological recognition elements. In **chapter 5**, the detection of the neuronal transmitter acetylcholine (ACh) by using the enzyme acetylcholine esterase (AChE) is demonstrated. AChE oxidises ACh to choline and acetic acid. The latter mentioned will cause a pH change. This pH change may be determined with pH-sensitive field-effect sensors, as it is demonstrated by utilising the FPGA-based LAPS and a CCD-type imaging sensor. Therefore, the enzyme AChE was immobilised on the sensor surfaces by means of a polyion-complex membrane. In order to guarantee a reasonable comparison, the

enzyme activity was chosen to be about 6 Units mm^{-2} for both sensors. Thereafter, the dynamic and static response of both sensors towards ACh concentrations in the range of 1 µM to 1 M was investigated. For a step response, by adding ACh resulting to a final concentration of 10 mM, the CCD-type sensor reacts faster (4.3 s) compared to the LAPS (13 s). A comparison of the sensor signals in terms of pH changes towards different ACh concentrations showed that both sensors had a similar behaviour up to 5 mM. The concentration-depending response of both sensors also is in a good agreement with the theoretically expected behaviour (see end of section 1.3.2) up to a concentration of about 3 mM. The lower detection limit is at about 0.1 mM with a pH-buffer concentration of 20 mM, as it was theoretically expected. By storing the LAPS chip at 4 °C, a long-term stability of at least 13 days was achieved. As discussed, both ACh-imaging sensors could be used to analyse the neuronal transmitter ACh during neuronal cell communication. However, an improving of the lateral resolution, especially regarding the LAPS, is required. This way, these sensors could be used to determine long-term cell degradation for investigating diseases, like Alzheimer and myasthenia.

The suitability of the FPGA-based LAPS as a whole-cell biosensor is demonstrated in **chapter 6** and **chapter 7**. Therefore, the metabolic activity of cells was investigated by determining their extracellular acidification by means of a pH-sensitive LAPS. The primary aim of these measurements was the development of a new monitoring system for biogas digesters. The biogas process plays a decisive role in the field of renewable energies. Regarding the anaerobic digestion, a large number of different organisms is involved in the production of biogas, which mainly consists of methane and carbon dioxide. By means of a cogeneration unit the produced biogas can further be transformed, to heat and electricity. To avoid expensive down times and losses in production, the process should ideally be monitored and controlled. Therefore, parameters of the digester, such as the pH value, the redox potential and the temperature, have to be monitored. However, to the large size of the digester, changes of the above mentioned parameters might affect to later to threaten the sensitive microorganisms. Thus, a new approach is to monitor the metabolic activity of relevant organisms involved in the anaerobic digestion, in order to determine their "welfare". This "welfare" can be investigated by determining the extracellular acidification that occurs by extraction of organic acids as metabolic waste product of the metabolism of microorganisms. These acids cause a pH-value change in the surrounding of the microbes, which could be detected by a LAPS. A fast acidification would refer to a high activity and a slow acidification might be a sign for a possible threat of the bio-digestion process. Since the sensor signal of the LAPS correlates almost linearly with the pH value when utilising a pH-sensitive transducer material, the directly measurable potential-change rate is affected by the pH-buffer strength of the measurement medium. To allow a better

comparison between measurements with different measurement media, the acidification rate is calculated by taking into account the pH-buffer capacity (see also Eq. (6.1) and (7.1)). Thus, the acidification rate is given as the number of H^+ ions produced per second and per cell.

In **chapter 6**, *Escherichia coli* as a model organism and lysogeny broth (LB) medium as measurement medium have been used. In a first step, measurements with *E. coli* in suspension with different cell densities from 2×10^9 cells ml^{-1} to 8×10^9 cells ml^{-1} have been carried out. The average acidification rate was about 5×10^4 H^+ s^{-1} per cell, which fits well to the values from literature. In a second step, the *E. coli* were immobilised on the sensor surface. In order to determine the acidification rate over time, it is necessary to fix the microbes on the sensor surface, since the used and acidified measurement medium has to be exchanged periodically. Therefore, an immobilisation technique to embed *E. coli* within polyacrylamide gel was developed. This allows to attach large number of cells near to the sensor surface without any additional surface-treatment steps. Furthermore, to compensate external influences, like sensor drift, temperature changes and external pH changes, an on-chip differential arrangement was introduced. For the differential arrangement, two wells with a height of about 160 µm were realised on the LAPS chip by means of photolithography. One well, the active area, was filled with *E. coli* embedded in polyacrylamide gel. The other well, the reference area, was filled with only polyacrylamide gel. Both wells can be read out by means of the addressability of the FPGA-based LAPS set-up. Since both wells would be affected by external influences in the same way, only the active area is affected in addition by the extracellular acidification of the bacteria. Thus, the differential signal is calculated by simply subtracting the signal of the reference area from the signal of the active area. Thereafter, the acidification rate is calculated from the differential signal. Several measurement cycles with 1.4×10^9 cells in 50 µl gel and LB medium demonstrated the suitability of the immobilisation technique and the on-chip differential set-up for acidification measurements. The achieved acidification rate was $(4 \pm 2) \times 10^4$ H^+ s^{-1} per cell in average. These results proof that the extracellular acidification of *E. coli* in the polyacrylamide gel is not suppressed by immobilisation, when compared to measurements with *E. coli* in suspension.

The sensitivity of the microorganism-based LAPS towards nutrient concentrations is demonstrated in **chapter 7**. At a high number of immobilised cells and/or at low nutrient concentrations, the transport of the nutrient into and through the gel layer is limited by diffusion. Under this condition, the nutrient concentration can be determined similar to enzyme-based field-effect sensors (see section 1.3.2). If the reaction kinetic is limited by diffusion, an equilibrium between the nutrient delivery to the cell layer and the product (organic acids) delivery to the bulk solution will occur and the product

concentration on the sensor surface will become a function of the substrate concentration. Utilising whole cells instead of single enzymes offers the advantage of determining all nutrients that can be metabolised (under creation of acids or bases) by the immobilised microorganism, simultaneously. This is exemplarily shown with *E. coli* as organism and glucose as nutrient. The bacteria were immobilised in polyacrylamide gel in a differential arrangement, as described in chapter 6. The measurement solution was phosphate buffered saline (PBS) with a low buffer capacity of 0.2 mM pH^{-1} and various glucose concentrations from 0.5 mM to 1.5 mM. With a sensitivity of (89.0 ± 1.5) mV per decade of glucose, the sensitivity towards glucose was demonstrated and the lower detection limit was found to be about 0.4 mM. By comparing the acidification rates it was found that the reaction is limited by diffusion due to the glucose transport.

Further measurements demonstrate the ability to investigate the metabolic activity in slurry from a biogas digester. Therefore, *E. coli* was immobilised in a differential set-up on the LAPS-chip surface. After adding glucose to the slurry, an extracellular acidification of the immobilised *E. coli* occurs. The differential signal decreased after some time, demonstrating that the glucose concentration decreases due to the metabolism of the organisms inside the slurry.

In further investigations, the sensitivity towards other nutrients metabolised by *E. coli* or other acid- or base-producing microbes should be investigated. Also, the influence of the cell density is an interesting task, since different amounts of immobilised cells would change the cell-based biosensor's behaviour from diffusion limitation to reaction limitation. This way, either the nutrient concentration or the metabolic activity of the cells can be investigated. Hence, a further approach for cell-based biosensors to investigate the status of the biogas process could be the immobilisation of different species of microbes in various cell densities on the LAPS-chip surface. The resulting response of each measurement spot then would indicate different parameters, like various nutrient concentrations, metabolic activities and/or the presence of inhibiting substances. These parameters combined by mathematical models or algorithms could give an early information about the status of the biogas digester.

Besides the monitoring of biogas processes, this microorganism-based biosensor would be interesting for medical and pharmaceutical fields. The bacteria-based LAPS may be used directly to observe the gut microbiota, since the processes related to the gut microbiota and the organisms involved in biogas digesters are similar; both perform anaerobic fermentation and consist of a wide diversity of anaerobic microorganism species. Recently, it is discussed in literature (e.g., [6]) that the activity and composition of the gut microbiota play an important role for e.g., diet, overweight, immunity reactions, allergies and health. The use of the microorganism-based LAPS to investigate the metabolic activity of enteric bacteria in the presence of e.g., drugs represents a further

possible applications field.

Furthermore, those microorganism-based biosensors that are sensitive towards nutrient concentrations and the metabolic activities of immobilised cells open a wide field of possible applications for e.g., cell-growth studies in fermentation processes. Their ability to be sensitive to all nutrients and also inhibiting substances that are affecting the metabolic activity of the immobilised organisms might serve as an overall indicator to define the status of a fermentation process. This might be also helpful to further optimise cell culturing in fermentation processes in the fields of food or pharmaceutical industry.

Utilising mammalian cells on the whole-cell-based LAPS enables to perform drug screening in medical research and drug development. But it might also be used in cases of personalised medicine to perform simultaneously *in vitro* screening of several drugs against tissues from a patient before applying these drugs to this patent. In this case, the development of a multi-analyte imaging technique with the OLED-based LAPS would be interesting, to e.g., observe the uptake of agents and the release of products simultaneously in addition to the extracellular acidification. Moreover, a combination of a microfluidic system on a LAPS chip allows to establish fully automatically measurement systems, like lab-on-a-chip systems. Here, LAPS offer the advantage to scan almost any position inside those microfluidic channels.

References

[1] T. Wagner. "Lichtadressierbare potentiometrische Sensoren für den Einsatz in der Pharmazie". German. PhD thesis. Philipps-Universität Marburg, 2008.

[2] K. Miyamoto, K. Kaneko, A. Matsuo, T. Wagner, S. Kanoh, M. J. Schöning, and T. Yoshinobu. "Miniaturized chemical imaging sensor system using an OLED display panel". In: *Procedia Engineering* 5 (2010), pp. 516–519. DOI: 10.1016/j.proeng.2010.09.160.

[3] M. George, W. J. Parak, I. Gerhardt, W. Moritz, F. Kaesen, H. Geiger, I. Eisele, and H. E. Gaub. "Investigation of the spatial resolution of the light-addressable potentiometric sensor". In: *Sensors and Actuators, A: Physical* 86.3 (2000), pp. 187–196. DOI: 10.1016/S0924-4247(00)00455-6.

[4] M. Nakao, S. Inoue, T. Yoshinobu, and H. Iwasaki. "High-resolution pH imaging sensor for microscopic observation of microorganisms". In: *Sensors and Actuators B: Chemical* 34.1-3 (1996), pp. 234–239. DOI: 10.1016/S0925-4005(96)01903-X.

[5] W. Moritz, T. Yoshinobu, F. Finger, S. Krause, M. Martin-Fernandez, and M. J. Schöning. "High resolution LAPS using amorphous silicon as the semiconductor material". In: *Sensors and Actuators B: Chemical* 103.1–2 (2004), pp. 436–441. DOI: 10.1016/j.snb.2004.04.073.

[6] A. M. O'Hara and F. Shanahan. "The gut flora as a forgotten organ". In: *EMBO Rep* 7.7 (2006), pp. 688–693. DOI: 10.1038/sj.embor.7400731.

9 Zusammenfassung und Ausblick

Die gleichzeitige Analyse von mehreren Analyten und die ortsaufgelöste Messung von Konzentrationsverteilungen mit einem einzelnen Sensorchip ist ein viel diskutiertes Feld in der Sensorentwicklung. Zusammen mit der Miniaturisierung ist dies ein entscheidender Entwicklungsschritt für Anwendungen und Prozesse, welche von Bio- und Chemosensoren profitieren. In Kombination mit biologischen Komponenten zur spezifischen Analytbestimmung, wie Enzymen oder Zellen, sind diese Biosensoren ein interessantes System für biotechnologische, medizinische oder pharmazeutische Applikationen. Ein vielversprechendes Sensorprinzip für diese Aufgaben ist der lichtadressierbare potentiometrische Sensor (LAPS). Ein LAPS ist ein Halbleiter-basierter potentiometrischer Sensor, welcher eine ortsaufgelöste Analytkonzentrationsbestimmung in wässrigen Lösungen erlaubt. Die Ortsauflösung wird mit einem fokussierten Lichtstrahl erreicht. Das Licht erzeugt einen Fotostrom, welcher mit der Analytkonzentration an der Sensoroberfläche im beleuchteten Bereich korreliert. Basierend auf einer früheren Doktorarbeit von Dr. T. Wagner wurden in dieser Promotion LAPS-Aufbauten weiterentwickelt. Des Weiteren wurde die Nutzung dieser LAPS-Aufbauten für biotechnologische, medizinische und pharmazeutische Anwendungen durch die Nutzung von Enzymen und Mikroorganismen demonstriert.

In dieser Arbeit wurden zunächst mehrere unterschiedliche LAPS-Aufbauten entwickelt. Der erste LAPS-Aufbau basiert auf einem „Field-programmable Gate Array“ (FPGA), welches ein 4×4 Leuchtdioden-Array (LED) ansteuert und somit 16 Messspots auf der Sensoroberfläche definiert. Mit dem FPGA können alle Messspots zum selben Zeitpunkt ausgelesen werden, um z.B. „Chemical Images“ der gesamten Sensoroberfläche in nur 200 ms zu erfassen. Mit diesem FPGA-basierte LAPS-Aufbau wurde das Frequenzverhalten von LAPS-Chips untersucht. In einem zweiten LAPS-Aufbau wurde ein kommerziell verfügbares „Organic-LED“-Display (OLED) als Lichtquelle benutzt. Das OLED-Display besitzt 96×64 Pixel mit einer Pixelgröße von $200\,\mu m \times 200\,\mu m$. Um Modulationsfrequenzen im kHz-Bereich zu erhalten, wurde eine neue Ansteuerungsmethode für das OLED-Display entwickelt. Mit dieser Ansteuerungsmethode können „Chemical Images“ der gesamten LAPS-Oberfläche in 2.5 min erfasste werden, was ca. 40-mal schneller ist, als mit der herkömmlichen OLED-Ansteuerungsmethode. Da die Ortsauflösung von LAPS nicht allein von der Lichtquelle definiert wird, sondern auch vom LAPS-Chip selbst, wurde die laterale Auflösung der LAPS-Strukturen untersucht.

Hierfür wurde ein dritter LAPS-Aufbau entwickelt, welcher eine einzelne Laserdiode auf einer verfahrbaren XY-Einheit benutzt. Durch Charakterisieren von speziell strukturierten LAPS-Chips wurde eine laterale Auflösung in der Größenordnung der OLED-Pixel nachgewiesen.

Neben den technologischen Weiterentwicklungen wurde mit dem FPGA-basierten LAPS-Aufbau erstmals der markierungsfreie Nachweis von Konzentrationsverteilungen biologischer Substanzen demonstriert. Mit einer Enzymschicht mit dem Enzym Acetylcholin-Esterase (AChE) wurde der Neurotransmitter Acetylcholin (ACh) nachgewiesen. Das dynamische und statische Ansprechverhalten sowie die Langzeitstabilität wurden charakterisiert und mit einem weiteren, Halbleiter-basierten Sensor, welcher das „Charge-coupled Devices"-Prinzip (CCD) nutzt, unter Verwendung der gleichen Enzymschicht, verglichen.

Die Verwendung des FPGA-basierten LAPS-Aufbau als zellbasierter Biosensor wurde mit dem Modelorganismus *Escherichia coli* gezeigt. Hier wurde die metabolische Aktivität von *E. coli* untersucht, indem die extrazelluläre Ansäuerung erfasst wurde. Dazu wurde eine Immobilisierungsstrategie entwickelt, bei welcher die Mikroorganismen in Polyacrylamidgel eingebettet wurden. Die Immobilisierung ist in einer Differenzanordnung realisiert worden, welche die Adressierbarkeit des LAPS nutzt, um somit externe Einflüsse wie Sensordrift, Temperaturschwankungen und externe pH-Wertänderungen zu kompensieren. Beim Vergleich der extrazellulären Ansäuerung von immobilisierten *E. coli* mit *E. coli*'s in Suspension wurden ähnliche Ansäuerungsraten festgestellt, was zeigt, dass die Immobilisierung keinen entscheidenden negativen Einfluss auf die metabolische Aktivität hatte. Weitere Messungen demonstrierten die Sensitivität dieses zellbasierten LAPS-Systems gegenüber unterschiedliche Nährstoffkonzentrationen, was am Beispiel von Glucose ausgeführt wurde. Die Möglichkeit der Erfassung der extrazellulären Ansäuerung von Mikroorganismen sowie die Sensitivität gegenüber Nährstoffkonzentrationen erlaubt es, übergeordnete Effekte wie Toxizität und pharmazeutische Aktivität, von komplexen Messmedien nachzuweisen.

Weiterführende Arbeiten, wozu sich der OLED-basierte LAPS-Aufbau eignen würde, ist ein „Cheimcal Imaging"-Sensor, welcher die Konzentrationsverteilung mehrerer Analyte gleichzeitig nachweisen könnte. Für die Untersuchung von Zellkommunikationen wäre eine weitere Verbesserung der lateralen Auflösung notwendig; ab einer Auflösung von ca. 10 µm wäre die Beobachtung von einzelnen Zellen möglich. Der vorgestellte *E. coli*-basierte LAPS hat neben dem Einsatz zur Überwachung von Biogasanalgen auch das Potenzial zur Untersuchung von anderen Bakteriengemeinschaften, wie z.B. Darmmikrobiota. Generell liegen die Einsatzmöglichkeiten des zellbasierten LAPS-Aufbaus zur Untersuchung der metabolischen Aktivität bei Anwendungen, wie im Bereich des Medikamenten-Screening oder der personalisierte Medizin.

List of publications

Publications in peer-reviewed journals

[1] C. F. Werner, T. Wagner, T. Yoshinobu, M. Keusgen, and M. J. Schöning. "Frequency behaviour of light-addressable potentiometric sensors". In: *Physica Status Solidi A: Applications and Materials Science* 210.5 (2013), pp. 884–891. DOI: 10.1002/pssa.201200929.

[2] C. F. Werner, S. Takenaga, H. Taki, K. Sawada, and M. J. Schöning. "Comparison of label-free ACh-imaging sensors based on CCD and LAPS". In: *Sensors and Actuators B: Chemical* 177 (2013), pp. 745–752. DOI: 10.1016/j.snb.2012.11.012.

[3] C. F. Werner, T. Wagner, K. Miyamoto, T. Yoshinobu, and M. J. Schöning. "High speed and high resolution chemical imaging based on a new type of OLED-LAPS set-up". In: *Sensors and Actuators B: Chemical* 175 (2012), pp. 118–122. DOI: 10.1016/j.snb.2011.12.102.

[4] C. F. Werner, S. Groebel, C. Krumbe, T. Wagner, T. Selmer, T. Yoshinobu, M. E. M. Baumann, M. Keusgen, and M. J. Schöning. "Nutrient concentration-sensitive microorganism-based biosensor". In: *Physica Status Solidi A: Applications and Materials Science* 209.5 (2012), pp. 900–904. DOI: 10.1002/pssa.201100801.

[5] T. Wagner, K. Miyamoto, C. F. Werner, M. J. Schöning, and T. Yoshinobu. "Utilising digital micro-mirror device (DMD) as scanning light source for light-addressable potentiometric sensors (LAPS)". In: *Sensor Letters* 9.2 (2011), pp. 812–815. DOI: 10.1166/sl.2011.1620.

[6] C. F. Werner, S. Schusser, H. Spelthahn, T. Wagner, T. Yoshinobu, and M. J. Schöning. "Field-programmable gate array based controller for multi spot light-addressable potentiometric sensors with integrated signal correction mode". In: *Electrochimica Acta* 56.26 (2011), pp. 9656–9660. DOI: 10.1016/j.electacta.2011.03.012.

[7] T. Wagner, C. F. Werner, K. Miyamoto, M. J. Schöning, and T. Yoshinobu. "Development and characterisation of a compact light-addressable potentiometric sensor (LAPS) based on the digital light processing (DLP) technology for flexible

chemical imaging". In: *Sensors and Actuators, B: Chemical* 170 (2012), pp. 34–39. DOI: 10.1016/j.snb.2010.12.003.

[8] C. F. Werner, C. Krumbe, K. Schumacher, S. Groebel, H. Spelthahn, M. Stellberg, T. Wagner, T. Yoshinobu, T. Selmer, M. Keusgen, M. E. M. Baumann, and M. J. Schöning. "Determination of the extracellular acidification of *Escherichia coli* by a light-addressable potentiometric sensor". In: *Physica Status Solidi A: Applications and Materials Science* 208.6 (2011), pp. 1340–1344. DOI: 10.1002/pssa.201001141.

[9] T. Wagner, C. F. B. Werner, K. Miyamoto, M. J. Schöning, and T. Yoshinobu. "A high-density multi-point LAPS set-up using a VCSEL array and FPGA control". In: *Sensors and Actuators B: Chemical* 154.2 (2011), pp. 124–128. DOI: 10.1016/j.snb.2010.03.009.

[10] T. Wagner, C. F. Werner, K. Miyamoto, H.-J. Ackermann, T. Yoshinobu, and M. J. Schöning. "FPGA-based LAPS device for the flexible design of sensing sites on functional interfaces". In: *Physica Status Solidi A: Applications and Materials Science* 207.4 (2010), pp. 844–849. DOI: 10.1002/pssa.200983320.

[11] J. R. Siqueira, R. M. Maki, F. V. Paulovich, C. F. Werner, A. Poghossian, M. C. F. de Oliveira, V. Zucolotto, O. N. Oliveira, and M. J. Schöning. "Use of information visualization methods eliminating cross talk in multiple sensing units investigated for a light-addressable potentiometric sensor". In: *Analytical Chemistry* 82.1 (2010), pp. 61–65. DOI: 10.1021/ac9024076.

[12] J. R. Siqueira Jr., C. F. Werner, M. Baecker, A. Poghossian, V. Zucolotto, O. N. Oliveira Jr., and M. J. Schöning. "Layer-by-layer assembly of carbon nanotubes incorporated in light-addressable potentiometric sensors". In: *Journal of Physical Chemistry C* 113.33 (2009), pp. 14765–14770. DOI: 10.1021/jp904777t.

Proceedings

[1] S. Takenaga, C. Herrera, C. F. Werner, M. Biselli, T. Schnitzler, M. Schöning, P. Öhlschläger, and T. Wagner. "Detection of the metabolic activity of cells by differential measurements based on a single light-adressable potentiometric sensor chip". In: *11. Dresdner Sensor-Symposium 2013*. Wunstorf: AMA Service GmbH, 2013, pp. 63–67. DOI: 10.5162/11dss2013/3.4.

[2] C. Wu, A. Poghossian, C. F. Werner, T. Bronder, M. Bäcker, P. Wang, and M. J. Schöning. "An application of a scanning light-addressable potentiometric sensor for label-free DNA detection". In: *11. Dresdner Sensor-Symposium 2013*. Wunstorf: AMA Service GmbH, 2013, pp. 164–168. DOI: 10.5162/11dss2013/A9.

[3] S. Takenaga, C. F. Werner, K. Sawada, and M. J. Schöning. "Comparison of label-free ACh image sensors based on CCD and LAPS". In: *IMCS 2012 - The 14th International Meeting on Chemical Sensors*. Ed. by R. Moos. Wunstorf (Germany): AMA Service GmbH, 2012, pp. 356–359. DOI: 10.5162/IMCS2012/4.2.6.

[4] S. Groebel, C. F. Werner, M. Reimann, N. Jörres, F. Jansen, J. Schiffels, B. Sprenger, M. E. M. Baumann, M. J. Schöning, and T. Selmer. "Entwicklung einer Sensor-Überwachung für Biogasanlagen auf Basis von Prozessdaten einer Parallelanlage". German. In: *10. Dresdner Sensor-Symposium: 05.–07. Dezember 2011, Dresden*. Ed. by G. Gerlach and A. Schütze. Dresden: TUDpress, 2011, pp. 81–84. DOI: 10.5162/10dss2011/4.3.

[5] C. F. Werner, A. Mansour, F.-M. Rateike, S. Schusser, T. Wagner, T. Yoshinobu, M. Keusgen, and M. J. Schöning. "Kompakter Aufbau eines lichtadressierbaren potentiometrischen Sensors mit verfahrbarem Diodenlaser". German. In: *10. Dresdner Sensor-Symposium: 05.–07. Dezember 2011, Dresden*. Ed. by G. Gerlach and A. Schütze. Dresden: TUDpress, 2011, pp. 277–280. DOI: 10.5162/10dss2011/14.3.

[6] C. F. Werner, T. Wagner, K. Miyamoto, T. Yoshinobu, and M. J. Schöninig. "High speed and high resolution chemical imaging based on a new type of OLED-LAPS set-up". In: *Procedia Engineering* 25 (2011), pp. 346–349. DOI: 10.1016/j.proeng.2011.12.085.

[7] C. F. Werner, S. Groebel, T. Wagner, T. Yoshinobu, T. Selmer, M. E. M. Baumann, and M. J. Schöning. "Überwachung der metabolischen Aktivität von Mikroorganismen zur Kontrolle des biologischen Prozesses im Biogasfermenter". German. In: *Energieträger der Zukunft: Fachtagung Braunschweig, 08. und 09. Juni 2011 / 6. Fachtagung Biogas 2011. VDI Energie und Umwelt*. Düsseldorf: VDI-Verlag, 2011, pp. 285–286. URL: http://d-nb.info/1013435907.

[8] C. F. Werner, H. Spelthahn, M. J. Schöning, C. Krumbe, T. Wagner, T. Yoshinobu, and M. Keusgen. "Neue Ansteuerungselektronik für LAPS-basierte Biosensoren zur gleichzeitigen ortsaufgelösten Messung der pH-Konzentration". German. In: *Sensoren und Messsysteme 2010: Vorträge der 15. ITG-GMA-Fachtagung vom 18. bis 19. Mai 2010 in Nürnberg / ITG-GMA Fachtagung Sensoren und Messsysteme 2010*. Ed. by R. Gerhard. Berlin, Offenbach: VDE Verlag GmBH, 2010, pp. 109–114. URL: http://d-nb.info/1002307023.

[9] C. F. Werner, S. Groebel, K. Schumacher, H. Spelthahn, T. Wagner, T. Selmer, M. E. M. Baumann, and M. J. Schöning. "Bestimmung der metabolischen Aktivität von Mikroorganismen während des Biogasbildungsprozesses". German. In: *9. Dresdner Sensor-Symposium: 07.–09. Dezember 2009, Dresden*. Ed. by G. Gerlach

and P. Hauptmann. Dresden: TUDpress, 2009, pp. 201–204. URL: http://d-nb.info/998316334.

[10] T. Wagner, C. F. Werner, K. Miyamoto, M. J. Schöning, and T. Yoshinobu. "A high-density multi-point LAPS set-up using a VCSEL array and FPGA control". In: *Procedia Chemistry* 1.1 (2009). Ed. by J. Brugger and D. Briand, pp. 1483–1486. DOI: 10.1016/j.proche.2009.07.370.

Oral and poster presentations

[1] C. F. Werner, C. Krumbe, T. Wagner, T. Yoshinobu, T. Selmer, M. Keusgen, and M. J. Schöning. "Measurement of saccharide concentrations using an *E. coli* cell-based LAPS". In: *Workshop Engineering of Functional Interfaces*. Hasselt (Belgium), 2013, p. 44.

[2] C. F. Werner, C. Krumbe, T. Wagner, T. Yoshinobu, M. Keusgen, and M. J. Schöning. "Lichtadressierbare potentiometrische Sensoren und deren Einsatz zur ortsaufgelösten Konzentrationsbestimmung". German. In: *8. Deutsches BioSensor Symposium*. Ed. by F. Lisdat. Wildau (Germany): TH Wildau, 2013, p. 45.

[3] C. F. Werner, S. Groebel, T. Wagner, T. Selmer, T. Yoshinobu, M. E. M. Baumann, M. Keusgen, and M. J. Schöning. "Light-addressable potentiometric sensors and their application for the determination of the metabolic activity of bacteria". In: *5. Graduiertentagung der FH Aachen*. Ed. by S. Schusser, C. Vaeßen, and M. J. Schöning. Jülich (Germany), 2012, p. 45. URL: http://nbn-resolving.de/urn/resolver.pl?urn:nbn:de:hbz:a96-opus-50425.

[4] C. F. Werner, T. Wagner, T. Yoshinobu, and M. J. Schöning. "Frequency behaviour of light-addressable potentiometric sensors". In: *Workshop Engineering of Functional Interfaces*. Zweibrücken (Germany), 2012, p. 91.

[5] S. Takenaga, C. F. Werner, K. Sawada, and M. J. Schöning. "Comparison of label-free ACh image sensors based on CCD and LAPS". In: *IMCS 2012 - The 14th International Meeting on Chemical Sensors*. Ed. by R. Moos. Wunstorf (Germany): AMA Service GmbH, 2012, p. 88.

[6] C. F. Werner, A. Mansour, F.-M. Rateike, S. Schusser, T. Wagner, T. Yoshinobu, M. Keusgen, and M. J. Schöning. "Kompakter Aufbau eines lichtadressierbaren potentiometrischen Sensors mit verfahrbarem Diodenlaser". German. In: *10. Dresdner Sensor-Symposium*. Dresden (Germany), 2011.

[7] C. F. Werner, S. Groebel, T. Wagner, T. Selmer, T. Yoshinobu, M. E. M. Baumann, M. Keusgen, and M. J. Schöning. "Determination of glucose concentration by means of a microorganism-based biosensor". In: *4. Graduiertentagung der FH Aachen*. Ed. by S. Schusser, C. Vaeßen, and M. J. Schöning. Aachen (Germany), 2011, p. 59. URL: http://nbn-resolving.de/urn/resolver.pl?urn:nbn:de:hbz:a96-opus-3530.

[8] C. F. Werner, T. Wagner, K. Miyamoto, T. Yoshinobu, and M. J. Schöning. "High speed and high resolution chemical imaging based on a new type of OLED-LAPS set-up". In: *Eurosensors XXV*. Athens (Greece), 2011.

[9] C. F. Werner, S. Groebel, T. Wagner, T. Selmer, T. Yoshinobu, M. E. M. Baumann, M. Keusgen, and M. J. Schöning. "Determination of nutrient concentration by means of a microorganism-based biosensor". In: *Workshop Engineering of Functional Interfaces*. Linz (Austria), 2011.

[10] C. F. Werner, S. Groebel, T. Wagner, T. Yoshinobu, T. Selmer, M. E. M. Baumann, and M. J. Schöning. "Überwachung der metabolischen Aktivität von Mikroorganismen zur Kontrolle des biologischen Prozesses im Biogasfermenter". German. In: *6. Fachtagung Biogas*. Braunschweig (Germany), 2011.

[11] C. F. Werner, S. Schusser, S. Groebel, H. Spelthahn, T. Wagner, T. Selmer, T. Yoshinobu, and M. J. Schöning. "Ortsaufgelöste Bestimmung der Ansäuerung von Mikroorganismen mit geregelter Spot-/Pixelkorrektur". German. In: *7. Deutsches BioSensor Symposium*. Ed. by D. Beckmann. Heilbad Heiligenstadt (Germany): Verlag Mainz, 2011, p. 40.

[12] C. F. Werner, C. Krumbe, S. Groebel, H. Spelthahn, T. Wagner, T. Yoshinobu, T. Selmer, M. Keusgen, and M. J. Schöning. "On-line determination of the condition of microorganisms by a light-addressable potentiometric sensor". In: *3. Graduiertentagung der FH Aachen*. Ed. by N. Schubert, C. Vaeßen, and M. J. Schöning. Aachen (Germany), 2010, p. 73. URL: http://nbn-resolving.de/urn/resolver.pl?urn:nbn:de:hbz:a96-opus-3386.

[13] C. F. Werner, S. Groebel, H. Spelthahn, C. Krumbe, T. Wagner, T. Yoshinobu, T. Selmer, M. Keusgen, M. J. Schöning, and S. Schusser. "Array-based light-addressable potentiometric sensor with integrated imaging correction mode". In: *EMNT 2010*. Mandelieu la Napoule (France), 2010, p. 067.

[14] C. F. Werner, S. Groebel, H. Spelthahn, T. Wagner, T. Yoshinobu, T. Selmer, M. Keusgen, and M. J. Schöning. "On-line determination of the condition of microorganisms by a light-addressable potentiometric sensor". In: *Workshop Engineering of Functional Interfaces*. Ed. by M. Keusgen, J. Jedelská-Keusgen, and L. Fernanda. Rauischholzhausen Castle (Germany), 2010, p. 47.

[15] C. F. Werner, H. Spelthahn, M. J. Schöning, C. Krumbe, T. Wagner, T. Yoshinobu, and M. Keusgen. "Neue Ansteuerungselektronik für LAPS-basierte Biosensoren zur gleichzeitigen ortsaufgelösten Messung der pH-Konzentration". German. In: *Sensoren und Messsysteme 2010*. Nürnberg (Germany), 2010.

[16] C. F. Werner, S. Groebel, K. Schumacher, H. Spelthahn, T. Wagner, T. Selmer, M. E. M. Baumann, and M. J. Schöning. "Bestimmung der metabolischen Aktivität von Mikroorganismen während des Biogasbildungsprozesses". German. In: *9. Dresdner Sensor-Symposium*. Dresden (Germany), 2009.

[17] C. F. Werner, S. Groebel, H. Spelthahn, T. Wagner, M. E. M. Baumann, and M. J. Schöning. "Optimising of the operation of a biogas fermenter by means of a field-effect biosensor based on a light-addressable potentiometric sensor (LAPS)". In: *2. Graduiertentagung der FH Aachen*. Ed. by M. J. Schöning, S. Crummenerl, S. Kowollik, and S. Groebel. Aachen (Germany), 2009, p. 61. URL: http://nbn-resolving.de/urn/resolver.pl?urn:nbn:de:hbz:a96-opus-3131.

[18] C. F. Werner, S. Groebel, K. Schumacher, T. Wagner, M. Stellberg, M. E. M. Baumann, and M. J. Schöning. "Biosensor to investigate the metabolic activity of acetogen bacteria". In: *Workshop Engineering of Functional Interfaces*. Ed. by P. Wagner. Hasselt (Belgium), 2009, p. 45.

[19] C. F. Werner, S. Groebel, H. Spelthahn, T. Wagner, M. E. M. Baumann, and M. J. Schöning. "Lichtadressierbarer potentiometrischer Sensor zur Überwachung von Biogasanlagen". German. In: *6. Deutsches BioSensor Symposium*. Ed. by G. Urban. Freiburg (Germany), 2009, p. 83.

Acknowledgements

The present dissertation would not have sprout unless the guidance, assistance and help of many well-meaning and pleasant persons. Hence, I would like to express my sincere appreciation to:

Prof. Dr. Michael J. Schöning for the supervision, for his confidence, for providing the freedom to further develop my skills, for providing me with the opportunity to work with a talented team of researchers and for attending in national and international conferences. It was a pleasure for me to be a part of his team at the FH Aachen, Institute of Nano- and Biotechnologies (INB). Thank you for all the great proof-reading of all manuscripts and thus, the compensating my weaknesses in spelling and grammar.

Prof. Dr. Michael Keusgen (University Marburg) for giving me the opportunity to do a Ph.D. under his supervision, for the proof-reading of the papers and the present thesis as well as for his always uncomplicated and friendly manner. Mrs. Prof. Dr. Petersen and Mr. Prof. Dr. Bünemann from the University Marburg for their attendance in the examination committee.

Prof. Dr. Tatsuo Yoshinobu (Tokoku University) for the close cooperation in the field of LAPS, for the fruitful discussions and for the opportunity to stay three months in Japan and work in his laboratory. Dr. Torsten Wagner (Tokoku University and INB) for his introduction and the long, interesting and fruitful discussions about LAPS, for the opportunity to work in the team "Opto-Switch", for his support during my stay in Japan, for all the assistance during my dissertation and for being a kind of unofficial supervisor. He was in a lot of areas, a role model and a source of inspiration for me. Thank you, for the time experimenting with things like, Linux, LaTeX, Python, micro controllers, ...

Prof. Dr. Marcus Baumann and Prof. Dr. Thorsten Selmer from INB for their support in the project "Bio-LAPS". Dr. Simone Groebel (INB) for the cooperation in the project "Bio-LAPS", for the cultivation of the microorganisms and for providing the technical support and the required material to conduct all the microbiological studies.

Dr. Shoko Takenaga (Toyohashi University and INB) for providing the possibility to work with the CCD-type chemical-imaging sensor, for working together on LAPS experiments and for all the Japanese culture and language skills. Dr. José R. Siqueira, Jr. (University of São Paulo and INB), Dr. Ko-ichiro Miyamoto (Tohoku University), Dr. Ulrich Bohrn (Siemens AG) and Dr. Chunsheng Wu (Zhejiang University and INB) for

the collaboration and their resulting publications.

Dr. Patrick Kirchner and Dr. Steffen Reisert who starts their Ph.D. thesis together with me at the INB, for all the helpful and inspiration discussions during a cup of tea and for all their support. The former and present Ph.D. students at the laboratory of Chemical Sensors and Biosensors (INB), Dr. Matthias Bäcker, Sebastian Schusser, Christina Huck, Jan Oberländer, Lars Breuer, Thomas Bronder, Dr. Niko Näther, Dr. Monika Turek and Dr. Maryam Abouzar for the friendly atmosphere and the solidarity during the daily work.

The students Katharina Schumacher, Ahmed Mansour, Christoph Krumbe and, Marc Reimann for their contributions to the matter of the present dissertation with their own work in the context of their research projects, diploma, bachelor and master theses. Max Krischer for improving the Scanning-LAPS software.

The members of the laboratory of Chemical Sensors and Biosensors (INB), David Rolka, Heiko Iken, Marcel Leinhos and Stefan Beging for fabricating all the LAPS chips, for their technical discussions and support and for the friendly atmosphere. Prof. Dr. Arshak Poghossian (INB) for the helpful discussions and advices. Benno Schneider (INB) for designing and printing of 3D objects to improve the LAPS set-ups. Thomas Schnitzler (INB) for the opportunity to use the laboratory of cell culture technology and for his professional support.

My friends and my family for their encouragement and support throughout the years.

Furthermore, this present thesis would not have been possible without financial support. Hence, I would like to express my gratitude to:

The German Federal Ministry of Food, Agriculture and Consumer Protection (BMELV) and the "Fachagentur Nachwachsende Rohstoffe e.V." (FNR) for financial support of the project "Bio-LAPS".

The Marubun Research Promotion Foundation (Japan) for the three month scholarship at the Tohoku University.

The FH Aachen for financial support in the frame of the promotion of Ph.D. students.

The German Federal Ministry of Education and Research (BMBF) for financial support within the research frame of "NanoMatFutur": 13N12585.

Curriculum vitae

The curriculum vitae is not part of the online version.

The curriculum vitae is not part of the online version.